ATOM INTERFEROMETRY FOR TESTS OF GENERAL RELATIVITY

Von der QUEST-Leibniz-Forschungsschule der
Gottfried Wilhelm Leibniz Universität Hannover

zur Erlangung des Grades

Doktor der Naturwissenschaften
- Dr. rer. nat. -

genehmigte Dissertation von

M.Sc. Sina Leon Loriani Fard

geboren am 06.10.1993
in Hamburg

2020

REFERENT
Prof. Dr. Ernst Maria Rasel
Institut für Quantenoptik
Leibniz Universität Hannover

KORREFERENT
Prof. Dr. Peter Wolf
LNE-SYRTE, Observatoire de Paris
Université PSL, CNRS

KORREFERENT
Prof. Dr. Wolfgang Ertmer
Institut für Quantenoptik
Leibniz Universität Hannover

VORSITZENDE DER PRÜFUNGSKOMMISSION
Prof. Dr. Michèle Heurs
Institut für Gravitationsphysik
Leibniz Universität Hannover

TAG DER PROMOTION: 07.10.2020

Für Opa.

تقدیم به پدربزرگم.

ABSTRACT

The search for a fundamental, self-consistent theoretical framework to cover phenomena over all energy scales is possibly the most challenging quest of contemporary physics. Approaches to reconcile quantum mechanics and general relativity entail the modification of their foundations such as the equivalence principle. This corner stone of general relativity is suspected to be violated in various scenarios and is therefore under close scrutiny. Experiments based on the manipulation of cold atoms are excellently suited to challenge its different facets. Freely falling atoms constitute ideal test masses for tests of the universality of free fall in interferometric setups. Moreover, the superposition of internal energy eigenstates provides the notion of a clock, which allows to perform tests of the gravitational redshift. Furthermore, as atom interferometers constitute outstanding phasemeters, they hold the promise to detect gravitational waves, another integral aspect of general relativity. In recent years, atom interferometers have developed into versatile sensors with excellent accuracy and stability, and allow to probe physics at the interface of quantum mechanics and general relativity without classical analog.

In this thesis, various aspects regarding tests of general relativity with atom interferometry have been theoretically investigated. This includes the analysis of fundamental effects as well as feasibility studies of experimental configurations. The work is partially focussed on a space-borne mission scenario for a dedicated quantum test of the universality of free fall beyond state-of-the-art by dropping matter waves of different elements [P1]. To enable the target accuracy at the level of 10^{-17}, a compensation scheme has been developed and discussed, mitigating the detrimental effects of imperfect test mass co-location upon release and relaxing the requirements on the source preparation by several orders of magnitude [P2]. In addition, it was demonstrated that the careful design of quantum degenerate sources is indispensable for these experiments, requiring tailored schemes to prepare miscible binary sources [P3]. The possibility to test the gravitational redshift with atom interferometers has also been examined in this thesis and connected to the ideas of clock interferometry. With the proof that closed light pulse atom interferometers without transitions between internal internal states are not sensitive to gravitational time dilation, an ongoing scientific debate has been resolved. Instead, certain configurations were shown to implement a quantum version of the special-relativistic twin paradox, for which an experiment has been proposed [P4]. Finally, requirements on atomic sources and atom optics for scenarios of gravitational wave detection on ground [P5, P6] and in space [P7] have been investigated.

Keywords: Atom interferometry, General Relativity, Equivalence Principle, Gravitational Wave Detection

ZUSAMMENFASSUNG

Die Suche nach einer fundamentalen, selbst-konsistenten Theorie zur Beschreibung physikalischer Phänomene über alle Energieskalen stellt wohl eine der wichtigsten Aufgaben der zeitgenössischen Physik dar. Ansätze zur Vereinigung von Quantenmechanik und allgemeiner Relativisitätstheorie haben Änderungen derer Grundlagen zur Folge. So wird das Äquivalenzprinzip, ein Eckpfeiler der allgemeinen Relativitätstheorie, in verschiedenem Szenarien möglicherweise verletzt und steht daher auf dem Prüfstand. Experimente mit kalten Atomen sind hervorragend dafür geeignet, die verschiedenen Aspekte des Prinzips zu untersuchen. Frei fallende Atome stellen ideale Testmassen für die Überprüfung der Universalität des Freien Falls in interferometrischen Anordnungen dar. Außerdem liefert die Überlagerung interner Energiezustände das Konzept einer Uhr und erlaubt damit, Tests der gravitativen Rotverschiebung durchzuführen. Darüber hinaus sind Atominterferometer vielversprechend für die Detektion von Gravitationswellen, eines weiteren Aspekts der allgemeinen Relativitätstheorie. Dank einer raschen Entwicklung in den letzten Jahren zeichnen sich diese Quantensensoren durch hohe Genauigkeit und Stabilität aus und ermöglichen einen Zugang zur Schnittstelle von Quantenmechanik und allgemeiner Relativitätstheorie, welcher die Möglichkeiten klassischer Sensoren überschreitet.

Im Rahmen dieser Arbeit wurden verschiedene Aspekte zu Tests der allgemeinen Relativitätstheorie mit Atominterferometrie theoretisch untersucht. Dies beinhaltet sowohl die Analyse fundamentaler Effekte als auch Machbarkeitsstudien experimenteller Konfigurationen. Ein Schwerpunkt liegt auf einem Szenario eines weltraumgestützten Quantentests der Universalität des freien Falls mit Materiewellen unterschiedlicher Elemente [P1]. Um die antizipierte relative Genauigkeit von 10^{-17} zu erreichen, wurde ein Schema erarbeitet, welches die nachteiligen Auswirkungen einer imperfekten Präparation der atomaren Ensembles kompensiert. Die experimentellen Anforderungen können somit um mehrere Größenordnungen erleichtert werden [P2]. Darüber hinaus wurden Konzepte zur Erzeugung ultra-kalter, mischbarer Zustände analysisert, welche für diese Experimente unerlässlich sind [P3]. Die Möglichkeit, die gravitative Rotverschiebung mit Atominterferometern zu testen, wurde ebenfalls in dieser Arbeit untersucht und mit den Konzepten der Interferometrie von Uhren verbunden. Mit dem allgemeinen Nachweis, dass geschlossene Lichtpuls-Atominterferometer ohne Übergänge zwischen internen Zuständen nicht auf gravitative Zeitdilatation sensitiv sind, wurde zur Aufklärung einer wissenschaftliche Debatte beigetragen. In dem Zuge wurde gezeigt, dass bestimmte Konfigurationen stattdessen eine Quantenversion des speziell-relativistischen Zwillingsparadoxons implementieren, für welches ein Experiment vorgeschlagen wurde [P4]. Schließlich wurden die Anforderungen an Atomquellen und Atomoptik für verschiedene Szenarien zur Messung von Gravitationswellen sowohl für terrestrische [P5, P6] als auch für weltraumgestützte [P7] Detektoren untersucht.

Schlagwörter: Atominterferometrie, allgemeine Relativitätstheorie, Äquivalenzprinzip, Gravitationswellendetektion

CONTENTS

INTRODUCTION

"This is all very interesting," he said, "but
it seems a strange occupation for grown men.
What good is it?"

— *Foundation* by Isaac Asimov [1]

1.1 MODERN PHYSICS AND BEYOND

In the long history of science and natural philosophy with its twists and turns, the development of quantum theory and general relativity about a hundred years ago marks an outstanding era. The progressing mathematization in the early modern period allowed to gradually replace the mere description of natural phenomena by increasingly abstract concepts [2, 3]. Eventually, this development culminated in the grand theories of the early 20th century which reached a level of abstraction and surreality that defies our everyday perception of the world entirely. Indeed, the concepts at the heart of quantum theory and general relativity compel us to abandon once undeniable facts and to accept that space is curved, time is relative and that objects can be at multiple places simultaneously.

And yet, the trust put in those theories has been substantiated time and time again by a plethora of experiments. Despite the discomfort it initially caused in the physics community[1], quantum mechanics could not be disregarded as it proved to be too successful in explaining phenomena on the microscopic level. It allowed to understand the observed quantization of charge [5], energy [6] and spin [7], and was rapidly advanced through theoretical developments in algebra and field theory incorporating special relativity [8]. The early postulation of the existence of neutrinos by Pauli to make sense of decay processes, decades before its (indirect) experimental verification is exemplary for the fruitful progress. Similarly, the gauge bosons and quarks were predicted long before being demonstrated in experiment. Today, the standard model unifies three of the four fundamental forces – the electromagnetic, weak and strong interaction – in a quantum-field theoretical framework and accounts for physics at the microscopic level with paramount success [9]. In the last decade, it found another major confirmation through experimental evidence of the Higgs mechanism [10–13].

General relativity, on the other hand, is the established theory of gravity, describing the fourth fundamental force as a geometric phenomenon which successfully models the world at the macroscopic scale. Unlike quantum theory, however, it was born out of aesthetic considerations rather than the need to explain immediate physical observations. After its foundations were laid by the Michelson-Morley [14] and the Eötvös [15] experiments, the correctly predicted perihelion advance of Mercury and the deflection of light by the Sun in 1919 [16] were first support-

---

1 The most prominent example is Einstein, who, despite substantially advancing quantum theory himself, considered it "not yet the real thing" [4].

ers of general relativity [17]. However, the accuracy of these experiments was debatable and insufficient invalidate alternative emerging alternative theories that avoid curved space time or the big bang. It was not before the early 1960s that the advent of space flight and the availabilty of new technology such as atomic clocks and radar ranging re-fueled experimental activities. In parallel, substantial efforts to create structured theoretical frameworks allowed to categorize competing theories of gravity (such as the Dicke framework [18] and the parametrized post-Newtonian (PPN) formalism [19]). In the following years (the "Golden Era" [20]), metric theories of gravity enjoyed a surge of experimental verifications. Thanks to the advances in technology, experiments could re-enact earlier tests with increased accuracy (such as tests of the equivalence principle and light deflection) and explore newly discovered features such as the time delay of light deflected off planets [21] (Shapiro delay) or the Nordtvedt effect of lunar precession [22, 23]. Later on, additional post-Newtonian physics like frame-dragging (Lense-Thirring effect) and the geodetic effect were demonstrated [24]. Many alternative theories, which agreed with the predictions of general relativity on the comparably weak gravitational phenomena in the solar system, were eventually ruled out in the analysis of binary pulsars. Shortly after the first discovery of such a system [25], the observed rate of change of its orbital period was accurately modeled by the loss of energy due to gravitational-wave radiation predicted by general relativity [26] and consolidated it as the prevailing theory in the late 1970s [27, 28]. Meanwhile, first indirect evidence for one of its most extreme features, the black hole, was provided by observations of characteristic X-rays emitted from a binary system [29, 30]. These developments were finally crowned by the spectacular scientific infrastructures and international collaborations of the 21st century. The first direct detection of gravitational waves from a binary merger in 2015 introduced a new tool for cosmological observation [31]. A global network of antennae [32] based on long-baseline light interferometers is being set up to complement electromagnetic astronomy. Finally, most recently, a global array of large telescopes was able to take the first picture of a black hole's silhouette [33].

Evidently, the confrontation of quantum theory and general relativity with experiments has so far only cemented their claim to model reality. However, their applicability is restricted to very different scopes (microscopic vs macroscopic). It seems desirable that the success story of the standard model in unifying very distinct forces in a single theory should be transferable to the consolidation of these two pillars of modern physics. Indeed, there is hope that they can be derived as the low-energy limit of some fundamental theory, the search of which is however riddled with mathematical and conceptual difficulties. Regarding the interface of gravitational and quantum phyics, there is no conclusive answer to fundamental questions like "What is the gravitational field of a massive object in spatial superposition?" [34, 35]. Another illustrative example is that the supposed differentiability of smooth manifolds constituting general relativity is incompatible with the energetic discreteness and spontaneous creation of matter on the minuscule scales of quantum field theory, leading to divergences (re-normalization problem) [36]. Moreover, whereas time is on an equal footing to spatial dimensions in general relativity, it has a prominent non-dynamical role in quantum mechanics, which constitutes a fundamental disagreement. Different approaches to quantum or emergent gravity

exist, such as loop quantum gravity or string theory [37]. However, the derivation of quantitative predictions for experiments from first principles is currently virtually impossible, which is also due to missing empirical guidance. General relativistic phenomena involving quantum effects are expected at the Planck scale[2], which is far beyond any observational capacities currently and the foreseeable future. Apart from the outlined rather conceptual strive for a more fundamental theory, cosmological observations strongly suggest physics beyond our current understanding. The prevailing model of big bang cosmology, the Λ-CDM model, successfully accounts for the observed expansion of the universe, structures in the distribution of galaxies and the cosmic microwave background [38]. However, it needs to assume the existence of dark energy and cold dark matter. Although there is compelling indirect evidence for these hypothetical concepts, modern science is downright oblivious to their nature and relation to known physics [39]. Even more, estimations state that baryonic matter incorporated in the Standard Model merely accounts for about 5% of the mass-energy of the universe [38].

In summary, despite of the individual success of quantum theory and general relativity, the open puzzles of physics are manifold and exciting. There are several reasons to assume that general relativity could be altered in some way, grounded in the belief that a comprehensive theory of all interactions also needs to include gravity with quantum features [37, 40]. The detection of minuscule deviations from the established fundamental theories is hence auspicious yet increasingly challenging. As strikingly demonstrated by the history of experimental gravity, the demand for sensors with ever-increasing accuracy is constantly growing. One exciting step was made by Pound and Rebka in 1959 with the redshift experiment, which employed the Mößbauer effect in the spectroscopy of gamma rays [41]. It did not only herald the "Golden Era" of experimental gravity [20] by measuring an effect that was previously inaccessible due to technological limitations – it also introduced quantum sensing into tests of general relativity.

1.2 MATTER-WAVE INTERFEROMETRY

Einstein's revolutionary approach to apply Planck's hypothetical quantization of energy to light reinforced the old corpuscular theory, which had constantly been challenged by experiments supporting the wave nature of light. And indeed, it turned out that it is governed by particle-wave duality, as "neither of [the two pictures] fully explains the phenomena of light, but together they do" [42]. In his seminal thesis in 1924 [43, 44], de Broglie transferred this idea to massive particles,

$$h\nu_0 = m_0 c^2, \tag{1.1}$$

associating some periodic phenomenon of the frequency ν_0 to the energy equivalent of the proper mass m_0, where h is the Planck constant and c the speed of light. This notion of the wave nature of matter has since then been exploited in a multitude of diffraction and interferometric experiments with neutrons, electrons and even molecules [45], demonstrating striking parallels to classical optics. Of particular

---

2 By combining the fundamental constants c, G and $\hbar$ (speed of light, the gravitational and Planck's reduced constant, respectively), one obtains scales of length, time and mass: $l_P = \sqrt{\hbar G/c^3} \sim 10^{-35}$ m, $t_P = l_P/c \sim 10^{-43}$ s and $m_P = \sqrt{\hbar c/G} \sim 10^{19}$ GeV/c^2.

historical importance for the interface of gravity and quantum mechanics is the neutron interferometer experiment by Collela, Overhauser and Werner, which, for the first time, demonstrated a gravity-induced phase shift in a quantum experiment in 1975 [46] .

The research field of cold atom physics is rooted in the coherent manipulation of internal quantum states of atoms through Stern-Gerlach setups [47], rf-resonances [48] and finally Ramsey's oscillatory field method that allowed to determine the transition frequency from an interference pattern with unprecedented accuracy [49]. This established the prosperous field of atomic clocks, ranging from microwave to optical fountain and lattice systems, with many applications in technology as well as fundamental science [50]. The quantum optics concepts for the manipulation of internal states were eventually transferred to the motional degrees of freedom, allowing for spatial superpositions and hence, finally, atom interferometry. Since the pioneering experiments of Kasevich and Chu in 1991 [51], atom interferometry has evolved into a versatile tool for inertial sensing [52] and tests of fundamental physics [53].

Atom interferometry is "the art of coherently manipulating the translational motion of atoms" [54] with electromagnetic fields. The prevalent type covered in this thesis is based on light pulses, which serve as beam splitters and mirrors to freely falling atoms [55]. They create a superposition of motional states, which are then recombined and brought to interference. The interference pattern is indicative of the (e.g. gravitationally induced) motion, as each atom-light interaction imprints a phase on the atomic wave function which encodes the atomic position with respect to the light beam. In analogy to the spectroscopy of internal energies in atomic clocks with respect to a local oscillator, atomic gravimeters measure the gravitationally induced Doppler-shift with respect to the light fields [56]. In these quantum systems, gravity is typically accounted for as Newtonian potential in the Schrödinger equation. However, the starting point of de Broglie's work involving (1.1) were the properties of rest mass energy under Lorentz transformations [43, 44]. As a result, the phase

$$\varphi_p = -\frac{m_0 c^2}{\hbar} \int d\tau \tag{1.2}$$

of a matter wave associated with a freely falling particle with rest mass m_0 is linked to proper time $\tau = \int d\tau$ through the Compton frequency $\omega_C = m_0 c^2 / \hbar$. Based on this concept, a classical particle that follows the geodesics of space time picks up a phase proportional to proper time as a quantum effect. In consequence, it is conceivable that atom interferometers are sensitive to general relativistic effects. Although this has been subject to early theoretical investigations [57], the role of general-relativistic time dilation in atom interferometry continued to be an open issue [58–60] and found renewed interest recently [P4, 61, 62].

1.3   SCOPE OF THE THESIS

The value of atom interferometry for tests of general relativity is two-fold. From a technological point of view, the properties of these quantum systems render them excellent sensors for precision experiments with the prospect to outperform their

classical counterparts [52, 63].. In addition, they offer the possibility to explore effects without classical equivalent such as the interaction of gravity with spin and entangled quantum states. In the frame of this thesis, several articles[3] were published regarding atom interferometry for tests of various aspects of general relativity [P1–P7]. The work comprises studies of technological limitations, mitigation strategies and assessment of their experimental feasibility as well as the analysis of fundamental effects. This dissertation shall provide the background and scientific context in which the work was conducted and concludes each chapter with a section summarizing the main results.

To this end, particular emphasis is put on the connection of the equivalence principle to low-energetic quantum systems in weak gravitational fields in Chapter 2. This serves to discuss the potential of atom-interferometric tests of the universality of free fall in a dedicated satellite mission [P1], which we have submitted to the European Space Agency in the context of its long-term science program. One of the major systematic effects in these experiments is caused by the coupling of gravity gradients to the imperfect co-location of the employed source masses. In [P2], we demonstrate a mitigation strategy, which allows to relax experimental requirements on the source preparation by several orders of magnitude, simultaneously leading to a reduced mission duration. In addition, we present a preparation scheme for a binary source and evaluate it with respect to tests of the universality of free fall in micro-gravity in [P3].

Furthermore, time dilation effects in these systems are elucidated in Chapter 3. In [P4], we conclusively answer the open question whether atom interferometers without transitions between internal states are sensitive to the gravitational redshift and could be used to measure it. This discussion is linked to clock interferometry by proposing an experiment that implements a quantum version of the special-relativistic twin paradox.

Finally, Chapter 4 illustrates the prospect of gravitational wave detection with atom interferometry. We discuss the requirements on the atomic source and atom optics for proposals of configurations on ground [P5, P6] and in space [P7].

The outlook in Chapter 5 anticipates further developments, highlighting the promising progress of space-borne atom interferometry and the construction of large infrastructures, and concludes this thesis.

---

[3] These are listed separately in the Publications section of the thesis.

THE UNIVERSALITY OF FREE FALL

```
06 23 22 46   CDR-EVA   This proves that Mr. Galileo was correct in his findings.
06 23 22 59   CC        Superb.
```

— Communication during Apollo 15 [64]

2.1 THE EQUIVALENCE PRINCIPLE

In the last minutes of the Apollo 15 mission, astronaut David Scott conducted a quick demonstration experiment: A feather and a hammer, dropped simultaneously from the same height, reached the moon surface at the same time [65]. This is an illustrative manifestation of the weak equivalence principle (WEP), which states that the free-fall acceleration is independent of the mass. The WEP has a long, ongoing history of staggering experimental support, ranging from the first drop tests of masses in free fall [66, 67] and on inclined planes [68] in the 16th century over pendulum experiments [69] and torsion balances [15] to modern setups based on improved balances [70] and lunar laser ranging [71]. The space-borne MICROSCOPE experiment based on capacitive sensing has most recently confirmed the WEP to a few parts in 10^{14} [72]. The discussion of this phenomenon is deeply intertwined with the development of the scientific method [68, 73], calculus in general [69] and differential geometry in particular [74, 75]. Indeed, its significance for gravitational theory is well-reflected by the fact that it constitutes the first pages of the historically most important works on that subject [69, 74]. Today, it constitutes one component of the modern Einstein equivalence principle (EEP) [20, 76]:

- WEAK EQUIVALENCE PRINCIPLE (WEP): Two test particles, initially co-located in space-time in position and velocity, will follow the same trajectory irrespective of their composition. It is also referred to as universality of free fall (UFF).

- LOCAL LORENTZ INVARIANCE (LLI): Any local non-gravitational experiment will yield an outcome which is independent of the velocity and orientation of the freely-falling frame.

- LOCAL POSITION INVARIANCE (LPI): Any local non-gravitational experiment will yield an outcome which is independent of where and when it is performed. As it can be directly related to comparing clocks at different positions, it is also referred to as universality of gravitational redshift (UGR).

Parallel to the role that the constancy of the speed of light holds for special relativity, the equivalence principle "is the heart and soul of gravitational theory" [20] as its validity implies that gravity needs to be a (geo-)metric phenomenon. Metric theories of gravity assume that there exists a symmetric tensor $g_{\mu\nu}$, which defines geodesics along which test bodies propagate and that in local Lorentz frames, all physical

laws follow special relativity [76, 77]. The theories differ only in how the metric comes about, i.e. how it is generated by the distribution of energy and mass and potentially other additional fields. The effect of gravity on the non-gravitational laws of physics is then captured by replacing the flat background (Minkowski) metric $\eta_{\mu\nu}$, in which they are formulated, by $g_{\mu\nu}$ and the partial derivatives by their covariant counterpart [76]. This is referred to as universal coupling, entailing that gravity is an effect of space-time curvature affecting all non-gravitational fields alike.

The historically first and arguably most natural metric theory is general relativity, with the gravitational coupling strength determined entirely through one tensor field $g_{\mu\nu}$ and a universal constant G. The fundamental total action is given by [74, 75]

$$S_{GR} = \frac{c^4}{16\pi G} \int R(g_{\mu\nu}) \sqrt{-g_{\mu\nu}} \, d^4x + S_m(g_{\mu\nu}) \ , \tag{2.1}$$

yielding the Einstein field equations when varied with respect to $g_{\mu\nu}$. The first term is the gravitational action, where the Ricci scalar $R(g_{\mu\nu})$ captures the space-time curvature, and c is the speed of light. $S_m(g_{\mu\nu})$ accounts for all non-gravitational contributions to the action caused by fields and interactions whose quantum description[1] is given through the standard model [78]. Early attempts towards a theory unifying a tensor theory of gravity and electromagnetism [79] were accompanied by the introduction of an additional scalar field ϕ. The resulting field equations indicated a varying gravitational coupling constant G [80]. This was further pursued in an effort to connect the discussion to Mach's principle (the energy-mass content of the universe defines the local value of G), resulting in the Jordan-Brans-Dicke theory [81–84]

$$S_{JBD} = \frac{c^4}{16\pi} \int \left(\phi R - \frac{\omega}{\phi} g^{\mu\nu} \partial_\mu \phi \partial_\nu \phi \right) \sqrt{-g_{\mu\nu}} \, d^4x + S_m(g_{\mu\nu}) \ . \tag{2.2}$$

with coupling function ω. This scalar-tensor theory is an example for a modification of general relativity that is still metric [20]: The derived field equations do not only involve the energy-mass content defined by S_m but also the additional field ϕ. The resulting metric $g_{\mu\nu}$ hence differs from the one of general relativity – however, the non-gravitational laws of physics still couple universally and exclusively to $g_{\mu\nu}$. More general scalar-tensor theories include a cosmological function $\lambda(\phi)$ [85–87], varying coupling $\omega(\phi)$ [88] and a self-interaction term $V(\phi)$, rendering the scalar field massive in the presence of matter (chameleon mechanism) [89]. In a similar spirit, there exists a plethora of alternative metric theories of gravity with various modifications of the gravitational action, with more or less physical and mathematical motivation (vector-tensor, tensor-vector-scalar (TeVeS), massive and quadratic gravity, $f(R)$ etc. [17, 20]). A successful framework to compare them in the weak-field limit of the solar system is the Parametrized Post-Newtonian (PPN) formalism [17, 19], which both fertilized the creation of alternative theories while also ruling many of them out. This detailed analysis confined to metric theories is based on the fortitude of the EEP, which to date has passed all experimental tests with flying colors [20].

---

1 The interface of quantum mechanics and general relativity is disussed in Section 2.2.

However there are opinions that the "bias towards [metric theories of gravity] is quite unjustified" [40]. It is argued that the development of physics suggests to replace absolute structures by dynamical entities, i.e. to obtain the values of fundamental constants through symmetry breaking at some scale [90]. This is reminiscent of the confirmed Higgs mechanism [10–13], which determines the mass of elementary particles by breaking electroweak symmetry. Similar to the above-mentioned dependency of the gravitational constant $G(\phi)$ on a scalar field, the electromagnetic coupling constant $\alpha_{EM}(\phi)$, the proton to electron mass ratio $m_p/m_e(\phi)$ and other parameters $k(\phi)$ of the standard model could be functions of some background scalar (dilaton) field in models motivated by string theory[2] [90, 92]. This has the important implication that the mass-energy of a body is then composition dependent, $m' = m(\alpha_{EM}(\phi), \frac{m_p}{m_e}(\phi)\ldots)$. Supposed that the coupling constants do not all depend on ϕ in a universal manner, the UFF is consequently violated since the derived free-fall acceleration is composition dependent [77, 90, 93]. Similarly, cosmological considerations suggest possible non-universal coupling of dark matter to the standard model [89, 94], for example through a light scalar field [95–97].

A variety of phenomenological models allow to parametrize additional couplings and resulting violation scenarios, such as the $TH\epsilon\mu$ [98] and the derived simplified c^2 [99] formalism studying anomalous electromagnetic coupling, and the general standard model extension (SME) framework surveying Lorentz violation [100, 101]. These models have in common that they parametrize the anomalous behaviour of some kind of energy E_X in a gravitational field, whereas the other energies E_Y are assumed to couple universally[3] [60]. Consequently, the energy $m'c^2$ of a system can be decomposed into the rest mass m of the constituting particles and the combination of EEP violating and respecting energies,

$$m'c^2 = mc^2 + E_X + \sum_{Y \neq X} E_Y \quad . \tag{2.3}$$

For example, a position dependence $E_X(\mathbf{r})$ would reflect an LPI violation, whereas a velocity dependence $E_X(\mathbf{v})$ would account for a violation of LLI. Remarkably, both would imply a violation of the UFF as the free fall is directly affected by the modified mass [76, 77, 90]. This is a manifestation of Schiff's principle [102] which states that, despite their difference in nature, the violation of one of the constituents of the EEP implies a violation of the others. Although this conjecture can not be proven in general[4] [20], it can be made plausible from energy conservation arguments in cyclic thought experiments for theories that are based on an invariant action principle [106, 107]. As most viable theories belong to this class, the ideas discussed here have a broad range of applications. Schiff's conjecture was vividly debated, in particular in view of expensive space programs testing UGR as it seemed sufficient to tests only parts of the EEP to infer bounds on violation on all three constituents[5]. However, their quantitative relationship is strongly dependent on the model and the

---

2 In fact, a variable α_{EM} was considered together with a dynamical G early on [81–83, 91]. Reverting to a theory that did not violate the EEP by assuming a constant α_{EM} actually resulted in (2.2), c.f. [90].
3 The label X, Y shall denote the energy type, for example electromagnetic or nuclear binding energy.
4 There are indeed counter-examples for specific cases [103–105].
5 "If Schiff's basic assumptions are as firmly established as he believes, then indeed this project is a waste of government funds" [108].

kind of energy that is assumed to behave abnormally. As sketched in [60], UGR tests could be more sensitive to an anomalous coupling of atomic hyperfine energies to gravity than UFF experiments, whereas they are outperformed in sensitivity when testing electromagnetic coupling.

Therefore, it is desirable to test all aspects of the EEP independently and with various combinations of test systems to explore a parameter set as versatile and as large as possible [40]. Today, EEP tests put strict constraints on competing models that attempt to reconcile quantum and gravitational theory, such as string theory [92, 109], M-theory and Brane-world scenarios [110–113] as these have to be significantly modified to comply with experimental bounds. Moreover, the results of EEP experiments can be linked to PPN parameters and therefore even aid in constraining alternative metric theories of gravity [20, 114]. Consequently, tests of the equivalence principle in all its facets are considered to be among the most sensitive probes of contemporary physics [40, 115].

2.2 QUANTUM SYSTEMS IN WEAK FIELDS

The mathematical concept encapsulating the equivalence principle and metric theories of gravity is that gravitation is a property of space-time which couples universally to all fields [116]. However, the non-gravitational laws of physics are known to be well-described by quantum theories, for which the minimal coupling scheme $\eta_{\mu\nu} \to g_{\mu\nu}$ is not straightforward [117]. It is not even clear how to combine quantum and classical fields in one expression like (2.1) [37]. Attempts to take the expectation value of the quantum fields (semi-classical gravity [118–120]) face fundamental problems [121]. The back-action of quantum fields on the metric leads to non-linear modifications of the Schrödinger equation [118] and suggests quantization of the gravitational field sourced by massive superpositions, which appears to be in conflict with experimental observations [122]. This discussion enters the realm of fundamental modifications of one or both theories by either "quantizing" gravity [37], "gravitizing" quantum mechanics [123] or requiring the development of an underlying unified theory of all interactions such as string theory. As such a conclusive theory is still elusive, one can resort to semi-classical theories which are suspected to give appropriate results in the given limit[6] [36]. Quantum field theory on static, curved spacetime allows for few quantitative predictions. The most prominent example is Hawking radiation [124], which is, however, too low in energy to be detected against the cosmic microwave background (or would require the existence and detectability of primordial black holes).

For applications where particle creation does not need to be considered, the theory can be simplified even further, resulting in a Schrödinger equation for the quantum system in which the gravitational field enters as a potential with relativistic corrections. In practice, this means starting from a Klein-Gordon or Dirac equation with a static gravitational background field and deriving a Hamiltonian for the non-relativistic limit [125–129]. In a different approach, first the non-relativistic limit of the gravitational theory is determined, which is then canonically quantized [130, 131]. For general-relativistic corrections at expansion order c^{-2}, the two

---

6 For example, the interaction of classical electromagnetic fields with quantized matter (i.e. first quantization) is a limit of quantum electrodynamics, which yields satisfying results in many applications.

strategies agree for a freely falling point particle. It can be argued that the quantum-field theoretical approach is substantiated by deeper reasoning [128], resolving possible ambiguities in the operator ordering at higher orders through systematic derivation. However, the other approach is closely related to the path integral formalism by Feynman [132], which allows for a more intuitive connection to atom interferometry [133]. To this end, the components of the metric tensor $g_{\mu\nu}$ are taken in the weak-field limit of the gravitational theory under consideration. In general relativity for example the weak field limit of the Schwarzschild metric[7] is given by $g_{00} = -(1 + 2U/c^2)$, $g_{0i} = 0$ and $g_{ij} = \delta_{ij}(1 - 2U/c^2)$, such that the free-fall action in this background field becomes

$$S_p = -\int mc\sqrt{-g_{\mu\nu}dx^\mu dx^\nu} \simeq -\int dt \left(mc^2 - \tfrac{1}{2}m\dot{\mathbf{r}}^2 + mU\right) = \int dt\, L \;, \quad (2.4)$$

with $U = GM/|\mathbf{r}|$ being the Newtonian gravitational potential (M is the mass of the Earth). For typical applications [55], the potential is expanded in a series around $|\mathbf{r}| \ll |\mathbf{R}|$, with $\mathbf{R}$ being the location of the experiment on the surface of the Earth or on board of a satellite. $\mathbf{r}$ and $\dot{\mathbf{r}}$ denote the position and velocity in the lab frame, respectively. With $U = GM/|\mathbf{R}| + \mathbf{g} \cdot \mathbf{r} + \tfrac{1}{2}\mathbf{r}^\mathsf{T}\Gamma\mathbf{r} + \dots$ and $g_i = \partial_i U$, $\Gamma_{ij} = \partial_i\partial_j U$, the resulting Lagrangian L is (to this order) quadratic in $\mathbf{r}, \dot{\mathbf{r}}$, which allows for an exact application of the path integral formalism. This relates the phase of a propagating quantum wave packet to the action evaluated along the classical trajectories [132, 133], $\varphi_p = S_p/\hbar$, and connects back to the earlier findings of de Broglie (1.2) by identifying $L/(mc^2) = -\int(d\tau/dt)dt$ as the non-relativistic limit of proper time. In addition to the free fall of atoms, a comprehensive treatment of atom interferometry also needs to take into account the light pulses constituting mirrors and beam splitters, which can be seamlessly included [125, 128, 131, 134, 135]. The total phase of a freely falling matter wave interacting with light is then given by

$$\varphi = S_p/\hbar + S_{em}/\hbar = -\omega_C\tau + S_{em}/\hbar \;, \qquad (2.5)$$

obtaining contributions from free propagation and from the classical action $S_{em} = -\int dt\,(V_k + V_p)$ describing atom-light interaction [P4, 59]. In light-pulse atom interferometry, the optical potential of a sequence of short light pulses comprises two contributions: $V_k(\mathbf{r}, t) = -\sum_l \hbar\mathbf{k}_l \cdot \mathbf{r}\,\delta(t - t_l)$ modifies the atomic motion and imprints a position-dependent phase, whereas $V_p(t) = -\sum_l \hbar\phi_l\,\delta(t - t_l)$ imprints the phase ϕ_l of the light pulse without affecting the motional state. t_l is the time at which the pulse with wave vector $\mathbf{k}_l$ is applied. In fact, the propagation phase $\varphi_p = -\omega_C\tau$ associated with time-dilation typically vanishes in gravimetry setups due to the interferometer geometry, as will be discussed in Chapter 3. The interferometer phase is then fully determined by the position of the atoms with respect to the light fields upon interaction for a linear potential. The free fall motion of the atoms is nevertheless described by the Lagrangian of (2.4), such that a possible violation of the UFF is parametrized by substituting the mass $m \to m'$ as in (2.3) in that expression [60]. For the error analysis of the experiments, pertubative methods allow to assess the effect of beyond-quadratic contributions to U and other

---

7 Greek indices conventionally run from 0 to 3, wheras latin indices count the spatial dimensions from 1-3. Following [76], the (-,+,+,+)-notation for the metric is assumed here. Here and in the following, "weak-field" or "non-relativistic limit" refers to this solution.

potentials as well as pulses of finite duration [136, 137]. In fact, approximating the complicated multi-photon scattering processes by infinitely short laser pulses is highly non-trivial and requires careful analysis for individual experiments.

In typical atom interferometry setups, the wave packets are sufficiently localized to allow for an association with world lines. However, even in the semi-classical limit of the path integral picture, the descriptive propagation of quantum states along classical trajectories shall not divert from the peculiarities of their quantum nature. Low-energetic quantum systems, including atomic interferometers and clocks as well as experiments involving neutrons, molecules or opto-mechanical systems, could shed light on the most fundamental questions on the interface of gravitation and quantum mechanics. This does not only include the conundrum around the semiclassical Schrödinger-Newton-equation [118] but also the interplay of gravity with spin and other features without classical equivalent, such as the mass-dependent dispersion of wave packets in a gravitational field [138–141]. Whereas experiments testing (2.4) may be understood as quantum tests of the (classical) equivalence principle, the formulation and sense of a "quantum equivalence principle" is subject to current research and discussion [128, 129, 142].

2.3   QUANTUM TESTS

The first atom interferometric tests of the UFF compared the free fall acceleration measured with atomic gravimeters to that of classical gravimeters, which track the acceleration of a corner-cube by means of laser interferometry [143, 144], and found agreement at the 10^{-8} level. Fully quantum experiments involve two types of matter waves, which differ in isotope [145–148] or element [148, 149]. Aspects of the EEP without classical counterpart are explored by monitoring the free fall of different spin states [150–152] and energy eigenstates [153], and have been proposed to be studied under the influence of entanglement [154]. The choice of test species is on the one hand subject to a trade-off between technical feasibility and expected sensitivity to possible violations, encoded in the anomalous energy coupling parametrized in (2.3). The latter is most likely increased for large mass ratios, however also differences in the neutron excess and baryon number charge weigh into the decision [101, 149, 155], as well as the comparison of bosons and fermions. On the other hand, test pairs with large similarities such as two isotopes of Rb often simplify the experimental requirements considerably. One significant limitation of these quantum tests of the UFF is the sensitivity of the sensors, which scales with the available free fall time. Indeed, large fountain setups, which allow drift times of some hundred milliseconds, foresee tests at the $10^{-13} - 10^{-15}$ range [148, 156, 157]. Recently, in such an experiment, the UFF was confirmed to parts in 10^{-12} with two isotopes of Rb, constituting the best atom-interferometric test of the UFF so far [158].

Several proposals aim for atom interferometry and clocks in space in order to enhance the sensitivity even further through unlimited free fall times and to make use of the unique properties of micro-gravity such as simplified atom optics and quiet environments [159–167]. In 2010, the satellite mission STE-QUEST was proposed to the M3 call in the Cosmic Vision program of the European Space Agency [168]. It targeted to test all aspects of the EEP independently by employing two

isotopes of rubidium for free fall tests and a microwave link for clock comparisons. In the competitive evaluation, the science case was rated high and the mission was selected for a phase A study. However, the technological readiness of the components related to the generation and manipulation of the ultracold atomic ensembles was rated critical and eventually another mission was selected.

Fortunately, the field has developed significantly within the last decade. The development of quantum mechanical UFF tests is closely connected to the progress in atomic gravimetry and gradiometry in general, which is a flourishing research area [52]. The technological maturity of atom-interferometric inertial sensors has considerably grown in the last years [169–172], such that they are competitive to classical gravimeters [173, 174], also on a commercial basis [175–177]. In parallel, the minituarization of these systems for mobile applications is accompanied by the development of compact atom interferometry setups targeted for micro-gravity operation, funded by several national space agencies. In particular, the ICE experiment [178] working on UFF tests on board of a zero-g plane with potassium (K) and rubidium (Rb), and the QUANTUS collaboration are the main agitators on this axis. The latter is pioneering atom interferometry in micro-gravity with quantum degenerate gases in drop-tower experiments [179–182] and a sounding rocket mission [183]. Key technologies that are indispensable for space-borne atom interferometry could be demonstrated, in particular the creation of ultra-cold ensembles through Bose-Einstein-Condensation (BEC) [179, 183], Delta-Kick Collimation [180, 181], atomic transport techniques [183, 184] and interferometry [180]. The repitition rate of a few experimental shots per day in the drop tower is expected to be significantly increased by two orders of magnitude thanks to the newly set up Einstein Elevator in Hanover [185] and similar facilities [186]. Longer micro-gravity duration is possible at the Cold Atom Lab (CAL) on the ISS, constructed and operated by JPL (NASA) [187]. A bilateral collaboration including German research teams currently allows for a variety of cold-atom experiments, including the recent creation of a BEC [188]. Continuing on this exciting path, subsequent sounding rocket missions built on the heritage of [183] will follow with a dual source of K and Rb. Moreover, the Bose-Einstein Condensate and Cold Atom Laboratory (BECCAL) [189] will succeed CAL on the ISS with improved capabilities with regards to atom interferometry. In particular, it will allow to study the concurrent operation of K and Rb.

2.4 PERSONAL CONTRIBUTION: ASPECTS OF SPACE-BORNE SCENARIOS

Fueled by this success story, one can dare to envision space-borne quantum tests of the EEP in a dedicated satellite mission. We have proposed such a scenario in [P1] and investigated specific aspects regarding the source preparation in [P2] and [P3].

[P1] UFF TEST AT 10^{-17} Built on the original STE-QUEST proposal [168] and its further developed mission scenario [115, 191], we present an atom-interferometry based concept for testing the UFF to parts in 10^{-17} in [P1]. Alongside with a potential successor of MICROSCOPE [72], this constitutes the proposal of a European collaboration to focus on EEP tests in the long-term planning of ESA's science program (Voyage 2050) to follow Cosmic Vision. The proposal comprises an overview over the mission concept and an order-of-magnitude estimation of the
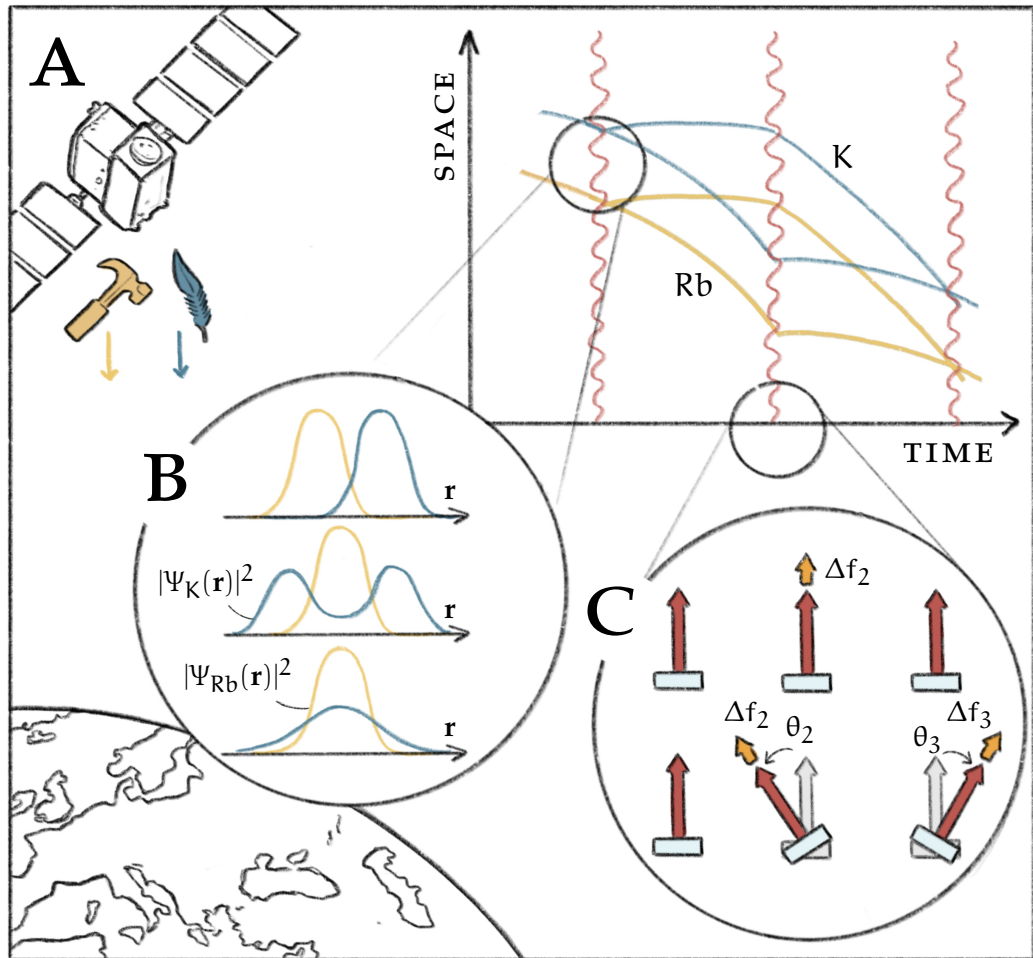
Figure 2.1: QUANTUM TEST OF THE UNIVERSALITY OF FREE FALL IN A SPACE MISSION.
(A) The concept that we present in [P1] foresees a satellite-based experiment operating two atom interferometers (Rb and K) simultaneously, targeting a test of the UFF to parts in 10^{-17}. **(B)** Systematic effects couple to the phase-space properties of the atomic ensembles and require careful source preparation schemes. In [P3], we develop a sequence to realize a miscible binary source with low expansion rate. An essential aspect is the miscibility of the species, which defines the center-of-mass overlap (co-location). The figure shows an immiscible (first row) and two miscible density distributions (second and third row). **(C)** As gravity gradients and rotations couple to a residual displacement of the input states, the imposed conditions are quite strict and represent a major limitation in these experiments. In [P2], we develop and apply a compensation scheme to the space mission, finding a relaxation of the source preparation requirements by several orders of magnitude. The method is a generalization of [190] to the case of time-varying gravity gradients and is schematically depicted by the effective wave vectors in the figure: Whereas static gradients may be compensated by a frequency shift at the second pulse of the interferometry sequence (first row), an inertial space mission as [P1] requires frequency shifts and tilts of the laser at the second and third pulse (second row).

main systematic and statistical limitations. The anticipated unprecedented accuracy is a consequence of the outlined technological advances and heritage from [72] as well as to the improved understanding of various detrimental effects.

[P2] GRAVITY-GRADIENT COMPENSATION   One particular challenge for tests of the UFF is the initial co-location of the two freely falling test masses upon release, as a displacement in position and momentum couples to residual rotations and potential gradients [190, 192]. Consequently, the initial kinematics have to be well-characterized [72], which constitutes a significant part of the mission duration in scenarios like STE-QUEST [191]. A recent proposal [190] alleviates the dependency on the source preparation based on a compensation mechanism that modifies the interferometry sequence, and has been successfully implemented in several experiments [157, 158, 193]. In [P2], we extend and apply this recipe to a space-borne UFF test scenario along the lines of [P1]. In such a configuration, in which the sensitive axis of the sensor is kept inertial with respect to a celestial reference frame, the gravitational potential in the satellite frame is time-dependent. We analyze the experimental modifications that allow to implement the compensation scheme in the presence of time-varying gravity gradients and assess its feasibility in the satellite environment. Moreover, by exploiting the spectral distribution of systematic effects, the metrological gain of signal demodulation is investigated. A potential UFF violation signal would be modulated at the orbital frequency in this system, whereas most systematic effects (including gravity gradients) are either constant or modulated at different frequencies. This combined strategy of gradient compensation and signal demodulation allows to relax the requirements on the source preparation by several orders of magnitude, while reducing the mission duration at the same time. Whereas in STE-QUEST [191], a spatial co-location in the order of nm limited the mission goal to few parts in 10^{-15}, the scenario of [P2] allows to reach 10^{-18} with μm displacement. Our findings remove one major obstacle towards space-borne quantum tests like [P1] with a target performance beyond state-of-the-art.

[P3] QUANTUM DEGENERATE BINARY SOURCE   Even these relaxed source conditions require a careful design of the interferometer input states. The phase-space properties of the atomic ensemble are decisive for the mitigation of many contributions to the systematic uncertainty such as wave front aberrations, mean-field effects and the aforementioned inertial couplings. In particular, the phase-space preparation schemes, which were designed for single species and successfully applied in micro-gravity environments [183, 194, 195], need to be transferred to mixtures. In [P3], we present a scaling approach for quantum-degenerate mixtures for a strategy to prepare binary sources based on the theoretical framework developed in [194]. The proposed scheme consists of several Delta-Kick collimation stages, assisted by Feshbach resonances to control the interspecies interaction. This allows to realize a miscible source with ultra-low kinetic expansion rate, which is suitable for experiments with seconds of drift time. The results and their applicability are discussed with regard to a quantum tests of the UFF with Rb and K along the lines of [P1, 191].

TIME DILATION

> ... is the same, in a relative way, but you're older ...
>
> — *Time* by Pink Floyd [196]

3.1 THE GRAVITATIONAL REDSHIFT

Time dilation is one of the most wondrous features of nature. Despite being an integral aspect of relativity, it was not until 1938 that special-relativistic time dilation was measured in an experiment [197]. Before, it had only been inferred from the constancy of the speed of light, which was experimentally supported by Michelson-Morley-type experiments [14]. In general relativity, the flow of time is affected by gravitational fields due to the equivalence of gravitational acceleration and inertial motion. With respect to some coordinate system (ct, x^i), the proper time interval $d\tau = \frac{1}{c}\sqrt{-g_{\mu\nu}dx^\mu dx^\nu}$ is related to the coordinate time interval dt via

$$d\tau = \left(-g_{00} - 2g_{i0}\frac{dx^i}{cdt} - g_{ij}\frac{dx^i}{cdt}\frac{dx^j}{cdt}\right)^{1/2} dt \simeq \left(1 + \frac{U}{c^2} - \frac{1}{2}\frac{v^2}{c^2}\right) dt \;, \quad (3.1)$$

defined by the local metric $g_{\mu\nu}$. Here, $v^2 = \delta_{ij}dx^i dx^j/dt^2$ and U are the velocity and Newtonian gravitational potential, respectively. The second equality assumes the weak-field and low-velocity limit of general relativity. Identically constructed clocks demonstrate a relative proper time difference of $\tau_A/\tau_B = \sqrt{g_{00}(A)/g_{00}(B)} \simeq 1 + \frac{1}{c^2}(U(A) - U(B))$ if kept fixed ($dx^i/dt = 0$) at different positions A and B. An observer that measures time by counting oscillations of some frequency standard given, for example, by an atomic transition, could come to the conclusion that the internal energy levels are shifted by the gravitational potential. This, in turn, would imply that a photon resonant to the transition of one atomic clock would not be able to drive excitations in the other, which could also be regarded as a gravitationally induced shift in the frequency of the photon (redshift if viewed from a higher position in the gravitational potential). The first experiment to successfully demonstrate this "apparent weight of photons" was the seminal work by Pound and Rebka in 1959 [41], which was soon to be followed by an upgraded version verifying the redshift to the percent level [198] and measurements of solar spectral lines [199]. An assumption that enters the outlined thought experiment is that the laws of physics governing the dynamics of the clocks do not depend on the location or time of the execution, which has been introduced in Chapter 2 as Local Position Invariance (LPI). This aspect of the EEP can hence be excellently tested by the measurements of clocks at different locations [200–202] and comparison of differently composed clocks at the same location, which serves as a null measurement and monitors possible time evolution of natural constants [203, 204]. The ACES experiment [163] to be flown on the ISS targets a test of the gravitational redshift to parts in 10^{-6}. A

popular occurrence of time dilation is in space-borne clocks as employed in GNSS[1], where it needs to be accounted for [205]. Even more, the analysis of two Galileo satellites, which were accidentally delivered to elliptical orbits, constitutes the best test of the gravitational redshift to date, confirming it to parts in 10^{-5} [206].

As alluded to in the introduction, de Broglie investigated energy under Lorentz transformation and arrived at the conclusion that the phase of a matter wave is connected to proper time (1.2). As these matter waves are put into a superposition of different heights in the gravitational potential, it appears that atom interferometry contains all ingredients to a device that is sensitive to gravitational time dilation. Naturally, the claim raised in [58] triggered some excitement: Re-interpretation of old gravimetry measurements with a standard Mach-Zehnder atom interferometer (MZI) yielded a 10^4-fold improvement over the at that time best LPI experiment [202]. The boost in performance was attributed to the pre-factor in (1.2), the Compton frequency $\omega_C \sim 10^{26}$ Hz, which exceeds typical microwave clock frequencies (as used in [202]) by many orders of magnitude. This sparked interest about relativistic effects and proper time in atom interferometry [59, 60, 155, 207–210]. Eventually, two major counter-arguments were presented in the debate following [58]:

- MISSING NOTION OF A CLOCK: The defining property of a clock is the periodic evolution between two states. In the widely used atomic clocks this is achieved by a superposition of internal states, the energy *difference* of which defines the oscillation frequency ('ticking rate'). An atom in a stationary state does not provide a physical signal at the Compton frequency, and hence does not represent a clock [60, 208, 209]. Another way to see this is that the Compton frequency enters the dynamics of the system only as an additive constant in L (first term in the integrand of (2.4)). This results in a global phase that is not observable [208], i.e. the corresponding time sequence of quantum states (ray in Hilbert space) is independent of ω_C [209].

- TIME-DILATION INSENSITIVE GEOMETRY: Evaluating (3.1) along the trajectories of an MZI results in a vanishing proper time difference between the two branches to this order, if the internal states are not changed. Hence, the phase of the MZI is independent of time dilation and is entirely caused by the atom-light interaction S_{em} in (2.5) [59, 60].

While there appears to be a general agreement that the standard MZI configuration is not susceptible to gravitational time dilation, the possibility to test the gravitational redshift with atom interferometers remained an open question. Recently, we have shown that the insensitivity to gravitational time dilation is general for closed atom interferometers without internal state transitions [P4]. In accordance with this rationale, schemes that involve these transitions during the interferometry sequence to measure the gravitational redshift in atom-interferometric setups have been put forward [61, 62]. The discussion touches on several captivating aspects: The duality of atoms constituting ideal test masses and clocks, and the unification of the outmost counter-intuitive concepts of (general) relativity and quantum mechanics, namely time dilation and spatial superposition.

---

1 Global Navigation Satellite Systems. Examples are the Global Positioning System (GPS) and the European counterpart Galileo.

3.2 COMPOSITE QUANTUM SYSTEMS IN WEAK FIELDS

In order to resolve the issue of the lacking concept of a clock, it was suggested to employ a superposition of internal degrees of freedom as input to the atom interferometer [208, 209, 211]. The phenomenology is intriguingly captured by the the thought experiment of [211]: The internal-state superposition constitutes a clock in the conventional sense, which is propagated along the arms of an interferometer in an additional motional superposition. These motional states are then brought to interference. In such a clock interferometer setup, where the branches move on different heights in the gravitational potential, gravitational time dilation could serve as a which-way marker, making the two paths distinguishable. Due to the complementarity between interferometric contrast and which-way information, the interference pattern would consequently vanish. Another theoretical study [208] comes to the same conclusion, however attributes the effect to the concurrent operation of two interferometers, one for each internal state. Detection at the end of the interferometer, which does not distinguish between internal states, leads to a beating of the interference patterns, which corresponds to the observed loss of contrast in the approach of [211]. These ideas on the phenomenology of a clock interferometer are presented on the general level of a thought-experiment, where the paths of a hypothetical setup differ in accumulated proper time. However, a cohesive treatment of such a composite quantum system[2] in gravity, including both its free fall as well as the interaction with light, and the proposal of a concrete implementation have been lacking.

With the increasing accuracy of atomic systems, relativistic post-Newtonian corrections become increasingly relevant. In the context of atom-light interaction, it was found that effects that appear anomalous in a Galilean (i.e. non-relativistic) framework could be resolved by including special-relativistic corrections [135]. The underlying idea is that the internal degrees of freedom of a composite system are effectively modeled by replacing the mass by $m \to m + E_{int}/c^2$ in the classical single particle Hamiltonian, which gives rise to correction terms $\hat{H}_{int} p^2 / 2(mc)^2$ in the corresponding quantum description to first-order in c^{-2}. A similar coupling of internal and external degrees of freedom is found for the non-relativistic limit of the system in a weak gravitational field, which has even been adduced as a possible decoherence mechanism [212]. In the limit of a quantum-field theoretical treatment [P4, 129], the composite particle Hamiltonian is given by

$$\hat{H} = \hat{H}_{int} + \frac{\hat{\mathbf{p}}^2}{2m} + mU(\hat{\mathbf{r}}) + \left(-\frac{\hat{\mathbf{p}}^2}{2m} + mU(\hat{\mathbf{r}}) \right) \frac{\hat{H}_{int}}{mc^2} + \hat{V}_{em} \ , \tag{3.2}$$

keeping terms up to c^{-2}. It is diagonal with respect to the internal states, i.e. it can be obtained from $\hat{H} = \sum_j \left[m_j c^2 + \hat{\mathbf{p}}^2 / 2m_j + m_j U(\hat{\mathbf{r}}) \right] |j\rangle\langle j|$ through first-order expansion in $(m_j - m)/m$. Here, $m_j = E_j/c^2$ is the mass corresponding to the energy eigenstate $|j\rangle$ of the atomic Hamiltonian $\hat{H}_{int} = \sum_j E_j |j\rangle\langle j|$ and m the rest mass. [128] discusses details and caveats in the derivation as well as potential conceptual issues. Remarkably, even in the presence of a gravitational field, the atom-light interaction $\hat{V}_{em}$ is determined by electric dipole coupling, plus a special

---

2 A composite system is to be understood here as a multi-level atom in the case where the internal degrees of freedom have to be taken into account.

relativistic Röntgen term [134, 135]. In principle, (3.2) involves additional terms proportional to $\hat{\mathbf{p}}^\top U(\hat{\mathbf{r}})\hat{\mathbf{p}}$ and $\hat{\mathbf{p}}^4$. However, as these do not couple to $\hat{H}_{int}$ at this order, they are not relevant to the following discussion.

3.3   PERSONAL CONTRIBUTION: QUANTUM TWIN PARADOX

In the geometry of an MZI, the proper time difference between the interferometer branches is vanishing for a linear potential, and the total phase is determined by the atom-light interaction only [59, 60]. We have generalized these findings to arbitrary geometries of closed atom interferometers without transitions between internal states and hence show that these systems are not susceptible to the gravitational redshift. Moreover, we connect the discussion to clock interferometry and propose an experiment that exhibits special-relativistic time dilation. The results of this work [P4] are summarized in the following.

[P4] SPECIAL-RELATIVISTIC TIME DILATION   We show that for a linear grav-itational potential[3], the proper time difference between the two branches of a closed light-pulse atom interferometer with arbitrary geometry is independent of gravity. This can be derived by means of a virial theorem and also be intuitively made plausible by transforming to a freely falling frame. These interferometers are hence not sensitive to gravitational time dilation, which is associated with the contribution to (3.1) involving the potential U. However, certain geometries exhibit special-relativistic time dilation (v^2 contribution to (3.1)). An example is the asymmetric Ramsey-Bordé configuration, in which one branch is left unaffected, while the other receives momentum in alternating directions such that it moves away and eventually returns to the first. One of our central results in [P4] is that the phase of light pulse atom interferometers associated with proper time (1.2) is either zero (such as in the case of the MZI), or of the form $\omega_C \Delta\tau = \frac{\hbar}{2m}K^2 T$, where m is the mass of the atom, and K, T geometry-dependent combinations of the momentum transfers and pulse timings, respectively. Asymmetric geometries that feature such a phase are used for recoil measurements of the ratio $\hbar/m$ for the determination of the fine-structure constant α [213, 214]. Indeed, this kinematic asymmetry is the origin of the difference in special-relativistic proper time between the interferometer arms. This is commonly illustrated by the twin paradox: Initially at the same position, one of them travels away and returns to find that the other has aged faster[4].

To perform a quantum version of the twin paradox, in which a single clocks is in a superposition of paths that differ in proper time, one could pick up the ideas developed in the previous section. By means of a cohesive framework that models all aspects of the atom interferometer including relativistic effects, we show in [P4] that certain configurations can realize the conceptual ideas of clock interferometry [208, 211]. Indeed, the propagation of an internal-state superposition through an asymmetric interferometer results in a loss of visibility that scales with the proper-

---

3 I.e. $U(\mathbf{r}) = \mathbf{g} \cdot \mathbf{r}$, which is the level of discussion of [58] and the subsequent publications.

4 The paradox in this situation lies in the fact that both twins could argue that from their perspective, it was the other one that moved away and returned. However, one of the twins changes inertial frames during this process, which resolves this alleged symmetry.
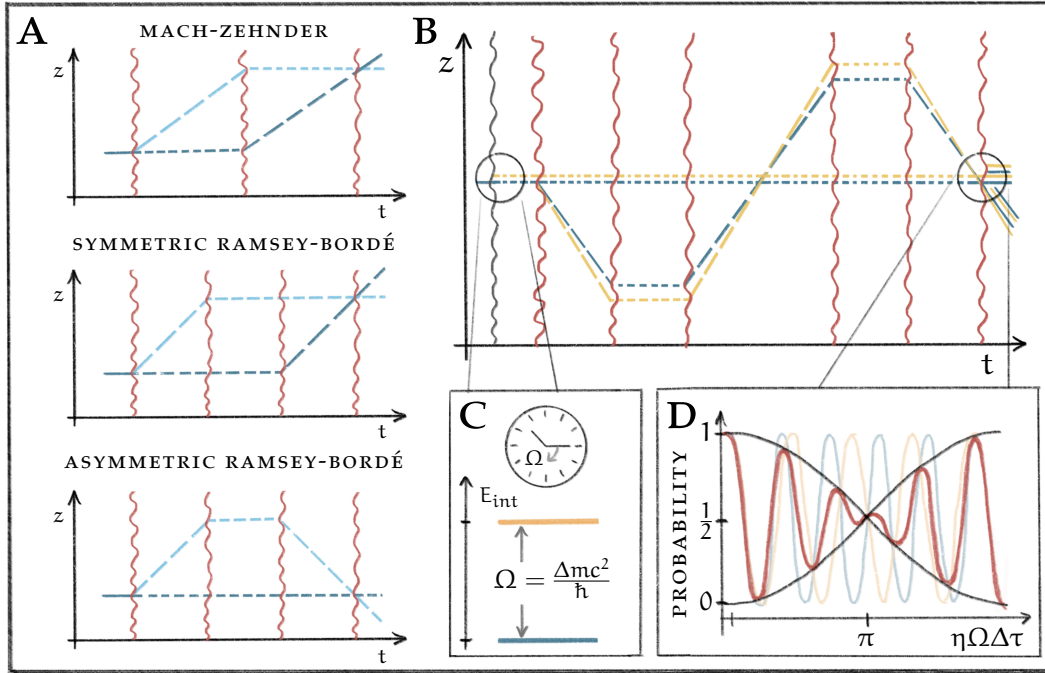
Figure 3.1: SPECIAL-RELATIVISTIC TIME DILATION IN ATOM INTERFEROMETRY. **(A)** The ticking rate of a hypothetical clock carried along the interferometer trajectories, denoted by the dashing length, allows to build an intuition on special-relativistic time dilation for different atom interferometer geometries. Indeed, the kinematic asymmetry of the Ramsey-Bordé configuration leads to a proper time difference. **(B)** Following the concepts of clock interferometry, we propose a geometry in [P4] which isolates this effect, hence implementing a quantum version of the classical twin paradox. **(C)** A superposition of internal states constitutes the notion of a clock, the frequency $\Omega = \Delta m c^2 / \hbar$ of which is defined by the effective mass difference Δm (i.e. energy splitting) between the internal states. It is supplied as input to the interferometer, which subsequently only manipulates the motional states. **(D)** In the presence of time dilation, this leads to a modulated visibility in the output port. This can be interpreted as the consequence of which-way information introduced by the proper time difference between the trajectories [211]. Another explanation [208] describes this phenomenon as the beatnote of two interferometers, one for each internal state. Our work in [P4] shows that the phase $\varphi(m)$ of geometries that are sensitive to proper time is dependent of the mass m. The beatnote of the two interferometers with phase $\varphi_{\pm} = \varphi(m \pm \Delta m/2)$ hence leads to the visibility modulation $\cos(\varphi_{+} - \varphi_{-}) = \cos(\eta \Omega \Delta \tau)$, which scales with the effective mass difference, parametrized by $\eta = 1/(1 - (\Delta m/2m)^2)$.

time difference between the branches as envisioned by [211]. Naturally, the effect is very small and the loss of contrast is not a favorable measurement observable. The alternative explanation is that two atom interferometers are operated simultaneously, one for each internal state [208]. In a two-level atom, which is effectively modeled by (3.2) with $j = 1, 2$, the phase of each individual interferometer is given by $\varphi_\pm = \omega_{C\pm}\Delta\tau = \frac{\hbar}{2m \pm \Delta m}K^2 T$. Here, the different internal states are associated with different effective masses, where $\Delta m = \Delta E/c^2$ depends on their energy difference $\Delta E = E_1 - E_2$. Consequently, by reading out the motional output ports of the interferometer, the beat note $\cos\left[\frac{1}{2}(\varphi_+ - \varphi_-)\right]\cos\left[\frac{1}{2}(\varphi_+ + \varphi_-)\right]$ of these two individual interferometers is recorded, which is identified as loss of visibility due to time-dilation-induced which-way information in the picture of [211]. The phase measurement of the individual masses (internal-state-dependent detection) is a considerably better observable of the same physical effect, owing to the excellent phase resolution of atom interferometers. Here, large fountain setups with long free fall times and large momentum transfer are advantageous as the sensitivity scales with $K^2 T$. To resolve the differential phase between the two internal states, their energy difference ΔE ought to be large, which favors alkaline-earth (like) species such as strontium (Sr) or ytterbium (Yb), which are typically used for optical clocks.

One key insight lies in the fact that for closed trajectories, the gravitational time dilation cancels with parts of the special relativistic time dilation. Their connection has to be accounted for in all tests of the redshift, which is achieved by carefully tracking the motion of the clock and subtracting the special relativistic contribution from the total time dilation (3.1) [201, 202, 206]. In atom-interferometric tests, this is evidently not possible as the position determination collapses the wave function, inhibiting an interferometric measurement. However, through elaborate arrangements one could distinguish the proper time contributions. This can be achieved through a new class of interferometers, such as proposed by [61] and [62]. While they are fundamentally different in implementation, they have in common that the clock is not initialized once before the interferometer as described above in the context of [P4]. The doubly differential scheme of [61] implements an internal-state superposition during the interferometic sequence at varying times such that certain sections of the interferometer can be isolated in the combination of subsequent measurements. These transitions between internal states during the sequence are identified as integral aspect and are used to replace the superposition of internal states in the geometry of [62]. These proposed experiments provide an exciting outlook for unprecedented atom-interferometric measurements of the gravitational redshift.

GRAVITATIONAL WAVES

> [The] universe has a soundtrack and that soundtrack is played on space itself,
> because space can wobble like a drum.
>
> — Janna Levin [215]

4.1 A NEW AVENUE FOR ASTRONOMY

Similar to the radiation sourced by accelerated electric charges, the acceleration of massive objects leads to space-time variations in the form of waves[1]. As alluded to in Chapter 1, there is compelling evidence for mass-energy distributions that are elusive to electromagnetic observation or neutrino detection [217] such that most of the universe remains invisible [38]. The detection of gravitational waves provides a new method to access these phenomena[2], allowing to monitor mergers of binary black holes and neutron stars and to shed light on processes like dark matter, cosmic strings and models of the early universe [218]. Apart from the immense astronomical value, gravitational wave astronomy has far-reaching implications for tests of general relativity as it probes the theory in the regime of strong fields and puts parameter bounds on the wave polarization and speed [20].

The first detection GW150914 of gravitational waves emitted by a binary black hole merger in 2015 therefore represents a milestone in the progress of modern physics [31]. The successful LIGO detectors were soon joined by the European Virgo collaboration, and together they have observed the mergers of ten solar mass binary black holes ($10^0 - 10^1 M_\odot$) [219]. Decades after first indirect evidence for gravitational radiation by the Hulse-Taylor neutron binary pulsar [25], the detection of gravitational waves [220] together with γ-ray bursts [221] constitutes the first multi-messenger observation of such an event. A global network of gravitational wave detectors based on long-baseline laser interferometry is under construction to complement the operating LIGO and Virgo observatories, allowing for significantly improved sky localization of the sources and facilitating multi-messenger operation [222]. These detectors and the planned upgraded versions of the third generation [223] are sensitive to gravitational waves of frequencies up to tens of kHz. At the lower end, they are limited by seismic and gravity gradient noise around 10 Hz, which had driven the consideration of space missions. The Laser-Interferometer-Space-Antenna LISA has been selected as L3 mission with launch date 2034 by the European space agency, designed for the mHz frequency band which is expected to be rich in gravitational wave sources [224]. The mission foresees three satellites connected via a laser link [225], and main technological concepts have been suc-

---

1 The physical reality of gravitational waves and methods to detect them had been subject to various debates [20, 216].
2 Gravitational wave detection is often labeled as a new sense to *listen* to the universe, with its sources being referred to as *loud* in analogy to *bright* sources of the conventional electromagnetic observation, which are associated with the optical sense.

cessfully demonstrated in a pathfinder mission [226, 227]. Pulsar timing arrays sensitive to mergers of supermassive black holes in the sub-µHz range complement the spectrum at very low frequencies [228].

The science case for multi-band gravitational wave astronomy is tantalizing as it allows to assess different energy scales and to follow an event through its evolution. The celebrated first detection GW150914, for example, radiated at mHz frequencies several years before the merger [229] within the sensitivity range of LISA. Such an early detection would have provided an early warning for terrestrial sensors to improve localization and facilitate multi-messenger observation. However, the intermediate frequency spectrum in the dezihertz range of 10 mHz to 10 Hz is not covered by these detectors. This regime encompasses the inspiral phase of stellar mass black hole binaries like GW150914 and coalescence of binaries involving neutron stars and black holes. Moreover, a detector sensitive at this frequency range would be able to observe white dwarf binaries and the merger of intermediate mass black holes in the order of $10^2 - 10^4 M_\odot$. In particular the latter represent an interesting science objective as their discovery may shed light on the evolution of supermassive black holes [P5, 230–233]. Finally, the change in position and orientation of a mid-band detector within the measurement time frame allows for improved angular localization of the source of a gravitational wave [233].

4.2   ATOM-INTERFEROMETRIC PHASEMETERS

Fueled by the early success of atom interferometers in inertial sensing [143, 234], first[3] proposals for gravitational wave detection were put forward and discussed [236–239]. Interferometric setups, where a beam of atoms with velocity v is coherently split and separated by a length L, feature a phase dependence $\phi \sim h_{GW} L / \lambda_{db}$. Here, h_{GW} denotes the strain of the gravitational wave and $\lambda_{db} = h/mv$ the wave length associated with the momentum of the atoms of mass m. As the phase response of light interferometers is very similar [238], however with significantly larger involved wavelength of the employed laser light $\lambda_L \gg \lambda_{db}$, atom interferometers first seemed to be very promising. However, the significantly smaller available baseline L and intrinsic sensor sensitivity $\sigma_\phi \sim 1/\sqrt{N}$, given by the flux of constituting particles $\dot{N}$ of the atoms quickly rendered these proposals unfeasible for typical parameters [239]. This approach, however, appears to be pursued further in concepts proposing free space matter wave links between space craft separated by several km [240].

Instead of measuring the phase shift in a single atom interferometer due to the influence of gravitational wave on atomic propagation, subsequent proposals [131, 241] suggested a gradiometric configuration, in which atom interferometers serve as phasemeters. As the phase of the laser is imprinted on the atomic wavefunction during atom-light interaction, a differential measurement between two atom interferometers that share the same light is susceptible to a gravitational wave induced phase shift of the light. This allows to scale up the base line for enhanced sensitivity. An advantage of a gradiometric scheme is that laser frequency and phase noise are largely suppressed as common mode [242, 243]. However, it remains a limiting fac-

---

3 First studies of the interaction of matter waves and gravitational waves were already performed in the 1970s [235].

tor due to the finite time delay between the two lasers constituting the two-photon transitions, limiting the base lines to a few km [244–246]. Alternatively, multi-arm configurations [131, 247] are considered in analogy to light interferometry. These setups allow to distinguish this noise by exploiting the polarization of gravitational waves.

Another significant limitation are fluctuations in the local gravitational field (Newtonian noise) that define the lower few Hz limit for terrestrial gravitational wave detectors [248]. By exploiting that Newtonian Noise and gravitational waves differ in their spatial distribution, an array of atom interferometers can discriminate these effects [249]. This allows to undercut the seismic limit and is the foundation of proposals for terrestrial gravitational wave detectors [P5, P6, 250]. The European Laboratory for Gravitation and Atom-interferometric Research (ELGAR) foresees a 2D-array of atomic gradiometers to measure gravitational waves in the deci-hertz band with a peak sensitivity at 1.7 Hz [P5, P6]. It could hence complement the frequency spectrum by filling the infrasound gap that is inaccessible to light interferometers, even in the planned upgraded third generation [223]. The MIGA experiment serves as a demonstrator to explore different technological and conceptual aspects [251].

An alternative strategy to mitigate laser frequency noise is the implementation of single photon transitions as first proposed in [252]. A single laser sent back and forth between the two atom interferometers circumvents the drawbacks associated with time delay of two-photon optics. Interestingly, this idea is very close to the utilization of separated clocks interrogated with the same light [253, 254] and requires only two satellites instead of three. In order to preserve enough intensity to drive transitions on both spacecraft [255], a heterodyne laser link was proposed, allowing to significantly increase the baseline [167, 256]. A collaboration on mid-band gravitational wave detection with precision atomic sensors (MAGIS) proposes a space mission based on these recent advances, anticipating to operate in the decihertz band [257]. Pathfinder experiments are planned to be conducted in the vertical MAGIS-100 long baseline setup at Fermi-lab [258].

The influence of a gravitational wave with strain h_{GW} and frequency ω on the phase difference $\Delta\phi \sim h_{GW} K L f(T\omega)$ in a gradiometric setup is determined by the baseline L, effective wave number K and pulse separation time T. The spectral response $f(T\omega)$ depends on the specific geometry and its resonance is, among other parameters, primarily defined by timings of the pulses. An inherent feature is hence the possibility to switch between operating modes. Broadband detection could be achieved by operating interleaved interferometers with different pulse timings. Upon discovery of a source, the choice of the appropriate pulse timing resonantly enhances the sensitivity of the sensor at the particular frequency, and could be dynamically changed to follow a signal [259, 260]. The effective wave number K is determined by the atom optical elements and is enhanced through large momentum transfer techniques. For two-photon beam splitters, this comprises sequential or higher-order Bragg and Raman scattering processes and/or Bloch oscillations in accelerated optical lattices. Large momentum transfer with one-photon manipulations can be achieved by sequential application of these pulses [261]. The phase expression shows a trade-off between baseline and effective momentum transfer.
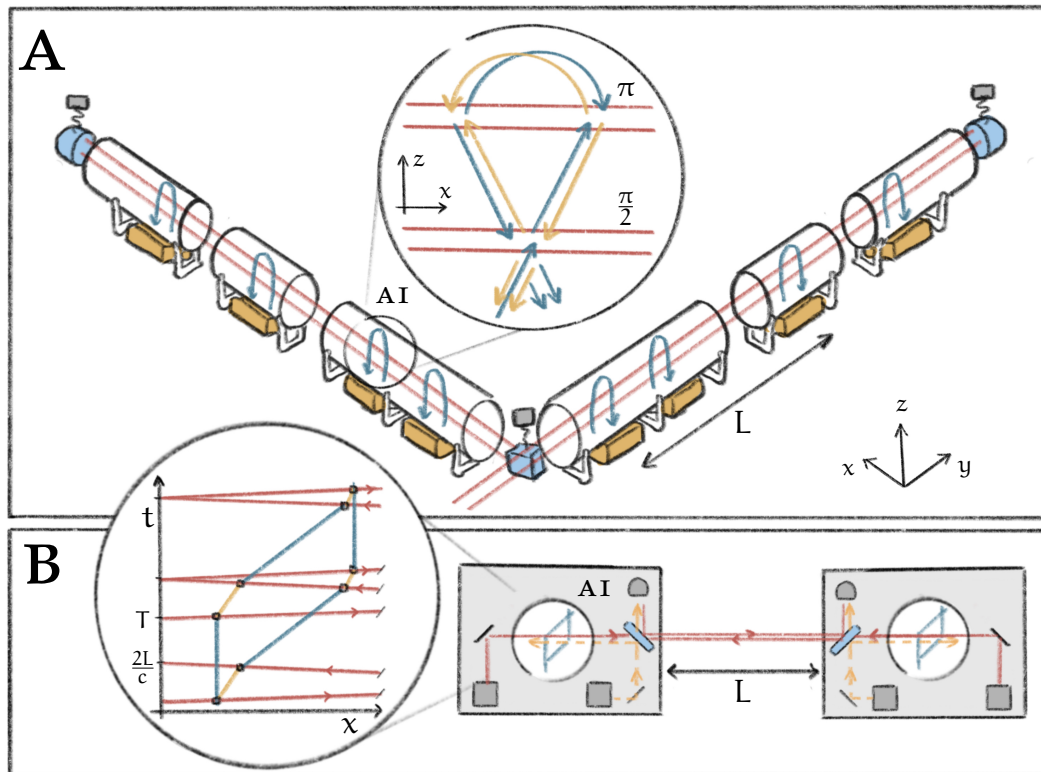
Figure 4.1: CONCEPTS FOR GRAVITATIONAL WAVE DETECTION WITH ATOM INTERFE-
ROMETRY. **(A)** The two-dimensional array of atom interferometers [P5, P6]
allows to effectively reject various noise sources, most notably gravity gradient
noise. In each interferometer, the atoms are vertically launched to pass two
separated interaction zones, which realize horizontal momentum transfer. In
[P6], we assess the requirements on the atomic source and beam splitters. **(B)**
The satellite concept of [167] is based on single-photon transitions, which enables
single-baseline operation . A phase-locking scheme allows for large base lines
and less stringent atom optics. As depicted in the inset, the atoms spend a
non-negligible time (in the order of seconds) in the excited state of the transition,
implying to use alkaline-earth(-like) species. In [P7], we perform a comparative
study of viable elements and assess different temperature and density regimes.

4.3   PERSONAL CONTRIBUTION: ATOMIC SOURCES AND OPTICS

Current proposals for atom interferometric gravitational wave detection comprise
two prevalent approaches: Single-baseline space missions based on single-photon
transitions [P7, 167, 257] and multi-dimensional terrestrial arrays with two-photon
excitations [P5, P6]. Both target the fruitful decihertz frequency regime which is not
accessed by existing and planned light interferometers, and have to face individual
technical and conceptual challenges. The requirements on the atomic source and
the atom optics processes are quite different and have been closely examined within
this thesis.

[P5, P6] TERRESTRIAL DETECTOR   In the main scenario of ELGAR, the lasers
constituting the beam splitters and mirrors will be realized by vertically separated
interaction zones. The atoms are launched with velocities in the order of m/s to

realize the designated interferometry duration. The anticipated gravitational wave strain sensitivity requires a (horizontal) momentum transfer in the order of 10^3 recoils while the atoms are falling through the light fields perpendicularly. We have conducted a numerical study to determine the required beam parameters that allow for large momentum transfer under these conditions in [P5, P6], which strongly favours the use of accelerated optical lattices. Our assessment of the source requirements suggests to employ alkaline species and two-photon transitions, owing to the technological heritage in particular with regard to large momentum transfer and phase-space engineering. To match the strict conditions on the source preparation imposed by the optics and systematic considerations, quantum degenerate sources (BECs) will have to be used. However, this has to be trade-off against the need for a high level of atomic flux to reach the level of required phase noise. Aside from needed significant improvements in source technology that loses less atoms to the cooling process, to concurrent operation of multiple interferometers is promising [262]. Moreover, entanglement for enhanced interferometry is actively pursued by several groups. The generation of non-classical input states through cavity feedback or atomic collisions with a metrological gain of 20 dB would allow for a 100-fold reduction of the required atomic flux.

[P7] SPACE-BORNE DETECTOR   The significantly longer base line available in space and the larger transition frequency of one-photon scenarios like MAGIS [167, 257] allows for comparably moderate atom optics in the order of tens of recoils. Due to the large distance between the spacecraft, the beam splitting scheme implies that the atoms spend seconds in the excited state of the transition. This calls for typical atomic clock species, which feature a large transition frequency and a long-lived excited state. The comparison of bosonic and fermionic species requires a trade-off between achievable excitation rates and excited state life time. Our study in [P7] comprises an exhaustive analysis of viable species for space-borne gravitational wave detection along the lines of [167, 257]. It contrasts different alkaline-earth(-like) elements with regard to fundamental properties and technical feasibility and identifies bosonic and fermionic Yb and Sr as the most promising candidates. One key aspect of the investigation considers the systematic requirements on the phase-space properties of the atomic ensembles. Different density and temperature regimes are compared, and to this end we developed a scaling description for interacting, non-degenerate ensembles to describe the intermediate regime between thermal and condensed sources. A central outcome of our study is that condensed sources are integral to meet the strict environmental requirements of such a mission.

5

SUMMARY AND OUTLOOK

Atom interferometry is a beautiful measurement concept that operates at the interface of quantum mechanics and general relativity. As such, it may shed light on models combining the two theories by providing a unique access to their non-relativistic limit. The description of the relativistic effects discussed in Chapter 3 require both, the notions of general relativity and quantum theory. Similarly, UFF tests involving spin, internal states and entanglement [150–154] and mass-dependent dispersion [138–141] are without classical equivalent. These concepts offer important guidance in the discussion of the equivalence principle in the context of quantum mechanics. Apart from these fundamental considerations, in a sense, the features and advantages of quantum mechanics are exploited to construct probes with high accuracy and stability [52]. They have been successfully applied to determine the gravitational constant G [263] and the fine structure constant α [213] with state-of-the-art accuracy. Moreover, the recent confirmation of the UFF to parts in 10^{-12} [158] demonstrates the pace at which atom interferometers catch up to the performance of their classical counterparts, which achieved the level of 10^{-14} recently [72].

This technological progress is accompanied by two major hallmarks, namely space maturity of compact systems and the construction of large-scale facilities and dedicated infrastructures. As sketched in Chapter 2, the technological readiness of different aspects of quantum systems for space applications has been demonstrated in various micro-gravity campaigns and will be further pursued in the next years [178–183, 186–189] . This is essential for a satellite mission as in [P1], where we propose an atom-interferometric test of the UFF with unprecedented accuracy to parts in 10^{-17}. The suggested concept foresees a dual-species experiment in an inertial configuration, which allows to discriminate various systematic effects from a potential UFF violation signal. This signal demodulation constitutes part of a strategy that we employ in [P2] to mitigate the detrimental influence of gravity gradients, which couple to the center-of-mass displacement of the two test masses in a drop test upon release. In this work, we apply a compensation scheme to alleviate the dependency on the source preparation. This does not only relax the requirements on the source co-location by several orders of magnitude but also leads to a reduced mission duration as compared to former proposals [191]. With regard to the environmental effects, the heritage of space missions with comparable scientific scope like LISA-Pathfinder [227] and MICROSCOPE [72, 264] is indispensable. In particular the latter features similar requirements on orbit and satellite control (residual drag, attitude, . . .). The support of national space agencies in the development of the required technology is emphasized through the implementation of dedicated research infrastructures, such as the new DLR-SI institute in Hanover for space-borne quantum inertial sensing and geodesy. Similarly, the French-German bilateral QUANTA collaboration, funded by CNES and DLR, explores space-borne geodesy with atom-interferometry. These

efforts in fostering technology and establishing institutional infrastructures are very promising and pave the way towards space-borne quantum tests of the UFF as studied in [P1, P2].

Another equally impressive trend is the set-up of large-scale atom interferometric facilities. The advantage of long experimental times and the corresponding increased sensitivity can also be obtained on Earth given large enough baselines. To this end, fountain experiments on the scale of several meters have been constructed, both with alkaline as well as alkaline-earth(-like) metals [148, 156, 157, 265]. The available scale factor allows for state-of-the-art measurements such as the recent UFF test [158] and is required to explore the relativistic effects discussed in Chapter 3. Our work [P4] proves that closed light-pulse atom interferometers without transitions between internal states are not sensitive to gravitational time dilation, which resolves a long-standing debate about the possibility to measure the gravitational redshift. Instead, we propose an experiment that demonstrates special-relativistic time dilation in atom interferometry. As this effect scales with the internal energy splitting, alkaline-earth(-like) metals such as Sr and Yb are strongly favoured due to their optical recombination (clock) transition. This requires the implementation of new atom optics techniques, such as magic Bragg beam splitting and recoil-free clock initialization [266]. Also, momentum transfer methods well understood for the two-photon transitions of alkaline species have to be transferred and up-scaled [267]. These tools are also useful for recently developed schemes for new types of atom interferometers [61, 62], which allow to access the gravitational time dilation by introducing internal state transitions during the interferometer sequence.

Finally, the large-scale setups serve as test beds to explore the technology required for the next generation of atom interferometric infrastructures in the km range [P5, P6, 250, 258], which are planned and in parts under construction. In particular the realization of large momentum transfer, atomic source manipulation and control of systematics such as the magnetic field, temperature and local gravity gradients over the entire extent of the baseline are challenges that will have to be faced. These insights are essential for the development of terrestrial gravitational wave detectors presented in Chapter 4 such as [P5, P6]. In this work, we assess the requirements on the atomic source and atom optics to realize the targeted strain sensitivity in the decihertz frequency band. Due to the comparably short baseline, the need for large momentum transfer and high atomic flux pose technological and conceptual challenges. Space-borne concepts alleviate the requirements on these aspects significantly and suggest to employ alkaline-earth(-like) species. In [P7], we conduct a thorough trade-off between different candidate elements and identify quantum degenerate Sr and Yb as most promising candidates.

Evidently, the increasing accuracy of atom interferometric sensors demands more sophisticated modeling and theoretical analysis. The path integral method alluded to in Chapter 2 is a powerful tool to assess major phase contributions and to discern various systematic effects as discussed in [P2, 55]. For a detailed uncertainty budget assessment and exhaustive modeling of experiments, this description is usually complemented by perturbative methods [136, 268] and a sensitivity formalism [269] inherited from the treatment of ion clocks [270]. Atom-light interaction, being the key component of the interferometric sequence, is a central pillar of

research and its analytic description can become arbitrarily complex [271, 272]. The dynamics of an atomic ensemble are conveniently described by virtue of a scaling approach for order-of-magnitude assessments, which allows to find parameters for source preparation sequences. In [P3], we use this technique to engineer a binary source for a UFF test in micro-gravity, based on a generalization [194] of the single-species scaling theory. For a specific scenario, such a study could be complemented by semi-classical N-particle simulations or numerical solutions to the Schrödinger equation for in-depth analysis. BECs, for which particle interactions play a superior role, are adequately modeled by the Gross-Pitaevskii equation, which is an amended Schrödinger equation with a non-linear density contribution [273]. As this description can also comprise the interaction with arbitrary light fields and external potentials, it is the most cohesive platform to numerically simulate an exact experimental sequence. Such a universal numeric atom interferometry simulator has been demonstrated in [274] will be extended to include single-photon beam splitting and internal state transitions to cover the full extent of metrologically relevant systems.

Of particular relevance for the discussion of sophisticated mission scenarios is the appropriate modeling of the time-dependent physical environment. The analysis in [P2] performs an analytical assessment of the order-of-magnitude effects by assuming a simplified configuration with a circular orbit and spherical gravitational potential. To avoid these restrictions, a complex simulator project was initiated within the frame of this thesis to incorporate the key aspects of a space mission. To this end, the final program shall feature a realistic gravitational potential model (such as [275]), orbits and satellite attitude as provided by space agencies to obtain the time-dependent gravitational potential in the frame of the satellite. Noise could be incorporated using the recorded spectra of residual linear and angular acceleration of the satellite of missions like [264]. This will serve as a simulation platform to assess future space missions based on atom interferometry for tests of fundamental physics, gravimetry and gravity gradiometry.

In conclusion, the recent progress in technological maturity, the establishment of dedicated infrastructures at large scales as well as the closing gap between quantum and classical sensors signalize an exciting and prosperous future for atom interferometry. Already the current generation of facilities [156] could measure the relativistic effects of [P4] and explore the related gravitational time dilation [61, 62]. The relentless strive for space seems to naturally lead to dedicated satellite missions like [P1, 115] beyond the technology demonstrators [183, 187, 189], requiring theoretical expertise on the mitigation of systematic effects [P2, P3]. Finally, the prospect of multi-band gravitational wave astronomy incorporating atom interferometric setups on ground [P5, P6] and in space [P7, 167] serves as thrilling long-term guidance.

BIBLIOGRAPHY

[1]   Isaac Asimov. *Foundation*. The Foundation Series 1. New York: Bantam Books, 2004. ISBN: 978-0-553-29335-7 (cit. on p. 1).

[2]   Norman Sieroka. *Philosophie der Physik: eine Einführung*. ger. Orig.-Ausg. C. H. Beck Wissen 2803. München: Beck, 2014. ISBN: 978-3-406-66794-7 (cit. on p. 1).

[3]   Hermann Weyl and Peter Pesic. *Mind and Nature: Selected Writings on Philosophy, Mathematics, and Physics*. en. Princeton: Princeton University Press, 2009. ISBN: 978-0-691-13545-8 (cit. on p. 1).

[4]   Albert Einstein, Max Born, and Hedwig Born. *The Born-Einstein Letters: Friendship, Politics, and Physics in Uncertain Times: Correspondence between Albert Einstein and Max and Hedwig Born from 1916 to 1955 with Commentaries by Max Born*. eng. Houndmills, Basingstoke, Hampshire ; New York: Macmillan, 2005. ISBN: 978-1-4039-4496-2 (cit. on p. 1).

[5]   R. A. Millikan. "On the Elementary Electrical Charge and the Avogadro Constant." In: *Physical Review* 2.2 (Aug. 1913), pp. 109–143. DOI: 10.1103/PhysRev.2.109 (cit. on p. 1).

[6]   J. Franck and G. Hertz. "Über Zusammenstöße Zwischen Elektronen Und Den Molekülen Des Quecksilberdampfes Und Die Ionisierungsspannung Desselben." en. In: *Physikalische Blätter* 23.7 (1967), pp. 294–301. ISSN: 1521-3722. DOI: 10.1002/phbl.19670230702 (cit. on p. 1).

[7]   Walther Gerlach and Otto Stern. "Der experimentelle Nachweis der Richtungsquantelung im Magnetfeld." de. In: *Zeitschrift für Physik* 9.1 (Dec. 1922), pp. 349–352. ISSN: 0044-3328. DOI: 10.1007/BF01326983 (cit. on p. 1).

[8]   P. Jordan and W. Pauli. "Zur Quantenelektrodynamik ladungsfreier Felder." de. In: *Zeitschrift für Physik* 47.3 (Feb. 1928), pp. 151–173. ISSN: 0044-3328. DOI: 10.1007/BF02055793 (cit. on p. 1).

[9]   Tom W.B. Kibble. "The Standard Model of Particle Physics." en. In: *European Review* 23.1 (Feb. 2015), pp. 36–44. ISSN: 1062-7987, 1474-0575. DOI: 10.1017/S1062798714000520 (cit. on p. 1).

[10] P. W. Higgs. "Broken Symmetries, Massless Particles and Gauge Fields." en. In: *Physics Letters* 12.2 (Sept. 1964), pp. 132–133. ISSN: 0031-9163. DOI: 10.1016/0031-9163(64)91136-9 (cit. on pp. 1, 9).

[11] F. Englert and R. Brout. "Broken Symmetry and the Mass of Gauge Vector Mesons." en. In: *Physical Review Letters* 13.9 (Aug. 1964), pp. 321–323. ISSN: 0031-9007. DOI: 10.1103/PhysRevLett.13.321 (cit. on pp. 1, 9).

[12] G. Aad et al. "Observation of a New Particle in the Search for the Standard Model Higgs Boson with the ATLAS Detector at the LHC." In: *Physics Letters B* 716.1 (Sept. 2012), pp. 1–29. ISSN: 0370-2693. DOI: 10.1016/j.physletb.2012.08.020 (cit. on pp. 1, 9).

[13]   S. Chatrchyan et al. "Observation of a New Boson at a Mass of 125 GeV with the CMS Experiment at the LHC." en. In: *Physics Letters B* 716.1 (Sept. 2012), pp. 30–61. ISSN: 0370-2693. DOI: 10.1016/j.physletb.2012.08.021 (cit. on pp. 1, 9).

[14]   A. A. Michelson and E. W. Morley. "On the Relative Motion of the Earth and the Luminiferous Ether." en. In: *American Journal of Science* s3-34.203 (Nov. 1887), pp. 333–345. ISSN: 0002-9599. DOI: 10.2475/ajs.s3-34.203.333 (cit. on pp. 1, 17).

[15]   Roland v Eötvös, Desiderius Pekár, and Eugen Fekete. "Beiträge Zum Gesetze Der Proportionalität von Trägheit Und Gravität." en. In: *Annalen der Physik* 373.9 (1922), pp. 11–66. ISSN: 1521-3889. DOI: 10.1002/andp.19223730903 (cit. on pp. 1, 7).

[16]   Frank Watson Dyson, Arthur Stanley Eddington, and C. Davidson. "IX. A Determination of the Deflection of Light by the Sun's Gravitational Field, from Observations Made at the Total Eclipse of May 29, 1919." In: *Philosophical Transactions of the Royal Society of London. Series A, Containing Papers of a Mathematical or Physical Character* 220.571-581 (Jan. 1920), pp. 291–333. DOI: 10.1098/rsta.1920.0009 (cit. on p. 1).

[17]   Clifford M. Will. *Theory and Experiment in Gravitational Physics*. Rev. ed. Cambridge [England] ; New York, NY, USA: Cambridge University Press, 1993. ISBN: 978-0-521-43973-2 (cit. on pp. 2, 8).

[18]   R. H. Dicke. *The Theoretical Significance of Experimental Relativity*. Documents on Modern Physics. New York: Gordon and Breach, 1964 (cit. on p. 2).

[19]   Clifford M. Will and Kenneth Nordtvedt Jr. "Conservation Laws and Preferred Frames in Relativistic Gravity. I. Preferred-Frame Theories and an Extended PPN Formalism." In: *The Astrophysical Journal* 177 (Nov. 1972), p. 757. ISSN: 0004-637X. DOI: 10.1086/151754 (cit. on pp. 2, 8).

[20]   Clifford M. Will. "The Confrontation between General Relativity and Experiment." en. In: *Living Reviews in Relativity* 17.1 (Dec. 2014). ISSN: 2367-3613, 1433-8351. DOI: 10.12942/lrr-2014-4 (cit. on pp. 2, 3, 7–10, 23).

[21]   Irwin I. Shapiro. "Fourth Test of General Relativity." In: *Physical Review Letters* 13.26 (Dec. 1964), pp. 789–791. DOI: 10.1103/PhysRevLett.13.789 (cit. on p. 2).

[22]   Kenneth Nordtvedt. "Equivalence Principle for Massive Bodies. I. Phenomenology." In: *Physical Review* 169.5 (May 1968), pp. 1014–1016. DOI: 10.1103/PhysRev.169.1014 (cit. on p. 2).

[23]   Kenneth Nordtvedt. "Equivalence Principle for Massive Bodies. II. Theory." In: *Physical Review* 169.5 (May 1968), pp. 1017–1025. DOI: 10.1103/PhysRev.169.1017 (cit. on p. 2).

[24]   C. W. F. Everitt et al. "Gravity Probe B: Final Results of a Space Experiment to Test General Relativity." en. In: *Physical Review Letters* 106.22 (May 2011). ISSN: 0031-9007, 1079-7114. DOI: 10.1103/PhysRevLett.106.221101 (cit. on p. 2).

[25]   R. A. Hulse and J. H. Taylor. "Discovery of a Pulsar in a Binary System." In: *The Astrophysical Journal Letters* 195 (Jan. 1975), pp. L51–L53. ISSN: 0004-637X. DOI: 10.1086/181708 (cit. on pp. 2, 23).

[26]   J. H. Taylor, L. A. Fowler, and P. M. McCulloch. "Measurements of General Relativistic Effects in the Binary Pulsar PSR1913 + 16." en. In: *Nature* 277.5696 (Feb. 1979), pp. 437–440. ISSN: 1476-4687. DOI: 10.1038/277437a0 (cit. on p. 2).

[27]   Russell A. Hulse. "The Discovery of the Binary Pulsar." In: *Reviews of Modern Physics* 66.3 (July 1994), pp. 699–710. DOI: 10.1103/RevModPhys.66.699 (cit. on p. 2).

[28]   Joseph H. Taylor. "Binary Pulsars and Relativistic Gravity." In: *Reviews of Modern Physics* 66.3 (July 1994), pp. 711–719. DOI: 10.1103/RevModPhys.66.711 (cit. on p. 2).

[29]   B. Louise Webster and Paul Murdin. "Cygnus X-1—a Spectroscopic Binary with a Heavy Companion ?" en. In: *Nature* 235.5332 (Jan. 1972), pp. 37–38. ISSN: 1476-4687. DOI: 10.1038/235037a0 (cit. on p. 2).

[30]   C. T. Bolton. "Identification of Cygnus X-1 with HDE 226868." en. In: *Nature* 235.5336 (Feb. 1972), pp. 271–273. ISSN: 1476-4687. DOI: 10.1038/235271b0 (cit. on p. 2).

[31]   B. P. Abbott et al. "Observation of Gravitational Waves from a Binary Black Hole Merger." In: *Physical Review Letters* 116.6 (Feb. 2016), p. 061102. ISSN: 0031-9007, 1079-7114. DOI: 10.1103/PhysRevLett.116.061102 (cit. on pp. 2, 23).

[32]   Gregory M. Harry. "Second Generation Gravitational Wave Detectors." In: *The Twelfth Marcel Grossmann Meeting*. WORLD SCIENTIFIC, Jan. 2012, pp. 628–644. ISBN: 978-981-4374-51-4. DOI: 10.1142/9789814374552_0032 (cit. on p. 2).

[33]   Kazunori Akiyama et al. "First M87 Event Horizon Telescope Results. I. The Shadow of the Supermassive Black Hole." en. In: *The Astrophysical Journal Letters* 875.1 (Apr. 2019), p. L1. ISSN: 2041-8205. DOI: 10.3847/2041-8213/ab0ec7 (cit. on p. 2).

[34]   Claus Kiefer. *Conceptual Problems in Quantum Gravity and Quantum Cosmology*. en. https://www.hindawi.com/journals/isrn/2013/509316/. Review Article. Aug. 2013. DOI: 10.1155/2013/509316 (cit. on p. 2).

[35]   Dean Rickles and Cécile M. DeWitt. "The Role of Gravitation in Physics: Report from the 1957 Chapel Hill Conference." In: *The Role of Gravitation in Physics: Report from the 1957 Chapel Hill Conference, Edited by Dean Rickles and Cécile M. DeWitt. ISBN: 978-3-945561-29-4, 2011* (Feb. 2011) (cit. on p. 2).

[36]   N. D. Birrell and P. C. W. Davies. *Quantum Fields in Curved Space*. en. Cambridge Monographs on Mathematical Physics. Cambridge [Cambridgeshire] ; New York: Cambridge University Press, 1982. ISBN: 978-0-521-23385-9 (cit. on pp. 2, 10).

[37] Claus Kiefer. "Conceptual Problems in Quantum Gravity and Quantum Cosmology." In: *ISRN Mathematical Physics* 2013 (2013), pp. 1–17. ISSN: 2090-4681. DOI: 10.1155/2013/509316. arXiv: 1401.3578 (cit. on pp. 3, 10).

[38] P. a. R. Ade et al. "Planck 2015 Results - XIII. Cosmological Parameters." en. In: *Astronomy & Astrophysics* 594 (Oct. 2016), A13. ISSN: 0004-6361, 1432-0746. DOI: 10.1051/0004-6361/201525830 (cit. on pp. 3, 23).

[39] Gianfranco Bertone and Tim M. P. Tait. "A New Era in the Search for Dark Matter." en. In: *Nature* 562.7725 (Oct. 2018), pp. 51–56. ISSN: 1476-4687. DOI: 10.1038/s41586-018-0542-z (cit. on p. 3).

[40] Thibault Damour. "Testing the Equivalence Principle: Why and How?" en. In: *Classical and Quantum Gravity* 13.11A (Nov. 1996), A33–A41. ISSN: 0264-9381, 1361-6382. DOI: 10.1088/0264-9381/13/11A/005 (cit. on pp. 3, 9, 10).

[41] R. V. Pound and G. A. Rebka. "Apparent Weight of Photons." en. In: *Physical Review Letters* 4.7 (Apr. 1960), pp. 337–341. ISSN: 0031-9007. DOI: 10.1103/PhysRevLett.4.337 (cit. on pp. 3, 17).

[42] Albert Einstein, Leopold Infeld, and Walter Isaacson. *The Evolution of Physics: From Early Concepts to Relativity and Quanta*. English. 2007 (cit. on p. 3).

[43] Louis de Broglie. "Recherches sur la théorie des Quanta." fr. PhD thesis. Migration - université en cours d'affectation, Nov. 1924 (cit. on pp. 3, 4).

[44] Jared W. Haslett. "Phase Waves of Louis deBroglie." en. In: *American Journal of Physics* 40.9 (Sept. 1972), pp. 1315–1320. ISSN: 0002-9505, 1943-2909. DOI: 10.1119/1.1986821 (cit. on pp. 3, 4).

[45] Yaakov Y. Fein, Philipp Geyer, Patrick Zwick, Filip Kiałka, Sebastian Pedalino, Marcel Mayor, Stefan Gerlich, and Markus Arndt. "Quantum Superposition of Molecules beyond 25 kDa." en. In: *Nature Physics* 15.12 (Dec. 2019), pp. 1242–1245. ISSN: 1745-2481. DOI: 10.1038/s41567-019-0663-9 (cit. on p. 3).

[46] R. Colella, A. W. Overhauser, and S. A. Werner. "Observation of Gravitationally Induced Quantum Interference." en. In: *Physical Review Letters* 34.23 (June 1975), pp. 1472–1474. ISSN: 0031-9007. DOI: 10.1103/PhysRevLett.34.1472 (cit. on p. 4).

[47] Wilhelm Hanle. "Üeber magnetische Beeinflussung der Polarisation der Resonanzfluoreszenz 1." de. In: (1924), p. 6 (cit. on p. 4).

[48] I. I. Rabi, J. R. Zacharias, S. Millman, and P. Kusch. "A New Method of Measuring Nuclear Magnetic Moment." en. In: *Physical Review* 53.4 (Feb. 1938), pp. 318–318. ISSN: 0031-899X. DOI: 10.1103/PhysRev.53.318 (cit. on p. 4).

[49] Norman F. Ramsey. "A New Molecular Beam Resonance Method." en. In: *Physical Review* 76.7 (Oct. 1949), pp. 996–996. ISSN: 0031-899X. DOI: 10.1103/PhysRev.76.996 (cit. on p. 4).

[50] M. S. Safronova, D. Budker, D. DeMille, Derek F. Jackson Kimball, A. Derevianko, and Charles W. Clark. "Search for New Physics with Atoms and Molecules." en. In: *Reviews of Modern Physics* 90.2 (June 2018). ISSN: 0034-6861, 1539-0756. DOI: 10.1103/RevModPhys.90.025008 (cit. on p. 4).

[51] Mark Kasevich and Steven Chu. "Atomic Interferometry Using Stimulated Raman Transitions." In: *Physical Review Letters* 67.2 (July 1991), pp. 181–184. DOI: 10.1103/PhysRevLett.67.181 (cit. on p. 4).

[52] Remi Geiger, Arnaud Landragin, Sébastien Merlet, and Franck Pereira Dos Santos. "High-Accuracy Inertial Measurements with Cold-Atom Sensors." en. In: (Mar. 2020). arXiv: 2003.12516 [physics, physics:quant-ph] (cit. on pp. 4, 5, 13, 29).

[53] Guglielmo M. Tino. *Atom Interferometry: Proceedings of the International School of Physics "Enrico Fermi", Course 188, Varenna on Lake Como, Villa Monastero, 15 - 20 July 2013 = Interferometria Atomica.* eng. Ed. by Guglielmo M. Tino and M. A. Kasevich. Amsterdam: IOS Press, 2014 (cit. on p. 4).

[54] Alexander D. Cronin, Jörg Schmiedmayer, and David E. Pritchard. "Optics and Interferometry with Atoms and Molecules." In: *Reviews of Modern Physics* 81.3 (July 2009), pp. 1051–1129. DOI: 10.1103/RevModPhys.81.1051 (cit. on p. 4).

[55] Jason M. Hogan, David M. S. Johnson, and Mark A. Kasevich. "Light-Pulse Atom Interferometry." In: (June 2008). arXiv: 0806.3261 [physics] (cit. on pp. 4, 11, 30).

[56] Dennis Schlippert. "Quantum Tests of the Universality of Free Fall." PhD thesis. Leibniz Universität Hannover, 2014 (cit. on p. 4).

[57] Christian J. Bordé. "Theoretical Tools for Atom Optics and Interferometry." en. In: *Comptes Rendus de l'Académie des Sciences - Series IV - Physics* 2.3 (Apr. 2001), pp. 509–530. ISSN: 12962147. DOI: 10.1016/S1296-2147(01)01186-6 (cit. on p. 4).

[58] Holger Müller, Achim Peters, and Steven Chu. "A Precision Measurement of the Gravitational Redshift by the Interference of Matter Waves." en. In: *Nature* 463.7283 (Feb. 2010), pp. 926–929. ISSN: 1476-4687. DOI: 10.1038/nature08776 (cit. on pp. 4, 18, 20).

[59] Wolfgang P. Schleich, Daniel M. Greenberger, and Ernst M. Rasel. "A Representation-Free Description of the Kasevich–Chu Interferometer: A Resolution of the Redshift Controversy." en. In: *New Journal of Physics* 15.1 (2013), p. 013007. ISSN: 1367-2630. DOI: 10.1088/1367-2630/15/1/013007 (cit. on pp. 4, 11, 18, 20).

[60] Peter Wolf, Luc Blanchet, Christian J. Bordé, Serge Reynaud, Christophe Salomon, and Claude Cohen-Tannoudji. "Does an Atom Interferometer Test the Gravitational Redshift at the Compton Frequency?" en. In: *Classical and Quantum Gravity* 28.14 (2011), p. 145017. ISSN: 0264-9381. DOI: 10.1088/0264-9381/28/14/145017 (cit. on pp. 4, 9–11, 18, 20).

[61]   Albert Roura. "Gravitational Redshift in Quantum-Clock Interferometry."
In: *Physical Review X* 10.2 (Apr. 2020), p. 021014. DOI: 10.1103/PhysRevX.10.
021014 (cit. on pp. 4, 18, 22, 30, 31).

[62]   Christian Ufrecht, Fabio Di Pumpo, Alexander Friedrich, Albert Roura,
Christian Schubert, Dennis Schlippert, Ernst M. Rasel, Wolfgang P. Schleich,
and Enno Giese. "An Atom Interferometer Testing the Universality of Free
Fall and Gravitational Redshift." In: (Jan. 2020). arXiv: 2001.09754 (cit. on
pp. 4, 18, 22, 30, 31).

[63]   Sven Abend, Matthias Gersemann, Christian Schubert, Dennis Schlippert,
Ernst M. Rasel, Matthias Zimmermann, Maxim A. Efremov, Albert Roura,
Frank A. Narducci, and Wolfgang P. Schleich. "Atom Interferometry and Its
Applications." en. In: (Jan. 2020). arXiv: 2001.10976 (cit. on p. 5).

[64]   NASA. *Apollo 15 Technical Air-To-Ground Voice Transcription*. 1971 (cit. on
p. 7).

[65]   Joseph Allen. *Apollo 15 Preliminary Science Report*. Tech. rep. NASA SP-289.
NASA National Aeronautics and Space Administration, 1972 (cit. on p. 7).

[66]   Stillman Drake. *History of Free Fall: Aristotle to Galileo ; with an Epilogue on
π in the Sky*. eng. Toronto: Wall & Thompson, 1989. ISBN: 978-0-921332-26-8
(cit. on p. 7).

[67]   Prabhakar Gondhalekar. *Grip of Gravity*. English. Cambridge, GBR: Cam-
bridge University Press, 2009. ISBN: 978-0-511-52528-5 (cit. on p. 7).

[68]   Galileo Galilei. *Two New Sciences: Including Centers of Gravity ; and Force of
Percussion*. English. Toronto: Wall & Thomson, 1990. ISBN: 978-0-921332-20-6
(cit. on p. 7).

[69]   Isaac Newton. *Philosophiae Naturalis Principia Mathematica*. First. London:
Jussu Societatis Regiae ac typis Josephi Streater, 1687 (cit. on p. 7).

[70]   T. A. Wagner, S. Schlamminger, J. H. Gundlach, and E. G. Adelberger.
"Torsion-Balance Tests of the Weak Equivalence Principle." en. In: *Classical
and Quantum Gravity* 29.18 (2012), p. 184002. ISSN: 0264-9381. DOI: 10.1088/
0264-9381/29/18/184002 (cit. on p. 7).

[71]   F Hofmann and J Müller. "Relativistic Tests with Lunar Laser Ranging." en.
In: *Classical and Quantum Gravity* 35.3 (Feb. 2018), p. 035015. ISSN: 0264-9381,
1361-6382. DOI: 10.1088/1361-6382/aa8f7a (cit. on p. 7).

[72]   Pierre Touboul et al. "MICROSCOPE Mission: First Results of a Space Test
of the Equivalence Principle." In: *Physical Review Letters* 119.23 (Dec. 2017),
p. 231101. DOI: 10.1103/PhysRevLett.119.231101 (cit. on pp. 7, 13, 15, 29).

[73]   Susannah Moore Dickerson. "Long-Time Atom Interferometry for Precision
Tests of Fundamental Physics." PhD thesis. Stanford University, 2014 (cit. on
p. 7).

[74]   A. Einstein. "Die Grundlage Der Allgemeinen Relativitätstheorie." en. In:
Annalen der Physik 354.7 (1916), pp. 769–822. ISSN: 1521-3889. DOI: 10.1002/
andp.19163540702 (cit. on pp. 7, 8).

[75]   David Hilbert. "Die Grundlagen Der Physik." In: *Mathematische Annalen* 92.1
(1924), pp. 1–32. ISSN: 1432-1807. DOI: 10.1007/BF01448427 (cit. on pp. 7, 8).

[76] Charles W. Misner, Kip S. Thorne, and John Archibald Wheeler. *Gravitation*. San Francisco: W. H. Freeman, 1973 (cit. on pp. 7–9, 11).

[77] R. H. Dicke. "Mach's Principle and Invariance under Transformation of Units." en. In: *Physical Review* 125.6 (Mar. 1962), pp. 2163–2167. ISSN: 0031-899X. DOI: 10.1103/PhysRev.125.2163 (cit. on pp. 8, 9).

[78] T. Damour. "Experimental Tests of Gravitational Theory." en. In: *The European Physical Journal C* 15.1-4 (Mar. 2000), pp. 121–124. ISSN: 1434-6044, 1434-6052. DOI: 10.1007/BF02683410 (cit. on p. 8).

[79] Thomas Appelquist, Alan Chodos, and Peter G. O. Freund, eds. *Modern Kaluza-Klein Theories*. Frontiers in Physics v. 65. Menlo Park, Calif: Addison-Wesley Pub. Co, 1987. ISBN: 978-0-201-09829-7 (cit. on p. 8).

[80] Carl H. Brans. "The Roots of Scalar-Tensor Theory: An Approximate History." en. In: (June 2005). arXiv: gr-qc/0506063 (cit. on p. 8).

[81] M. Fierz. "Über die physikalische Deutung der erweiterten Gravitationstheorie P. Jordans." de. In: (1956). DOI: 10.5169/SEALS-112699 (cit. on pp. 8, 9).

[82] P. Jordan. "Die physikalischen Weltkonstanten." de. In: *Naturwissenschaften* 25.32 (Aug. 1937), pp. 513–517. ISSN: 1432-1904. DOI: 10.1007/BF01498368 (cit. on pp. 8, 9).

[83] P. Jordan. "Über die kosmologische Konstanz der Feinstrukturkonstanten." de. In: *Zeitschrift für Physik* 113.9 (Sept. 1939), pp. 660–662. ISSN: 0044-3328. DOI: 10.1007/BF01340095 (cit. on pp. 8, 9).

[84] C. Brans and R. H. Dicke. "Mach's Principle and a Relativistic Theory of Gravitation." In: *Physical Review* 124.3 (Nov. 1961), pp. 925–935. DOI: 10.1103/PhysRev.124.925 (cit. on p. 8).

[85] Peter G. Bergmann. "Comments on the Scalar-Tensor Theory." en. In: *International Journal of Theoretical Physics* 1.1 (May 1968), pp. 25–36. ISSN: 1572-9575. DOI: 10.1007/BF00668828 (cit. on p. 8).

[86] Robert V. Wagoner. "Scalar-Tensor Theory and Gravitational Waves." In: *Physical Review D* 1.12 (June 1970), pp. 3209–3216. DOI: 10.1103/PhysRevD.1.3209 (cit. on p. 8).

[87] Jacob D. Bekenstein. "Are Particle Rest Masses Variable? Theory and Constraints from Solar System Experiments." In: *Physical Review D* 15.6 (Mar. 1977), pp. 1458–1468. DOI: 10.1103/PhysRevD.15.1458 (cit. on p. 8).

[88] Kenneth Nordtvedt Jr. "Post-Newtonian Metric for a General Class of Scalar-Tensor Gravitational Theories and Observational Consequences." en. In: *The Astrophysical Journal* 161 (Sept. 1970), p. 1059. ISSN: 0004-637X, 1538-4357. DOI: 10.1086/150607 (cit. on p. 8).

[89] Justin Khoury and Amanda Weltman. "Chameleon Fields: Awaiting Surprises for Tests of Gravity in Space." In: *Physical Review Letters* 93.17 (Oct. 2004), p. 171104. DOI: 10.1103/PhysRevLett.93.171104 (cit. on pp. 8, 9).

[90] Thibault Damour. "Theoretical Aspects of the Equivalence Principle." en. In: *Classical and Quantum Gravity* 29.18 (Aug. 2012), p. 184001. ISSN: 0264-9381. DOI: 10.1088/0264-9381/29/18/184001 (cit. on p. 9).

[91]   P. a. M. Dirac. "The Cosmological Constants." en. In: *Nature* 139.3512 (Feb. 1937), pp. 323–323. ISSN: 1476-4687. DOI: 10.1038/139323a0 (cit. on p. 9).

[92]   T. Damour and A. M. Polyakov. "The String Dilation and a Least Coupling Principle." en. In: *Nuclear Physics B* 423.2 (July 1994), pp. 532–558. ISSN: 0550-3213. DOI: 10.1016/0550-3213(94)90143-0 (cit. on pp. 9, 10).

[93]   Charles W. Misner, Kip S. Thorne, John Archibald Wheeler, and David Kaiser. *Gravitation*. Princeton, N.J: Princeton University Press, 2017. ISBN: 978-0-691-17779-3 (cit. on p. 9).

[94]   Justin Khoury and Amanda Weltman. "Chameleon Cosmology." In: *Physical Review D* 69.4 (Feb. 2004), p. 044026. DOI: 10.1103/PhysRevD.69.044026 (cit. on p. 9).

[95]   Sean M. Carroll, Sonny Mantry, Michael J. Ramsey-Musolf, and Christoper W. Stubbs. "Dark-Matter-Induced Violation of the Weak Equivalence Principle." In: *Physical Review Letters* 103.1 (July 2009), p. 011301. DOI: 10.1103/PhysRevLett.103.011301 (cit. on p. 9).

[96]   Sean M. Carroll, Sonny Mantry, and Michael J. Ramsey-Musolf. "Implications of a Scalar Dark Force for Terrestrial Experiments." In: *Physical Review D* 81.6 (Mar. 2010), p. 063507. DOI: 10.1103/PhysRevD.81.063507 (cit. on p. 9).

[97]   Rachel Bean, Éanna É. Flanagan, and Mark Trodden. "Adiabatic Instability in Coupled Dark Energy/Dark Matter Models." en. In: *Physical Review D* 78.2 (July 2008), p. 023009. ISSN: 1550-7998, 1550-2368. DOI: 10.1103/PhysRevD.78.023009 (cit. on p. 9).

[98]   Kean Loon Lee, Nils B. Jørgensen, I-Kang Liu, Lars Wacker, Jan J. Arlt, and Nick P. Proukakis. "Phase Separation and Dynamics of Two-Component Bose-Einstein Condensates." en. In: *Physical Review A* 94.1 (July 2016). ISSN: 2469-9926, 2469-9934. DOI: 10.1103/PhysRevA.94.013602 (cit. on p. 9).

[99]   Luc Blanchet. "A Class of Nonmetric Couplings to Gravity." In: *Physical Review Letters* 69.4 (July 1992), pp. 559–562. DOI: 10.1103/PhysRevLett.69.559 (cit. on p. 9).

[100] Quentin G. Bailey and V. Alan Kostelecký. "Signals for Lorentz Violation in Post-Newtonian Gravity." en. In: *Physical Review D* 74.4 (Aug. 2006), p. 045001. ISSN: 1550-7998, 1550-2368. DOI: 10.1103/PhysRevD.74.045001 (cit. on p. 9).

[101] V. Alan Kostelecký and Jay D. Tasson. "Matter-Gravity Couplings and Lorentz Violation." In: *Physical Review D* 83.1 (Jan. 2011), p. 016013. DOI: 10.1103/PhysRevD.83.016013 (cit. on pp. 9, 12).

[102] L. I. Schiff. "Possible New Experimental Test of General Relativity Theory." en. In: *Physical Review Letters* 4.5 (Mar. 1960), pp. 215–217. ISSN: 0031-9007. DOI: 10.1103/PhysRevLett.4.215 (cit. on p. 9).

[103] Hans C. Ohanian. "Comment on the Schiff Conjecture." en. In: *Physical Review D* 10.6 (Sept. 1974), pp. 2041–2042. ISSN: 0556-2821. DOI: 10.1103/PhysRevD.10.2041 (cit. on p. 9).

[104] Wei-Tou Ni. "Equivalence Principles and Electromagnetism." en. In: *Physical Review Letters* 38.7 (Feb. 1977), pp. 301–304. ISSN: 0031-9007. DOI: `10.1103/PhysRevLett.38.301` (cit. on p. 9).

[105] A. Coley. "Schiff's Conjecture on Gravitation." en. In: *Physical Review Letters* 49.12 (Sept. 1982), pp. 853–855. ISSN: 0031-9007. DOI: `10.1103/PhysRevLett.49.853` (cit. on p. 9).

[106] K. Nordtvedt. "Quantitative Relationship between Clock Gravitational "Red-Shift" Violations and Nonuniversality of Free-Fall Rates in Nonmetric Theories of Gravity." en. In: *Physical Review D* 11.2 (Jan. 1975), pp. 245–247. ISSN: 0556-2821. DOI: `10.1103/PhysRevD.11.245` (cit. on p. 9).

[107] Mark P Haugan. "Energy Conservation and the Principle of Equivalence." en. In: *Annals of Physics* 118.1 (Mar. 1979), pp. 156–186. ISSN: 00034916. DOI: `10.1016/0003-4916(79)90238-0` (cit. on p. 9).

[108] R. H. Dicke. "Eötvös Experiment and the Gravitational Red Shift." en. In: *American Journal of Physics* 28.4 (Apr. 1960), pp. 344–347. ISSN: 0002-9505, 1943-2909. DOI: `10.1119/1.1935801` (cit. on p. 9).

[109] T. R. Taylor and G. Veneziano. "Dilaton Couplings at Large Distances." en. In: *Physics Letters B* 213.4 (Nov. 1988), pp. 450–454. ISSN: 0370-2693. DOI: `10.1016/0370-2693(88)91290-7` (cit. on p. 10).

[110] I. Antoniadis, S. Baessler, M. Büchner, V. V. Fedorov, S. Hoedl, A. Lambrecht, V. V. Nesvizhevsky, G. Pignol, K. V. Protasov, S. Reynaud, and Yu. Sobolev. "Short-Range Fundamental Forces." en. In: *Comptes Rendus Physique*. Ultra Cold Neutron Quantum States 12.8 (Oct. 2011), pp. 755–778. ISSN: 1631-0705. DOI: `10.1016/j.crhy.2011.05.004` (cit. on p. 10).

[111] Roy Maartens and Kazuya Koyama. "Brane-World Gravity." en. In: *Living Reviews in Relativity* 13.1 (Sept. 2010), p. 5. ISSN: 1433-8351. DOI: `10.12942/lrr-2010-5` (cit. on p. 10).

[112] Valerii A. Rubakov. "Large and Infinite Extra Dimensions." en. In: *Physics-Uspekhi* 44.9 (2001), p. 871. DOI: `10.1070/PU2001v044n09ABEH001000` (cit. on p. 10).

[113] E. G. Adelberger, J. H. Gundlach, B. R. Heckel, S. Hoedl, and S. Schlamminger. "Torsion Balance Experiments: A Low-Energy Frontier of Particle Physics." en. In: *Progress in Particle and Nuclear Physics* 62.1 (Jan. 2009), pp. 102–134. ISSN: 0146-6410. DOI: `10.1016/j.ppnp.2008.08.002` (cit. on p. 10).

[114] James G. Williams, Slava G. Turyshev, and Dale H. Boggs. "Progress in Lunar Laser Ranging Tests of Relativistic Gravity." In: *Physical Review Letters* 93.26 (Dec. 2004), p. 261101. DOI: `10.1103/PhysRevLett.93.261101` (cit. on p. 10).

[115] Brett Altschul. "Quantum Tests of the Einstein Equivalence Principle with the STE–QUEST Space Mission." en. In: *Advances in Space Research* 55.1 (Jan. 2015), pp. 501–524. ISSN: 0273-1177. DOI: `10.1016/j.asr.2014.07.014` (cit. on pp. 10, 13, 31).

[116] Steven Weinberg. *Gravitation and Cosmology: Principles and Applications of the General Theory of Relativity*. New York: Wiley, 1972. ISBN: 978-0-471-92567-5 (cit. on p. 10).

[117] Philip K. Schwartz and Domenico Giulini. "Post-Newtonian Corrections to Schrödinger Equations in Gravitational Fields." en. In: (Dec. 2018). arXiv: 1812.05181 (cit. on p. 10).

[118] T. W. B. Kibble and S. Randjbar-Daemi. "Non-Linear Coupling of Quantum Theory and Classical Gravity." en. In: *Journal of Physics A: Mathematical and General* 13.1 (Jan. 1980), pp. 141–148. ISSN: 0305-4470. DOI: 10.1088/0305-4470/13/1/015 (cit. on pp. 10, 12).

[119] André Lichnérowicz, Marie-Antoinette Tonnelat, Centre National de la Recherche Scientifique, and -. *Les théories relativistes de la gravitation: [actes du colloque international], Royaumont, 21-27 juin 1959*. French. Paris: Centre National de la Recherche Scientifique, 1962 (cit. on p. 10).

[120] L. Rosenfeld. "On Quantization of Fields." en. In: *Nuclear Physics* 40 (Jan. 1963), pp. 353–356. ISSN: 0029-5582. DOI: 10.1016/0029-5582(63)90279-7 (cit. on p. 10).

[121] S. Carlip. "Is Quantum Gravity Necessary?" en. In: *Classical and Quantum Gravity* 25.15 (July 2008), p. 154010. ISSN: 0264-9381. DOI: 10.1088/0264-9381/25/15/154010 (cit. on p. 10).

[122] Don N. Page and C. D. Geilker. "Indirect Evidence for Quantum Gravity." en. In: *Physical Review Letters* 47.14 (Oct. 1981), pp. 979–982. ISSN: 0031-9007. DOI: 10.1103/PhysRevLett.47.979 (cit. on p. 10).

[123] Roger Penrose. "On the Gravitization of Quantum Mechanics 1: Quantum State Reduction." en. In: *Foundations of Physics* 44.5 (May 2014), pp. 557–575. ISSN: 1572-9516. DOI: 10.1007/s10701-013-9770-0 (cit. on p. 10).

[124] S. W. Hawking. "Particle Creation by Black Holes." en. In: *Communications in Mathematical Physics* 43.3 (Aug. 1975), pp. 199–220. ISSN: 1432-0916. DOI: 10.1007/BF02345020 (cit. on p. 10).

[125] Claus Lämmerzahl. "A Hamilton Operator for Quantum Optics in Gravitational Fields." In: *Physics Letters A* 203.1 (1995), pp. 12–17 (cit. on pp. 10, 11).

[126] Claus Kiefer and Tejinder P. Singh. "Quantum Gravitational Corrections to the Functional Schrödinger Equation." In: *Physical Review D* 44.4 (1991), p. 1067 (cit. on p. 10).

[127] Domenico Giulini and Andre Grossardt. "The Schrödinger–Newton Equation as a Non-Relativistic Limit of Self-Gravitating Klein–Gordon and Dirac Fields." en. In: *Classical and Quantum Gravity* 29.21 (Oct. 2012), p. 215010. ISSN: 0264-9381. DOI: 10.1088/0264-9381/29/21/215010 (cit. on p. 10).

[128] Philip K. Schwartz and Domenico Giulini. "Post-Newtonian Corrections to Schrödinger Equations in Gravitational Fields." en. In: *Classical and Quantum Gravity* 36.9 (Apr. 2019), p. 095016. ISSN: 0264-9381. DOI: 10.1088/1361-6382/ab0fbd (cit. on pp. 10–12, 19).

[129]   C Anastopoulos and B L Hu. "Equivalence Principle for Quantum Systems: Dephasing and Phase Shift of Free-Falling Particles." en. In: *Classical and Quantum Gravity* 35.3 (Feb. 2018), p. 035011. ISSN: 0264-9381, 1361-6382. DOI: 10.1088/1361-6382/aaa0e8 (cit. on pp. 10, 12, 19).

[130]   Shigeru Wajima, Masumi Kasai, and Toshifumi Futamase. "Post-Newtonian Effects of Gravity on Quantum Interferometry." In: *Physical Review D* 55.4 (Feb. 1997), pp. 1964–1970. DOI: 10.1103/PhysRevD.55.1964 (cit. on p. 10).

[131]   Savas Dimopoulos, Peter W. Graham, Jason M. Hogan, Mark A. Kasevich, and Surjeet Rajendran. "Atomic Gravitational Wave Interferometric Sensor." en. In: *Physical Review D* 78.12 (Dec. 2008). ISSN: 1550-7998, 1550-2368. DOI: 10.1103/PhysRevD.78.122002 (cit. on pp. 10, 11, 24, 25).

[132]   R. P. Feynman. "Space-Time Approach to Non-Relativistic Quantum Mechanics." In: *Reviews of Modern Physics* 20.2 (Apr. 1948), pp. 367–387. DOI: 10.1103/RevModPhys.20.367 (cit. on p. 11).

[133]   Pippa Storey and Claude Cohen-Tannoudji. "The Feynman Path Integral Approach to Atomic Interferometry. A Tutorial." en. In: *Journal de Physique II* 4.11 (Nov. 1994), pp. 1999–2027. ISSN: 1155-4312, 1286-4870. DOI: 10.1051/jp2:1994103 (cit. on p. 11).

[134]   Karl-Peter Marzlin. "Dipole Coupling of Atoms and Light in Gravitational Fields." en. In: *Physical Review A* 51.1 (Jan. 1995), pp. 625–631. ISSN: 1050-2947, 1094-1622. DOI: 10.1103/PhysRevA.51.625 (cit. on pp. 11, 20).

[135]   Matthias Sonnleitner and Stephen M. Barnett. "Mass-Energy and Anomalous Friction in Quantum Optics." en. In: *Physical Review A* 98.4 (Oct. 2018), p. 042106. ISSN: 2469-9926, 2469-9934. DOI: 10.1103/PhysRevA.98.042106 (cit. on pp. 11, 19, 20).

[136]   A. Bertoldi, F. Minardi, and M. Prevedelli. "Phase Shift in Atom Interferometers: Corrections for Nonquadratic Potentials and Finite-Duration Laser Pulses." en. In: *Physical Review A* 99.3 (Mar. 2019), p. 033619. ISSN: 2469-9926, 2469-9934. DOI: 10.1103/PhysRevA.99.033619 (cit. on pp. 12, 30).

[137]   Christian Ufrecht and Enno Giese. "Perturbative Operator Approach to High-Precision Light-Pulse Atom Interferometry." In: *Physical Review A* 101.5 (May 2020), p. 053615. DOI: 10.1103/PhysRevA.101.053615 (cit. on p. 12).

[138]   Claus Lämmerzahl. "On the Equivalence Principle in Quantum Theory." en. In: *General Relativity and Gravitation* 28.9 (Sept. 1996), pp. 1043–1070. ISSN: 1572-9532. DOI: 10.1007/BF02113157 (cit. on pp. 12, 29).

[139]   Lorenza Viola and Roberto Onofrio. "Testing the Equivalence Principle through Freely Falling Quantum Objects." In: *Physical Review D* 55.2 (Jan. 1997), pp. 455–462. DOI: 10.1103/PhysRevD.55.455 (cit. on pp. 12, 29).

[140]   P. C. W. Davies. "Quantum Mechanics and the Equivalence Principle." en. In: *Classical and Quantum Gravity* 21.11 (May 2004), pp. 2761–2772. ISSN: 0264-9381. DOI: 10.1088/0264-9381/21/11/017 (cit. on pp. 12, 29).

[141]   E. Kajari, N. L. Harshman, E. M. Rasel, S. Stenholm, G. Süßmann, and W. P. Schleich. "Inertial and Gravitational Mass in Quantum Mechanics." en. In: *Applied Physics B* 100.1 (July 2010), pp. 43–60. ISSN: 0946-2171, 1432-0649. DOI: 10.1007/s00340-010-4085-8 (cit. on pp. 12, 29).

[142]   Magdalena Zych and Časlav Brukner. "Quantum Formulation of the Einstein Equivalence Principle." en. In: *Nature Physics* (Aug. 2018). ISSN: 1745-2473, 1745-2481. DOI: 10.1038/s41567-018-0197-6 (cit. on p. 12).

[143]   Achim Peters, Keng Yeow Chung, and Steven Chu. "Measurement of Gravitational Acceleration by Dropping Atoms." en. In: *Nature* 400.6747 (Aug. 1999), pp. 849–852. ISSN: 1476-4687. DOI: 10.1038/23655 (cit. on pp. 12, 24).

[144]   S Merlet, Q Bodart, N Malossi, A Landragin, F Pereira Dos Santos, O Gitlein, and L Timmen. "Comparison between Two Mobile Absolute Gravimeters: Optical versus Atomic Interferometers." en. In: *Metrologia* 47.4 (Aug. 2010), pp. L9–L11. ISSN: 0026-1394, 1681-7575. DOI: 10.1088/0026-1394/47/4/L01 (cit. on p. 12).

[145]   Sebastian Fray and Martin Weitz. "Atom-Based Test of the Equivalence Principle." In: *Space Science Reviews* 148.1 (Dec. 2009), pp. 225–232. ISSN: 1572-9672. DOI: 10.1007/s11214-009-9566-x (cit. on p. 12).

[146]   A. Bonnin, N. Zahzam, Y. Bidel, and A. Bresson. "Simultaneous Dual-Species Matter-Wave Accelerometer." en. In: *Physical Review A* 88.4 (Oct. 2013). ISSN: 1050-2947, 1094-1622. DOI: 10.1103/PhysRevA.88.043615 (cit. on p. 12).

[147]   C. C. N. Kuhn, G. D. McDonald, K. S. Hardman, S. Bennetts, P. J. Everitt, P. A. Altin, J. E. Debs, J. D. Close, and N. P. Robins. "A Bose-Condensed, Simultaneous Dual-Species Mach–Zehnder Atom Interferometer." en. In: *New Journal of Physics* 16.7 (2014), p. 073035. ISSN: 1367-2630. DOI: 10.1088/1367-2630/16/7/073035 (cit. on p. 12).

[148]   Lin Zhou, Shitong Long, Biao Tang, Xi Chen, Fen Gao, Wencui Peng, Weitao Duan, Jiaqi Zhong, Zongyuan Xiong, Jin Wang, Yuanzhong Zhang, and Mingsheng Zhan. "Test of Equivalence Principle at 10^{-8} Level by a Dual-Species Double-Diffraction Raman Atom Interferometer." en. In: *Physical Review Letters* 115.1 (July 2015). ISSN: 0031-9007, 1079-7114. DOI: 10.1103/PhysRevLett.115.013004 (cit. on pp. 12, 30).

[149]   D. Schlippert, J. Hartwig, H. Albers, L. L. Richardson, C. Schubert, A. Roura, W. P. Schleich, W. Ertmer, and E. M. Rasel. "Quantum Test of the Universality of Free Fall." en. In: *Physical Review Letters* 112.20 (May 2014). ISSN: 0031-9007, 1079-7114. DOI: 10.1103/PhysRevLett.112.203002 (cit. on p. 12).

[150]   M. G. Tarallo, T. Mazzoni, N. Poli, D. V. Sutyrin, X. Zhang, and G. M. Tino. "Test of Einstein Equivalence Principle for o-Spin and Half-Integer-Spin Atoms: Search for Spin-Gravity Coupling Effects." en. In: *Physical Review Letters* 113.2 (July 2014). ISSN: 0031-9007, 1079-7114. DOI: 10.1103/PhysRevLett.113.023005 (cit. on pp. 12, 29).

[151] Xiao-Chun Duan, Xiao-Bing Deng, Min-Kang Zhou, Ke Zhang, Wen-Jie
       Xu, Feng Xiong, Yao-Yao Xu, Cheng-Gang Shao, Jun Luo, and Zhong-Kun
       Hu. "Test of the Universality of Free Fall with Atoms in Different Spin
       Orientations." en. In: *Physical Review Letters* 117.2 (July 2016), p. 023001. ISSN:
       0031-9007, 1079-7114. DOI: 10.1103/PhysRevLett.117.023001 (cit. on pp. 12,
       29).

[152] Ke Zhang, Min-Kang Zhou, Yuan Cheng, Le-Le Chen, Qin Luo, Wen-Jie
       Xu, Lu-Shuai Cao, Xiao-Chun Duan, and Zhong-Kun Hu. "Testing the
       Universality of Free Fall at 10^{-10} Level by Comparing the Atoms in Different
       Hyperfine States with Bragg Diffraction." In: (May 2018). arXiv: 1805.07758
       (cit. on pp. 12, 29).

[153] G. Rosi, G. D'Amico, L. Cacciapuoti, F. Sorrentino, M. Prevedelli, M. Zych,
       Č. Brukner, and G. M. Tino. "Quantum Test of the Equivalence Principle
       for Atoms in Coherent Superposition of Internal Energy States." en. In:
       Nature Communications 8 (June 2017), p. 15529. ISSN: 2041-1723. DOI: 10.1038/
       ncomms15529 (cit. on pp. 12, 29).

[154] Remi Geiger and Michael Trupke. "Proposal for a Quantum Test of the
       Weak Equivalence Principle with Entangled Atomic Species." en. In: *Physical
       Review Letters* 120.4 (Jan. 2018). ISSN: 0031-9007, 1079-7114. DOI: 10.1103/
       PhysRevLett.120.043602 (cit. on pp. 12, 29).

[155] Michael A. Hohensee, Holger Müller, and R. B. Wiringa. "Equivalence
       Principle and Bound Kinetic Energy." en. In: *Physical Review Letters* 111.15
       (Oct. 2013). ISSN: 0031-9007, 1079-7114. DOI: 10.1103/PhysRevLett.111.
       151102 (cit. on pp. 12, 18).

[156] J. Hartwig, S. Abend, C. Schubert, D. Schlippert, H. Ahlers, K. Posso-Trujillo,
       N. Gaaloul, W. Ertmer, and E. M. Rasel. "Testing the Universality of Free
       Fall with Rubidium and Ytterbium in a Very Large Baseline Atom Interfer-
       ometer." en. In: *New Journal of Physics* 17.3 (2015), p. 035011. ISSN: 1367-2630.
       DOI: 10.1088/1367-2630/17/3/035011 (cit. on pp. 12, 30, 31).

[157] Chris Overstreet, Peter Asenbaum, Tim Kovachy, Remy Notermans, Jason
       M. Hogan, and Mark A. Kasevich. "Effective Inertial Frame in an Atom
       Interferometric Test of the Equivalence Principle." In: (Nov. 2017). arXiv:
       1711.09986 (cit. on pp. 12, 15, 30).

[158] Peter Asenbaum, Chris Overstreet, Minjeong Kim, Joseph Curti, and Mark A.
       Kasevich. "Atom-Interferometric Test of the Equivalence Principle at the
       10^{-12} Level." In: (May 2020). arXiv: 2005.11624 (cit. on pp. 12, 15, 29, 30).

[159] C. Jentsch, T. Müller, E. M. Rasel, and W. Ertmer. "HYPER: A Satellite Mis-
       sion in Fundamental Physics Based on High Precision Atom Interferometry."
       en. In: *General Relativity and Gravitation* 36.10 (Oct. 2004), pp. 2197–2221. ISSN:
       0001-7701. DOI: 10.1023/B:GERG.0000046179.26175.fa (cit. on p. 12).

[160] G. M. Tino et al. "Precision Gravity Tests with Atom Interferometry in
       Space." In: *Nuclear Physics B - Proceedings Supplements*. Proceedings of the IV
       International Conference on Particle and Fundamental Physics in Space 243-
       244 (Oct. 2013), pp. 203–217. ISSN: 0920-5632. DOI: 10.1016/j.nuclphysbps.
       2013.09.023 (cit. on p. 12).

[161] A. Trimeche, B. Battelier, D. Becker, A. Bertoldi, P. Bouyer, C. Braxmaier, E. Charron, R. Corgier, M. Cornelius, K. Douch, N. Gaaloul, S. Herrmann, J. Müller, E. Rasel, C. Schubert, H. Wu, and F. Pereira dos Santos. "Concept Study and Preliminary Design of a Cold Atom Interferometer for Space Gravity Gradiometry." In: (Mar. 2019). arXiv: 1903.09828 (cit. on p. 12).

[162] Kai Bongs et al. "Development of a Strontium Optical Lattice Clock for the SOC Mission on the ISS." en. In: *Comptes Rendus Physique*. The Measurement of Time / La Mesure Du Temps 16.5 (June 2015), pp. 553–564. ISSN: 1631-0705. DOI: 10.1016/j.crhy.2015.03.009 (cit. on p. 12).

[163] L. Cacciapuoti and Ch. Salomon. "Space Clocks and Fundamental Tests: The ACES Experiment." en. In: *The European Physical Journal Special Topics* 172.1 (June 2009), pp. 57–68. ISSN: 1951-6355, 1951-6401. DOI: 10.1140/epjst/e2009-01041-7 (cit. on pp. 12, 17).

[164] Luigi Cacciapuoti. "I-SOC Scientific Requirements." en. In: (2017), p. 107 (cit. on p. 12).

[165] S. Origlia, M. S. Pramod, S. Schiller, Y. Singh, K. Bongs, R. Schwarz, A. Al-Masoudi, S. Dörscher, S. Herbers, S. Häfner, U. Sterr, and Ch. Lisdat. "Towards an Optical Clock for Space: Compact, High-Performance Optical Lattice Clock Based on Bosonic Atoms." en. In: *Physical Review A* 98.5 (Nov. 2018), p. 053443. ISSN: 2469-9926, 2469-9934. DOI: 10.1103/PhysRevA.98.053443 (cit. on p. 12).

[166] Jason Williams, Sheng-wey Chiow, Nan Yu, and Holger Müller. "Quantum Test of the Equivalence Principle and Space-Time Aboard the International Space Station." en. In: *New Journal of Physics* 18.2 (2016), p. 025018. ISSN: 1367-2630. DOI: 10.1088/1367-2630/18/2/025018 (cit. on p. 12).

[167] Jason M. Hogan and Mark A. Kasevich. "Atom-Interferometric Gravitational-Wave Detection Using Heterodyne Laser Links." en. In: *Physical Review A* 94.3 (Sept. 2016). ISSN: 2469-9926, 2469-9934. DOI: 10.1103/PhysRevA.94.033632 (cit. on pp. 12, 25–27, 31).

[168] ESA. *STE-QUEST Assessment Study Report*. Tech. rep. ESA/SRE(2013)6. European Space Agency, 2013 (cit. on pp. 12, 13).

[169] Yannick Bidel, Olivier Carraz, Renée Charrière, Malo Cadoret, Nassim Zahzam, and Alexandre Bresson. "Compact Cold Atom Gravimeter for Field Applications." In: *Applied Physics Letters* 102.14 (Apr. 2013), p. 144107. ISSN: 0003-6951. DOI: 10.1063/1.4801756 (cit. on p. 13).

[170] Zhong-Kun Hu, Bu-Liang Sun, Xiao-Chun Duan, Min-Kang Zhou, Le-Le Chen, Su Zhan, Qiao-Zhen Zhang, and Jun Luo. "Demonstration of an Ultrahigh-Sensitivity Atom-Interferometry Absolute Gravimeter." In: *Physical Review A* 88.4 (Oct. 2013), p. 043610. DOI: 10.1103/PhysRevA.88.043610 (cit. on p. 13).

[171] C. Freier, M. Hauth, V. Schkolnik, B. Leykauf, M. Schilling, H. Wziontek, H.-G. Scherneck, J. Müller, and A. Peters. "Mobile Quantum Gravity Sensor with Unprecedented Stability." en. In: *Journal of Physics: Conference Series* 723 (June 2016), p. 012050. ISSN: 1742-6596. DOI: 10.1088/1742-6596/723/1/012050 (cit. on p. 13).

[172] B. Fang, I. Dutta, P. Gillot, D. Savoie, J. Lautier, B. Cheng, C. L. Garrido Alzar, R. Geiger, S. Merlet, F. Pereira Dos Santos, and A. Landragin. "Metrology with Atom Interferometry: Inertial Sensors from Laboratory to Field Applications." en. In: *Journal of Physics: Conference Series* 723 (June 2016), p. 012049. ISSN: 1742-6596. DOI: 10.1088/1742-6596/723/1/012049 (cit. on p. 13).

[173] Guochang Xu, ed. *Sciences of Geodesy - I*. en. Berlin, Heidelberg: Springer Berlin Heidelberg, 2010. DOI: 10.1007/978-3-642-11741-1 (cit. on p. 13).

[174] R. P. Middlemiss, A. Samarelli, D. J. Paul, J. Hough, S. Rowan, and G. D. Hammond. "Measurement of the Earth Tides with a MEMS Gravimeter." en. In: *Nature* 531.7596 (Mar. 2016), pp. 614–617. ISSN: 1476-4687. DOI: 10.1038/nature17397 (cit. on p. 13).

[175] Vincent Ménoret, Pierre Vermeulen, Nicolas Le Moigne, Sylvain Bonvalot, Philippe Bouyer, Arnaud Landragin, and Bruno Desruelle. "Gravity Measurements below 10 -9 g with a Transportable Absolute Quantum Gravimeter." En. In: *Scientific Reports* 8.1 (Aug. 2018), p. 12300. ISSN: 2045-2322. DOI: 10.1038/s41598-018-30608-1 (cit. on p. 13).

[176] AOsense. *AOSense, Inc.* en-US. URL: https://aosense.com/ (cit. on p. 13).

[177] Muquans. *Muquans - Precision Quantum Sensors*. en-US. URL: https://www.muquans.com/ (cit. on p. 13).

[178] B. Barrett, P. Cheiney, B. Battelier, F. Napolitano, and P. Bouyer. "Multidimensional Atom Optics and Interferometry." en. In: *Physical Review Letters* 122.4 (Feb. 2019). ISSN: 0031-9007, 1079-7114. DOI: 10.1103/PhysRevLett.122.043604 (cit. on pp. 13, 29).

[179] T. van Zoest et al. "Bose-Einstein Condensation in Microgravity." en. In: *Science* 328.5985 (June 2010), pp. 1540–1543. ISSN: 0036-8075, 1095-9203. DOI: 10.1126/science.1189164 (cit. on pp. 13, 29).

[180] H. Müntinga et al. "Interferometry with Bose-Einstein Condensates in Microgravity." en. In: *Physical Review Letters* 110.9 (Feb. 2013). ISSN: 0031-9007, 1079-7114. DOI: 10.1103/PhysRevLett.110.093602 (cit. on pp. 13, 29).

[181] Jan Rudolph, Waldemar Herr, Christoph Grzeschik, Tammo Sternke, Alexander Grote, Manuel Popp, Dennis Becker, Hauke Müntinga, Holger Ahlers, Achim Peters, Claus Lämmerzahl, Klaus Sengstock, Naceur Gaaloul, Wolfgang Ertmer, and Ernst M. Rasel. "A High-Flux BEC Source for Mobile Atom Interferometers." en. In: *New Journal of Physics* 17.6 (2015), p. 065001. ISSN: 1367-2630. DOI: 10.1088/1367-2630/17/6/065001 (cit. on pp. 13, 29).

[182] Christian Vogt, Marian Woltmann, Sven Herrmann, Claus Lämmerzahl, Henning Albers, Dennis Schlippert, Ernst M. Rasel, and PRIMUS. "Evaporative Cooling from an Optical Dipole Trap in Microgravity." In: *Physical Review A* 101.1 (Jan. 2020), p. 013634. DOI: 10.1103/PhysRevA.101.013634 (cit. on pp. 13, 29).

[183] Dennis Becker et al. "Space-Borne Bose–Einstein Condensation for Precision Interferometry." En. In: *Nature* 562.7727 (Oct. 2018), p. 391. ISSN: 1476-4687. DOI: 10.1038/s41586-018-0605-1 (cit. on pp. 13, 15, 29, 31).

[184]   R Corgier, S Amri, W Herr, H Ahlers, J Rudolph, D Guéry-Odelin, E M Rasel, E Charron, and N Gaaloul. "Fast Manipulation of Bose–Einstein Condensates with an Atom Chip." en. In: *New Journal of Physics* 20.5 (May 2018), p. 055002. ISSN: 1367-2630. DOI: 10.1088/1367-2630/aabdfc (cit. on p. 13).

[185]   Christian Lotz. *Novel Active Driven Drop Tower Facility for Microgravity Experiments Investigating Production Technologies on the Example of Substrate-Free Additive Manufacturing | Elsevier Enhanced Reader*. en. 18. DOI: 10.1016/j.asr.2018.01.010 (cit. on p. 13).

[186]   Gabriel Condon, Martin Rabault, Brynle Barrett, Laure Chichet, Romain Arguel, Hodei Eneriz-Imaz, Devang Naik, Andrea Bertoldi, Baptiste Battelier, Arnaud Landragin, and Philippe Bouyer. "All-Optical Bose-Einstein Condensates in Microgravity." In: (June 2019). arXiv: 1906.10063 (cit. on pp. 13, 29).

[187]   Ethan R. Elliott, Markus C. Krutzik, Jason R. Williams, Robert J. Thompson, and David C. Aveline. "NASA's Cold Atom Lab (CAL): System Development and Ground Test Status." En. In: *npj Microgravity* 4.1 (Aug. 2018), p. 16. ISSN: 2373-8065. DOI: 10.1038/s41526-018-0049-9 (cit. on pp. 13, 29, 31).

[188]   David C. Aveline, Jason R. Williams, Ethan R. Elliott, Chelsea Dutenhoffer, James R. Kellogg, James M. Kohel, Norman E. Lay, Kamal Oudrhiri, Robert F. Shotwell, Nan Yu, and Robert J. Thompson. "Observation of Bose–Einstein Condensates in an Earth-Orbiting Research Lab." en. In: *Nature* 582.7811 (June 2020), pp. 193–197. ISSN: 1476-4687. DOI: 10.1038/s41586-020-2346-1 (cit. on pp. 13, 29).

[189]   Kai Frye et al. "The Bose-Einstein Condensate and Cold Atom Laboratory." In: (Dec. 2019). arXiv: 1912.04849 (cit. on pp. 13, 29, 31).

[190]   Albert Roura. "Circumventing Heisenberg's Uncertainty Principle in Atom Interferometry Tests of the Equivalence Principle." en. In: *Physical Review Letters* 118.16 (Apr. 2017). ISSN: 0031-9007, 1079-7114. DOI: 10.1103/PhysRevLett.118.160401 (cit. on pp. 14, 15).

[191]   D N Aguilera et al. "STE-QUEST—Test of the Universality of Free Fall Using Cold Atom Interferometry." en. In: *Classical and Quantum Gravity* 31.11 (June 2014), p. 115010. ISSN: 0264-9381, 1361-6382. DOI: 10.1088/0264-9381/31/11/115010 (cit. on pp. 13, 15, 29).

[192]   J. P. Blaser. "Can the Equivalence Principle Be Tested with Freely Orbiting Masses?" en. In: *Classical and Quantum Gravity* 18.13 (June 2001), pp. 2509–2514. ISSN: 0264-9381. DOI: 10.1088/0264-9381/18/13/313 (cit. on p. 15).

[193]   G. D'Amico, G. Rosi, S. Zhan, L. Cacciapuoti, M. Fattori, and G. M. Tino. "Canceling the Gravity Gradient Phase Shift in Atom Interferometry." en. In: *Physical Review Letters* 119.25 (Dec. 2017). ISSN: 0031-9007, 1079-7114. DOI: 10.1103/PhysRevLett.119.253201 (cit. on p. 15).

[194]   Robin Corgier. "Engineered Atomic States for Precision Interferometry." eng. PhD thesis. Leibniz Universität Hannover, 2019. DOI: http://dx.doi.org/10.15488/5152 (cit. on pp. 15, 31).

[195]   S. Amri, R. Corgier, D. Sugny, E. M. Rasel, N. Gaaloul, and E. Charron. "Optimal Control of the Transport of Bose-Einstein Condensates with Atom Chips." En. In: *Scientific Reports* 9.1 (Mar. 2019), p. 5346. ISSN: 2045-2322. DOI: 10.1038/s41598-019-41784-z (cit. on p. 15).

[196]   Pink Floyd. *Time*. Abbey Road Studios (London, UK), 1973 (cit. on p. 17).

[197]   Herbert E. Ives and G. R. Stilwell. "An Experimental Study of the Rate of a Moving Atomic Clock." en. In: *Journal of the Optical Society of America* 28.7 (July 1938), p. 215. ISSN: 0030-3941. DOI: 10.1364/JOSA.28.000215 (cit. on p. 17).

[198]   R. V. Pound and J. L. Snider. "Effect of Gravity on Nuclear Resonance." In: *Physical Review Letters* 13.18 (Nov. 1964), pp. 539–540. DOI: 10.1103/PhysRevLett.13.539 (cit. on p. 17).

[199]   James William Brault. "The Gravitational Red Shift in the Solar Spectrum." PhD thesis. 1962 (cit. on p. 17).

[200]   J. C. Hafele and Richard E. Keating. "Around-the-World Atomic Clocks: Predicted Relativistic Time Gains." en. In: *Science* 177.4044 (July 1972), pp. 166–168. ISSN: 0036-8075, 1095-9203. DOI: 10.1126/science.177.4044.166 (cit. on p. 17).

[201]   J. C. Hafele and Richard E. Keating. "Around-the-World Atomic Clocks: Observed Relativistic Time Gains." en. In: *Science* 177.4044 (July 1972), pp. 168–170. ISSN: 0036-8075, 1095-9203. DOI: 10.1126/science.177.4044.168 (cit. on pp. 17, 22).

[202]   R. F. C. Vessot, M. W. Levine, E. M. Mattison, E. L. Blomberg, T. E. Hoffman, G. U. Nystrom, B. F. Farrel, R. Decher, P. B. Eby, C. R. Baugher, J. W. Watts, D. L. Teuber, and F. D. Wills. "Test of Relativistic Gravitation with a Space-Borne Hydrogen Maser." en. In: *Physical Review Letters* 45.26 (Dec. 1980), pp. 2081–2084. ISSN: 0031-9007. DOI: 10.1103/PhysRevLett.45.2081 (cit. on pp. 17, 18, 22).

[203]   J. Guéna, M. Abgrall, D. Rovera, P. Rosenbusch, M. E. Tobar, Ph. Laurent, A. Clairon, and S. Bize. "Improved Tests of Local Position Invariance Using ^{87}Rb and ^{133}Cs Fountains." In: *Physical Review Letters* 109.8 (Aug. 2012), p. 080801. DOI: 10.1103/PhysRevLett.109.080801 (cit. on p. 17).

[204]   Jean-Philippe Uzan. "Varying Constants, Gravitation and Cosmology." en. In: *Living Reviews in Relativity* 14.1 (Mar. 2011), p. 2. ISSN: 1433-8351. DOI: 10.12942/lrr-2011-2 (cit. on p. 17).

[205]   Neil Ashby. "Relativity in the Global Positioning System." en. In: *Living Reviews in Relativity* 6.1 (Jan. 2003), p. 1. ISSN: 1433-8351. DOI: 10.12942/lrr-2003-1 (cit. on p. 18).

[206]   P. Delva, N. Puchades, E. Schönemann, F. Dilssner, C. Courde, S. Bertone, F. Gonzalez, A. Hees, Ch. Le Poncin-Lafitte, F. Meynadier, R. Prieto-Cerdeira, B. Sohet, J. Ventura-Traveset, and P. Wolf. "Gravitational Redshift Test Using Eccentric *Galileo* Satellites." en. In: *Physical Review Letters* 121.23 (Dec. 2018), p. 231101. ISSN: 0031-9007, 1079-7114. DOI: 10.1103/PhysRevLett.121.231101 (cit. on pp. 18, 22).

[207] Holger Müller, Achim Peters, and Steven Chu. "Müller, Peters & Chu Reply." en. In: *Nature* 467.7311 (Sept. 2010), E2–E2. ISSN: 1476-4687. DOI: 10.1038/nature09341 (cit. on p. 18).

[208] Supurna Sinha and Joseph Samuel. "Atom Interferometry and the Gravitational Redshift." en. In: *Classical and Quantum Gravity* 28.14 (2011), p. 145018. ISSN: 0264-9381. DOI: 10.1088/0264-9381/28/14/145018 (cit. on pp. 18–22).

[209] Felix Finster, Olaf Müller, Marc Nardmann, Jürgen Tolksdorf, and Eberhard Zeidler, eds. *Quantum Field Theory and Gravity*. en. Basel: Springer Basel, 2012. DOI: 10.1007/978-3-0348-0043-3 (cit. on pp. 18, 19).

[210] Wolfgang P. Schleich, Daniel M. Greenberger, and Ernst M. Rasel. "Redshift Controversy in Atom Interferometry: Representation Dependence of the Origin of Phase Shift." In: *Physical Review Letters* 110.1 (Jan. 2013), p. 010401. DOI: 10.1103/PhysRevLett.110.010401 (cit. on p. 18).

[211] Magdalena Zych, Fabio Costa, Igor Pikovski, and Časlav Brukner. "Quantum Interferometric Visibility as a Witness of General Relativistic Proper Time." en. In: *Nature Communications* 2 (Oct. 2011), p. 505. ISSN: 2041-1723. DOI: 10.1038/ncomms1498 (cit. on pp. 19–22).

[212] Igor Pikovski. "Macroscopic Quantum Systems and Gravitational Phenomena." PhD Thesis. Universität Wien, 2014 (cit. on p. 19).

[213] Richard H. Parker, Chenghui Yu, Weicheng Zhong, Brian Estey, and Holger Müller. "Measurement of the Fine-Structure Constant as a Test of the Standard Model." en. In: *Science* 360.6385 (Apr. 2018), pp. 191–195. ISSN: 0036-8075, 1095-9203. DOI: 10.1126/science.aap7706 (cit. on pp. 20, 29).

[214] Pierre Cladé, François Nez, François Biraben, and Saïda Guellati-Khelifa. "State of the Art in the Determination of the Fine-Structure Constant and the Ratio h/m_u." en. In: *Comptes Rendus Physique*. The New International System of Units / Le Nouveau Système International d'unités 20.1 (Jan. 2019), pp. 77–91. ISSN: 1631-0705. DOI: 10.1016/j.crhy.2018.12.003 (cit. on p. 20).

[215] Janna Levin. *The sound the universe makes*. TED talk. Longbeach California. Mar. 2011. URL: https://www.ted.com/talks/janna_levin_the_sound_the_universe_makes (cit. on p. 23).

[216] Peter R. Saulson. "Josh Goldberg and the Physical Reality of Gravitational Waves." en. In: *General Relativity and Gravitation* 43.12 (Dec. 2011), pp. 3289–3299. ISSN: 1572-9532. DOI: 10.1007/s10714-011-1237-z (cit. on p. 23).

[217] Shin'ichiro Ando et al. "Colloquium: Multimessenger Astronomy with Gravitational Waves and High-Energy Neutrinos." In: *Reviews of Modern Physics* 85.4 (Oct. 2013), pp. 1401–1420. DOI: 10.1103/RevModPhys.85.1401 (cit. on p. 23).

[218] Dr Karsten Amaro. "The Gravitational Universe." en. In: (2013), p. 20 (cit. on p. 23).

[219] R. Abbott et al. "GWTC-1: A Gravitational-Wave Transient Catalog of Compact Binary Mergers Observed by LIGO and Virgo during the First and Second Observing Runs." In: *Physical Review X* 9.3 (Sept. 2019), p. 031040. DOI: 10.1103/PhysRevX.9.031040 (cit. on p. 23).

[220] B. P. Abbott et al. "GW170817: Observation of Gravitational Waves from a Binary Neutron Star Inspiral." In: *Physical Review Letters* 119.16 (Oct. 2017), p. 161101. DOI: 10.1103/PhysRevLett.119.161101 (cit. on p. 23).

[221] A. Goldstein et al. "An Ordinary Short Gamma-Ray Burst with Extraordinary Implications: Fermi -GBM Detection of GRB 170817A." en. In: *The Astrophysical Journal* 848.2 (Oct. 2017), p. L14. ISSN: 2041-8205. DOI: 10.3847/2041-8213/aa8f41 (cit. on p. 23).

[222] B. P. Abbott et al. "Prospects for Observing and Localizing Gravitational-Wave Transients with Advanced LIGO, Advanced Virgo and KAGRA." en. In: *Living Reviews in Relativity* 21.1 (Apr. 2018), p. 3. ISSN: 1433-8351. DOI: 10.1007/s41114-018-0012-9 (cit. on p. 23).

[223] M. Punturo et al. "The Einstein Telescope: A Third-Generation Gravitational Wave Observatory." en. In: *Classical and Quantum Gravity* 27.19 (Sept. 2010), p. 194002. ISSN: 0264-9381. DOI: 10.1088/0264-9381/27/19/194002 (cit. on pp. 23, 25).

[224] Scott A. Hughes. "A Brief Survey of LISA Sources and Science." In: *AIP Conference Proceedings* 873.1 (Nov. 2006), pp. 13–20. ISSN: 0094-243X. DOI: 10.1063/1.2405017 (cit. on p. 23).

[225] Klaus Abich et al. "In-Orbit Performance of the GRACE Follow-on Laser Ranging Interferometer." In: *Physical Review Letters* 123.3 (July 2019), p. 031101. DOI: 10.1103/PhysRevLett.123.031101 (cit. on p. 23).

[226] Armano et al. "Charge-Induced Force Noise on Free-Falling Test Masses: Results from LISA Pathfinder." In: *Physical Review Letters* 118.17 (Apr. 2017), p. 171101. DOI: 10.1103/PhysRevLett.118.171101 (cit. on p. 24).

[227] M Armano et al. "LISA Pathfinder Platform Stability and Drag-Free Performance." en. In: *PHYS. REV. D* (2019), p. 14 (cit. on pp. 24, 29).

[228] B. B. P. Perera et al. "The International Pulsar Timing Array: Second Data Release." en. In: *Monthly Notices of the Royal Astronomical Society* 490.4 (Dec. 2019), pp. 4666–4687. ISSN: 0035-8711. DOI: 10.1093/mnras/stz2857 (cit. on p. 24).

[229] Alberto Sesana. "Prospects for Multiband Gravitational-Wave Astronomy after GW150914." en. In: *Physical Review Letters* 116.23 (June 2016). ISSN: 0031-9007, 1079-7114. DOI: 10.1103/PhysRevLett.116.231102 (cit. on p. 24).

[230] Manuel Arca Sedda et al. "The Missing Link in Gravitational-Wave Astronomy: Discoveries Waiting in the Decihertz Range." In: (May 2020). arXiv: 1908.11375 (cit. on p. 24).

[231] Kevin A. Kuns, Hang Yu, Yanbei Chen, and Rana X. Adhikari. "Astrophysics and Cosmology with a Decihertz Gravitational-Wave Detector: TianGO." en. In: *arXiv:1908.06004 [astro-ph, physics:gr-qc]* (June 2020). arXiv: 1908.06004 [astro-ph, physics:gr-qc] (cit. on p. 24).

[232]   Yousef Abou El-Neaj et al. "AEDGE: Atomic Experiment for Dark Matter and Gravity Exploration in Space." In: (Oct. 2019). arXiv: 1908.00802 (cit. on p. 24).

[233]   Peter W. Graham and Sunghoon Jung. "Localizing Gravitational Wave Sources with Single-Baseline Atom Interferometers." en. In: *Physical Review D* 97.2 (Jan. 2018). ISSN: 2470-0010, 2470-0029. DOI: 10.1103/PhysRevD.97.024052 (cit. on p. 24).

[234]   T. L. Gustavson, A. Landragin, and M. A. Kasevich. "Rotation Sensing with a Dual Atom-Interferometer Sagnac Gyroscope." en. In: *Classical and Quantum Gravity* 17.12 (June 2000), pp. 2385–2398. ISSN: 0264-9381. DOI: 10.1088/0264-9381/17/12/311 (cit. on p. 24).

[235]   B. Linet and P. Tourrenc. "Changement de phase dans un champ de gravitation: Possibilité de détection interférentielle." fr. In: *Canadian Journal of Physics* 54.11 (June 1976), pp. 1129–1133. ISSN: 0008-4204, 1208-6045. DOI: 10.1139/p76-136 (cit. on p. 24).

[236]   Raymond Y. Chiao and Achilles D. Speliotopoulos. "Towards MIGO, the Matter-Wave Interferometric Gravitational-Wave Observatory, and the Intersection of Quantum Mechanics with General Relativity." In: *Journal of Modern Optics* 51.6-7 (Apr. 2004), pp. 861–899. ISSN: 0950-0340. DOI: 10.1080/09500340408233603 (cit. on p. 24).

[237]   Albert Roura, Dieter R. Brill, B. L. Hu, Charles W. Misner, and William D. Phillips. "Gravitational Wave Detectors Based on Matter Wave Interferometers (MIGO) Are No Better than Laser Interferometers (LIGO)." In: *Physical Review D* 73.8 (Apr. 2006), p. 084018. DOI: 10.1103/PhysRevD.73.084018 (cit. on p. 24).

[238]   P. Delva, M. -C. Angonin, and P. Tourrenc. "A Comparison between Matter Wave and Light Wave Interferometers for the Detection of Gravitational Waves." en. In: *Physics Letters A* 357.4 (Sept. 2006), pp. 249–254. ISSN: 0375-9601. DOI: 10.1016/j.physleta.2006.04.103 (cit. on p. 24).

[239]   G. M. Tino and F. Vetrano. "Is It Possible to Detect Gravitational Waves with Atom Interferometers?" en. In: *Classical and Quantum Gravity* 24.9 (Apr. 2007), pp. 2167–2178. ISSN: 0264-9381. DOI: 10.1088/0264-9381/24/9/001 (cit. on p. 24).

[240]   Pan-Pan Wang, Yajie Wang, Yu-jie Tan, Cheng-Gang Shao, and Zhong-Kun Hu. "Establishing the Quasi-Inertial Reference System Based on Free-Falling Atom and Its Application on Gravity Experiments." en. In: *Classical and Quantum Gravity* (2020). ISSN: 0264-9381. DOI: 10.1088/1361-6382/ab81ce (cit. on p. 24).

[241]   Pacôme Delva and Ernst Rasel. "Matter Wave Interferometry and Gravitational Waves." In: *Journal of Modern Optics* 56.18-19 (Oct. 2009), pp. 1999–2004. ISSN: 0950-0340. DOI: 10.1080/09500340903326169 (cit. on p. 24).

[242]   Savas Dimopoulos, Peter W. Graham, Jason M. Hogan, Mark A. Kasevich, and Surjeet Rajendran. "Gravitational Wave Detection with Atom Interferometry." en. In: *Physics Letters B* 678.1 (July 2009), pp. 37–40. ISSN: 0370-2693. DOI: 10.1016/j.physletb.2009.06.011 (cit. on p. 24).

[243] M. Snadden, J. McGuirk, P. Bouyer, K. Haritos, and M. Kasevich. "Measurement of the Earth's Gravity Gradient with an Atom Interferometer-Based Gravity Gradiometer." en. In: *Physical Review Letters* 81.5 (Aug. 1998), pp. 971–974. ISSN: 0031-9007, 1079-7114. DOI: 10.1103/PhysRevLett.81.971 (cit. on p. 24).

[244] J. Le Gouët, P. Cheinet, J. Kim, D. Holleville, A. Clairon, A. Landragin, and F. Pereira Dos Santos. "Influence of Lasers Propagation Delay on the Sensitivity of Atom Interferometers." en. In: *The European Physical Journal D* 44.3 (Sept. 2007), pp. 419–425. ISSN: 1434-6060, 1434-6079. DOI: 10.1140/epjd/e2007-00218-2. arXiv: physics/0701023 (cit. on p. 25).

[245] Jason M. Hogan, David M. S. Johnson, Susannah Dickerson, Tim Kovachy, Alex Sugarbaker, Sheng-wey Chiow, Peter W. Graham, Mark A. Kasevich, Babak Saif, Surjeet Rajendran, Philippe Bouyer, Bernard D. Seery, Lee Feinberg, and Ritva Keski-Kuha. "An Atomic Gravitational Wave Interferometric Sensor in Low Earth Orbit (AGIS-LEO)." en. In: *General Relativity and Gravitation* 43.7 (July 2011), pp. 1953–2009. ISSN: 0001-7701, 1572-9532. DOI: 10.1007/s10714-011-1182-x (cit. on p. 25).

[246] Michael Hohensee, Shau-Yu Lan, Rachel Houtz, Cheong Chan, Brian Estey, Geena Kim, Pei-Chen Kuan, and Holger Müller. "Sources and Technology for an Atomic Gravitational Wave Interferometric Sensor." en. In: *General Relativity and Gravitation* 43.7 (July 2011), pp. 1905–1930. ISSN: 1572-9532. DOI: 10.1007/s10714-010-1118-x (cit. on p. 25).

[247] Jan Harms, Bram J. J. Slagmolen, Rana X. Adhikari, M. Coleman Miller, Matthew Evans, Yanbei Chen, Holger Müller, and Masaki Ando. "Low-Frequency Terrestrial Gravitational-Wave Detectors." In: *Physical Review D* 88.12 (Dec. 2013), p. 122003. DOI: 10.1103/PhysRevD.88.122003 (cit. on p. 25).

[248] M. Beccaria et al. "Relevance of Newtonian Seismic Noise for the VIRGO Interferometer Sensitivity." en. In: *Classical and Quantum Gravity* 15.11 (Nov. 1998), p. 3339. ISSN: 0264-9381. DOI: 10.1088/0264-9381/15/11/004 (cit. on p. 25).

[249] W. Chaibi, R. Geiger, B. Canuel, A. Bertoldi, A. Landragin, and P. Bouyer. "Low Frequency Gravitational Wave Detection with Ground-Based Atom Interferometer Arrays." en. In: *Physical Review D* 93.2 (Jan. 2016). ISSN: 2470-0010, 2470-0029. DOI: 10.1103/PhysRevD.93.021101 (cit. on p. 25).

[250] Ming-Sheng Zhan et al. "ZAIGA: Zhaoshan Long-Baseline Atom Interferometer Gravitation Antenna." In: *International Journal of Modern Physics D* 29.04 (May 2019), p. 1940005. ISSN: 0218-2718. DOI: 10.1142/S0218271819400054 (cit. on pp. 25, 30).

[251] B. Canuel et al. "Exploring Gravity with the MIGA Large Scale Atom Interferometer." En. In: *Scientific Reports* 8.1 (Sept. 2018), p. 14064. ISSN: 2045-2322. DOI: 10.1038/s41598-018-32165-z (cit. on p. 25).

[252]   Nan Yu and Massimo Tinto. "Gravitational Wave Detection with Single-Laser Atom Interferometers." en. In: *General Relativity and Gravitation* 43.7 (July 2011), pp. 1943–1952. ISSN: 1572-9532. DOI: 10.1007/s10714-010-1055-8 (cit. on p. 25).

[253]   S. Kolkowitz, I. Pikovski, N. Langellier, M. D. Lukin, R. L. Walsworth, and J. Ye. "Gravitational Wave Detection with Optical Lattice Atomic Clocks." en. In: *Physical Review D* 94.12 (Dec. 2016). ISSN: 2470-0010, 2470-0029. DOI: 10.1103/PhysRevD.94.124043 (cit. on p. 25).

[254]   Matthew A. Norcia, Julia R. K. Cline, and James K. Thompson. "Role of Atoms in Atomic Gravitational-Wave Detectors." en. In: *Physical Review A* 96.4 (Oct. 2017). ISSN: 2469-9926, 2469-9934. DOI: 10.1103/PhysRevA.96.042118 (cit. on p. 25).

[255]   Peter L. Bender. "Comparison of Atom Interferometry with Laser Interferometry for Gravitational Wave Observations in Space." en. In: *Physical Review D* 89.6 (Mar. 2014). ISSN: 1550-7998, 1550-2368. DOI: 10.1103/PhysRevD.89.062004 (cit. on p. 25).

[256]   Sheng-wey Chiow, Jason Williams, and Nan Yu. "Laser-Ranging Long-Baseline Differential Atom Interferometers for Space." en. In: *Physical Review A* 92.6 (Dec. 2015). ISSN: 1050-2947, 1094-1622. DOI: 10.1103/PhysRevA.92.063613 (cit. on p. 25).

[257]   Peter W. Graham, Jason M. Hogan, Mark A. Kasevich, Surjeet Rajendran, and Roger W. Romani. "Mid-Band Gravitational Wave Detection with Precision Atomic Sensors." In: (Nov. 2017). arXiv: 1711.02225 (cit. on pp. 25–27).

[258]   Jon Coleman. "MAGIS-100 at Fermilab." In: (Dec. 2018). arXiv: 1812.00482 (cit. on pp. 25, 30).

[259]   Peter W. Graham, Jason M. Hogan, Mark A. Kasevich, and Surjeet Rajendran. "Resonant Mode for Gravitational Wave Detectors Based on Atom Interferometry." en. In: *Physical Review D* 94.10 (Nov. 2016). ISSN: 2470-0010, 2470-0029. DOI: 10.1103/PhysRevD.94.104022 (cit. on p. 25).

[260]   C. Schubert, D. Schlippert, S. Abend, E. Giese, A. Roura, W. P. Schleich, W. Ertmer, and E. M. Rasel. "Scalable, Symmetric Atom Interferometer for Infrasound Gravitational Wave Detection." In: *arXiv:1909.01951 [quant-ph]* (Sept. 2019). arXiv: 1909.01951 [quant-ph] (cit. on p. 25).

[261]   Peter W. Graham, Jason M. Hogan, Mark A. Kasevich, and Surjeet Rajendran. "New Method for Gravitational Wave Detection with Atomic Sensors." en. In: *Physical Review Letters* 110.17 (Apr. 2013). ISSN: 0031-9007, 1079-7114. DOI: 10.1103/PhysRevLett.110.171102 (cit. on p. 25).

[262]   D. Savoie, M. Altorio, B. Fang, L. A. Sidorenkov, R. Geiger, and A. Landragin. "Interleaved Atom Interferometry for High-Sensitivity Inertial Measurements." In: *Science Advances* 4.12 (Dec. 2018). ISSN: 2375-2548. DOI: 10.1126/sciadv.aau7948 (cit. on p. 27).

[263] G. Rosi, F. Sorrentino, L. Cacciapuoti, M. Prevedelli, and G. M. Tino. "Precision Measurement of the Newtonian Gravitational Constant Using Cold Atoms." en. In: *Nature* 510.7506 (June 2014), pp. 518–521. ISSN: 0028-0836, 1476-4687. DOI: 10.1038/nature13433 (cit. on p. 29).

[264] Pierre Touboul et al. "Space Test of the Equivalence Principle: First Results of the MICROSCOPE Mission." en. In: *Classical and Quantum Gravity* 36.22 (Oct. 2019), p. 225006. ISSN: 0264-9381. DOI: 10.1088/1361-6382/ab4707 (cit. on pp. 29, 31).

[265] E. Wodey, D. Tell, E. M. Rasel, D. Schlippert, R. Baur, U. Kissling, B. Kölliker, M. Lorenz, M. Marrer, U. Schläpfer, M. Widmer, C. Ufrecht, S. Stuiber, and P. Fierlinger. "A Scalable High-Performance Magnetic Shield for Very Long Baseline Atom Interferometry." en. In: *Review of Scientific Instruments* 91.3 (Mar. 2020), p. 035117. ISSN: 0034-6748, 1089-7623. DOI: 10.1063/1.5141340 (cit. on p. 30).

[266] E. A. Alden, K. R. Moore, and A. E. Leanhardt. "Two-Photon $E1$-$M1$ Optical Clock." In: *Physical Review A* 90.1 (July 2014), p. 012523. DOI: 10.1103/PhysRevA.90.012523 (cit. on p. 30).

[267] Jan Rudolph, Thomas Wilkason, Megan Nantel, Hunter Swan, Connor M. Holland, Yijun Jiang, Benjamin E. Garber, Samuel P. Carman, and Jason M. Hogan. "Large Momentum Transfer Clock Atom Interferometry on the 689 Nm Intercombination Line of Strontium." In: (Oct. 2019). arXiv: 1910.05459 (cit. on p. 30).

[268] Christian Ufrecht. "Theoretical Approach to High-Precision Atom Interferometry." en. Dissertation. Universität Ulm, Aug. 2019. ISBN: 9781671434431. DOI: http://dx.doi.org/10.18725/OPARU-17923 (cit. on p. 30).

[269] P. Cheinet, B. Canuel, F. Pereira Dos Santos, A. Gauguet, F. Yver-Leduc, and A. Landragin. "Measurement of the Sensitivity Function in a Time-Domain Atomic Interferometer." In: *IEEE Transactions on Instrumentation and Measurement* 57.6 (June 2008), pp. 1141–1148. ISSN: 0018-9456. DOI: 10.1109/TIM.2007.915148 (cit. on p. 30).

[270] G. J. Dick. *Local Oscillator Induced Instabilities in Trapped Ion Frequency Standards*. Tech. rep. California Inst of Technology Pasadena CA Jet Propulsion Lab, 1987 (cit. on p. 30).

[271] Holger Müller, Sheng-wey Chiow, and Steven Chu. "Atom-Wave Diffraction between the Raman-Nath and the Bragg Regime: Effective Rabi Frequency, Losses, and Phase Shifts." en. In: *Physical Review A* 77.2 (Feb. 2008), p. 023609. ISSN: 1050-2947, 1094-1622. DOI: 10.1103/PhysRevA.77.023609 (cit. on p. 31).

[272] Jan-Niclas Siemß, Florian Fitzek, Sven Abend, Ernst M. Rasel, Naceur Gaaloul, and Klemens Hammerer. "Analytic Theory for Bragg Atom Interferometry Based on the Adiabatic Theorem." In: (Feb. 2020). arXiv: 2002.04588 (cit. on p. 31).

[273] C. J. Pethick and H. Smith. *Bose–Einstein Condensation in Dilute Gases*. Second. Cambridge: Cambridge University Press, 2008. ISBN: 978-0-521-84651-6. DOI: 10.1017/CBO9780511802850 (cit. on p. 31).

[274]   Florian Fitzek, Jan-Niclas Siemß, Stefan Seckmeyer, Holger Ahlers, Ernst M. Rasel, Klemens Hammerer, and Naceur Gaaloul. "Universal Atom Interferometer Simulator – Elastic Scattering Processes." In: (Feb. 2020). arXiv: 2002.05148 (cit. on p. 31).

[275]   Nikolaos K. Pavlis, Simon A. Holmes, Steve C. Kenyon, and John K. Factor. "The Development and Evaluation of the Earth Gravitational Model 2008 (EGM2008)." en. In: *Journal of Geophysical Research: Solid Earth* 117.B4 (2012). ISSN: 2156-2202. DOI: 10.1029/2011JB008916 (cit. on p. 31).

PUBLICATIONS

[P1]   Baptiste Battelier et al. "Exploring the Foundations of the Universe with Space Tests of the Equivalence Principle." In: (2019). URL: http://arxiv.org/abs/1908.11785 (cit. on pp. v, vi, 5, 13–15, 29–31).

[P2]   Sina Loriani, Christian Schubert, Dennis Schlippert, Wolfgang Ertmer, Franck Pereira Dos Santos, Ernst Maria Rasel, Naceur Gaaloul, and Peter Wolf. "Resolution of the Co-Location Problem in Satellite Quantum Tests of the Universality of Free Fall." In: (June 2020). URL: http://arxiv.org/abs/2006.08729 (cit. on pp. v, vi, 5, 13–15, 29–31, 57).

[P3]   Robin Corgier, Sina Loriani, Holger Ahlers, Katerine Posso-Trujillo, Christian Schubert, Ernst M. Rasel, Eric Charron, and Naceur Gaaloul. "Interacting quantum mixtures for precision atom interferometry." In: (2020). URL: http://arxiv.org/abs/2007.05007 (cit. on pp. v, vi, 5, 13–15, 31).

[P4]   Sina Loriani, Alexander Friedrich, Christian Ufrecht, Fabio Di Pumpo, Stephan Kleinert, Sven Abend, Naceur Gaaloul, Christian Meiners, Christian Schubert, Dorothee Tell, Étienne Wodey, Magdalena Zych, Wolfgang Ertmer, Albert Roura, Dennis Schlippert, Wolfgang P. Schleich, Ernst M. Rasel, and Enno Giese. "Interference of clocks: A quantum twin paradox." In: *Science Advances* 5.10 (Oct. 2019), eaax8966. ISSN: 2375-2548. DOI: 10.1126/sciadv.aax8966 (cit. on pp. v, vi, 4, 5, 11, 18–22, 30, 31, 57).

[P5]   Benjamin Canuel et al. "ELGAR - a European Laboratory for Gravitation and Atom-interferometric Research." In: *Classical and Quantum Gravity* (2020). ISSN: 0264-9381. DOI: 10.1088/1361-6382/aba80e (cit. on pp. v, vi, 5, 24–27, 30, 31).

[P6]   Benjamin Canuel et al. "Technologies for the ELGAR large scale atom interferometer array." In: (2020). URL: http://arxiv.org/abs/2007.04014 (cit. on pp. v, vi, 5, 25–27, 30, 31).

[P7]   Sina Loriani, Dennis Schlippert, Christian Schubert, Sven Abend, Holger Ahlers, Wolfgang Ertmer, Jan Rudolph, Jason M. Hogan, Mark A. Kasevich, Ernst M. Rasel, and Naceur Gaaloul. "Atomic source selection in space-borne gravitational wave detection." In: *New Journal of Physics* 21.6 (2019), p. 063030. DOI: 10.1088/1367-2630/ab22d0 (cit. on pp. v, vi, 5, 26, 27, 30, 31, 57).

The publications [P2, P4, P7] are attached in the following.

Resolution of the Co-Location Problem
in Satellite Quantum Tests of the Universality of Free Fall

Sina Loriani,[1, *] Christian Schubert,[1] Dennis Schlippert,[1] Wolfgang Ertmer,[1]
Franck Pereira Dos Santos,[2] Ernst Maria Rasel,[1] Naceur Gaaloul,[1, †] and Peter Wolf[2, ‡]

[1]*Institut für Quantenoptik, Leibniz Universität Hannover,*
Welfengarten 1, D-30167 Hannover, Germany
[2]*LNE-SYRTE, Observatoire de Paris, Université PSL, CNRS,*
Sorbonne Université 61 avenue de l'Observatoire 75014 Paris

A major challenge common to all Galilean drop tests of the Universality of Free Fall (UFF) is the required control over the initial kinematics of the two test masses upon release due to coupling to gravity gradients and rotations. In this work, we present a two-fold mitigation strategy to significantly alleviate the source preparation requirements in space-borne quantum tests of the UFF, using a compensation mechanism together with signal demodulation. To this end, we propose a scheme to reduce the gravity-gradient-induced uncertainties in an atom-interferometric experiment in a dedicated satellite mission and assess the experimental feasibility. We find that with moderate parameters, the requirements on the initial kinematics of the two masses can be relaxed by five orders of magnitude. This does not only imply a significantly reduced mission time but also allows to reduce the differential acceleration uncertainty caused by co-location imperfections below the 10^{-18} level.

I. INTRODUCTION

The Equivalence Principle is a remarkable concept of physics as it threads its way through scientific history, facilitating our understanding of gravity since the times of Galileo and Newton. Postulating the equivalence of inertial and gravitational mass implies the same free fall acceleration of objects of different composition, which has been labeled as the Weak Equivalence Principle or Universality of Free Fall (UFF). This notion, together with the principle of Relativity, today lays the foundation for General Relativity (GR), which constitutes the present perception of the macroscopic world. Even more, in its modern formulation comprising the UFF, Local Lorentz Invariance and Local Position Invariance, the Einstein Equivalence Principle (EEP) consolidates the assumptions required to comprehend gravity as a purely geometrical phenomenon and therefore serves as classification for gravitational theories [1]. Gravity is however the only fundamental force of nature that could not yet be integrated into the Standard Model, which explains particle phenomena on the microscopic scale with outstanding success, ranging from high-energy physics as observed in particle colliders to the ultra-cold realm of atom optics. Moreover, the significance of Dark Energy and Dark Matter for cosmological considerations supports the strive to unveil a more fundamental, general theory that yields General Relativity and the Standard Model as low energy limits. Attempts to find such a theory predict a violation of the EEP by introducing additional forces or fields that break the universal coupling of gravity to matter [2, 3]. As a consequence, despite its elegant simplicity and its hitherto unchallenged success, the Equivalence Principle

is subject to a large variation of validation tests including, for example, tests of the gravitational redshift of clocks, or of local Lorentz Invariance. Among those experiments, special attention is paid to the UFF, as Schiff's conjecture [4] and arguments based on energy conservation [5] indicate that violation of one of the constituents of EEP implies a violation of the others, and UFF tests are likely to be the most promising route to detect such a violation.

In experiments searching for a UFF violation, the figure of merit is given by the Eötvös parameter $\eta = \Delta a / g$ which quantifies the differential acceleration $\Delta a = \mathbf{n} \cdot (\mathbf{a}_A - \mathbf{a}_B)$ of two test masses A and B. The sensitive axis $\mathbf{n}$ denotes the direction along which the local gradient $g = \mathbf{n} \cdot \mathbf{g}$ of the gravitational field is measured. To date, all experiments have confirmed the UFF, corresponding to $\eta = 0$, with ever-increasing accuracies, which lie at $\delta\eta \sim 10^{-13}$ - 10^{-14} [6–8]. As a rather recent development, inertial-sensitive matter wave interferometry opened up a new pathway in testing the UFF by comparing the gravitation-induced phase shift for two different, freely falling matter waves. As such, they belong to the class of Galilean drop tests, as opposed to force balance experiments, and significantly extend the set of test-mass pairs to a wide range of atomic species. This is of great importance in constraining various composition-dependent violation scenarios such as dilaton models [3] motivated by String theory and parametrized frameworks such as the Standard Model Extension [2, 9]. Moreover, the coupling of gravity to matter can be investigated on a quantum-mechanical level by introducing spin degrees of freedom [10, 11], superposition of electronic states [12] and by studying the effect of gravity onto the internal dynamics [13–15]. So far, the UFF has been tested in the 10^{-7}-10^{-12}-range [11, 12, 16–21] in different atom interferometry setups with various isotopes and elements. Since the sensitivity scales with the free fall time of the atoms, large atomic fountain experiments and space-borne missions predict accuracies in the 10^{-15}

regime [22–25] and beyond [26], competing with the best classical tests [6–8].

It is, however, well known that the accuracy of drop tests is limited by the preparation of the two sources [27]. Indeed, any deviation from a uniform gravitational field leads to an acceleration that depends on the initial coordinates of a test mass, that is its initial position $\mathbf{r}_0$ and velocity $\mathbf{v}_0$, irrespective of whether that test mass is macroscopic or a matter wave. In particular, gravity gradients Γ, the second order derivative of the local gravitational field, give rise to a spurious (time-dependent) differential acceleration

$$\Delta \mathbf{a}_{GG} = \Gamma \left(\Delta \mathbf{r}_0 + \Delta \mathbf{v}_0 t \right) , \tag{1}$$

which, a priori, can not be distinguished from the linear acceleration that is to be measured. Consequently, in an experiment searching for minuscule violations of the UFF, the initial co-location of the two test masses in position $\Delta \mathbf{r}_0 = \mathbf{r}_{0,A} - \mathbf{r}_{0,B}$ and velocity $\Delta \mathbf{v}_0 = \mathbf{v}_{0,A} - \mathbf{v}_{0,B}$ has to be accurately determined, since uncertainties in the initial kinematics directly translate into a systematic uncertainty $\delta \Delta \mathbf{a}_{GG} = \Gamma \left(\delta \Delta \mathbf{r}_0 + \delta \Delta \mathbf{v}_0 t \right)$ in the measurement of the differential acceleration Δa [28].

In quantum tests of the UFF, the test masses are two carefully prepared wave packets. In phase space, these quantum states follow statistical distributions around experimentally realized means. Due to their statistical nature, a certain number ν of realizations is required in order to determine the mean differential position and velocity within desired uncertainty $\delta \Delta \mathbf{r}_0$ and $\delta \Delta \mathbf{v}_0$, given by

$$\delta \Delta r_{0,i} = \frac{\sigma_{r,0,i}}{\sqrt{\nu N/2}} \quad \text{and} \quad \delta \Delta v_{0,i} = \frac{\sigma_{v,0,i}}{\sqrt{\nu N/2}}, \tag{2}$$

where $\sigma_{r,0,i}$ and $\sigma_{v,0,i}$ denote the spatial extent and velocity width of one atomic ensemble, respectively [29]. N is the number of atoms in the atomic sample and $i = x, y, z$ denotes the spatial coordinate. One realization corresponds to imaging the atomic cloud in situ or after time-of-flight to infer spatial or velocity-related properties, respectively. Given that the number N of atoms per shot is limited and that the product of the sizes $\sigma_{r,0,i}$ and $\sigma_{v,0,i}$ is fundamentally constrained by Heisenberg's principle, the number ν of required verification shots can be fairly high and make up a large part of a measurement campaign. As an example, the uncertainty in the differential mean position $\delta \Delta \mathbf{r}_0$ of the two test masses has to be determined to the nm level to keep the effect of (1) below $\delta \eta = 10^{-15}$ in a space-borne UFF test [22]. For an atom interferometer with typical experimental parameters, this requires $\nu \sim 10^5$ shots with $N = 10^6$ atoms. In view of this unfavorable scaling, considering even more ambitious scenarios targeting $\delta \eta = 10^{-17}$ is futile, as the displacement would need to be controlled at the 10 pm level.

However, these long integration times can be avoided by artificially introducing accelerations that compensate the gravity gradient induced acceleration (1) and hence alleviate the dependency on the initial preparation, as proposed in [30] and already implemented in ground-based experiments [21, 25, 31]. In this work, we generalize this compensation technique to space-borne missions with time-dependent gravity gradients, and study its feasibility in combination with signal demodulation, in which one takes advantage of the spectral separation between the target signal and the gravity-gradient-induced perturbation [8]. With this two-fold strategy, the determination of the initial position (velocity) to the μm (μm/s) level is sufficient, compatible with state-of-the-art laboratory capabilities, such that only a few verification shots ν are required. Even more, this allows to integrate gravity gradient induced acceleration uncertainties below the 10^{-18} level in atom-interferometric tests of the UFF within favorable experimental parameter scales.

II. GRAVITY GRADIENT COMPENSATION

A. Model

The Mach-Zehnder configuration [32] is the most common atom interferometer geometry for inertial applications. A beam-splitter ($\pi/2$) light grating creates a coherent superposition of momentum states, which propagate freely for a duration T before being redirected by a mirror (π) pulse such that after an equal propagation time T, a final $\pi/2$ beam-splitter recombines the two wave packets. The two output ports of the interferometer differ in momentum, and their relative population is a function of the accumulated differential phase ϕ between the two interferometer branches. In our analysis, we follow a semi-classical description, in which the phase shift is evaluated by inserting the classical trajectories into the phase expression [33–35]

$$\begin{aligned} \phi = \ &\mathbf{r}_0 \cdot \mathbf{k}_{\text{eff}}^{(1)} \\ &- 2 \frac{\mathbf{r}_u(T) + \mathbf{r}_l(T)}{2} \cdot \mathbf{k}_{\text{eff}}^{(2)} \\ &+ \frac{\mathbf{r}_u(2T) + \mathbf{r}_l(2T)}{2} \cdot \mathbf{k}_{\text{eff}}^{(3)} \end{aligned} \tag{3}$$

for a Mach-Zehnder configuration. Here, $\mathbf{k}_{\text{eff}}^{(j)}$ is the wave vector of the jth light pulse ($j = 1, 2, 3$), and $\mathbf{r}_u$ ($\mathbf{r}_l$) the classical position of the wave packet on the upper (lower) branch of the interferometer upon interaction with the light in a coordinate system tied to the satellite frame. Typically, the three pulses $\mathbf{k}_{\text{eff}}^{(j)} = \mathbf{k}_{\text{eff}} = k_{\text{eff}} \mathbf{n}$ are identical, where $\mathbf{n}$ indicates the sensitive axis of the interferometer. The projection of the atoms' free fall acceleration $\mathbf{a}$ on this axis gives rise to the leading order phase shift, $\phi_a = k_{\text{eff}} \mathbf{n} \cdot \mathbf{a} T^2$, which allows to directly assess the Eötvös parameter η in a differential measurement. This treatment is exact for Lagrangians up to quadratic order in position and velocity, hence serving the purpose to study the effects related to gravity gradients (see Appendix A for details). The duration of atom-light-interaction τ is assumed to be small compared to
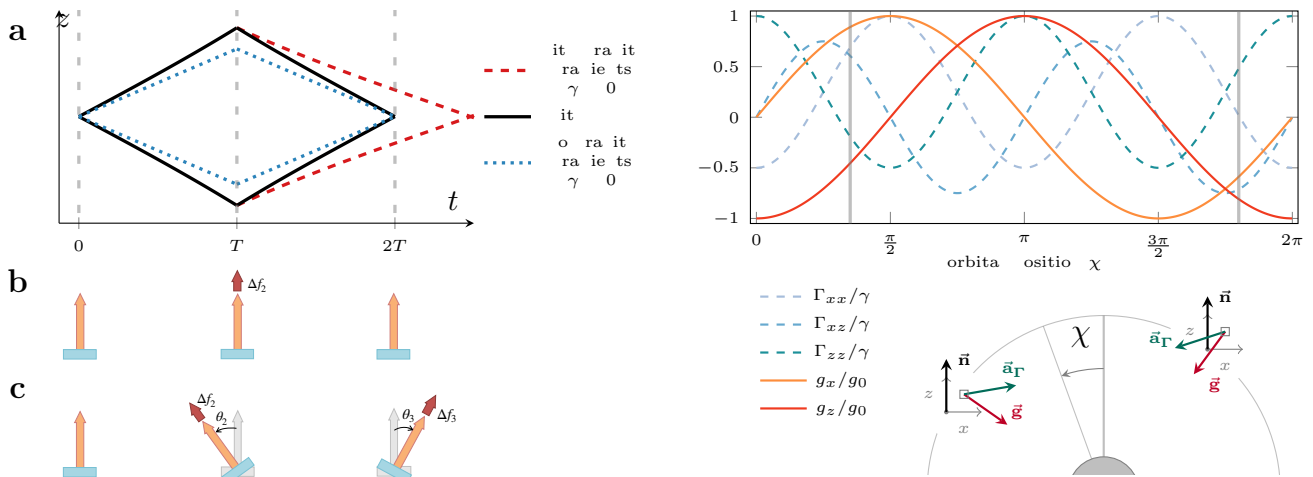
Figure 1. **Gravity gradient compensation in a space mission.** (**a**) In the presence of gravity gradients, the straight trajectories (blue, dashed) of the atoms in a freely falling frame get deformed, leading to an open (red, long dashes) interferometer. It is closed (solid, black) through (**b**) application of an appropriate frequency shift [30] at the second pulse. (**c**) In this work, the gradient compensation technique is extended to two dimensions by tilting the laser and changing it in frequency at the second as well as at the third light pulse. (**d**) This is required to mitigate the varying local values of the gravity gradient tensor components in the satellite frame in an inertial space mission. The effective acceleration $\mathbf{a}_\Gamma$ due to gradients and due to linear gravitational acceleration $\mathbf{g}$ shall only depict the changes in direction over an orbit and are not to scale. The sensitive axis and the satellite position on the orbit are labelled by $\mathbf{n}$ and χ respectively.

the pulse separation time T, which is the case for space-borne experiments with long drift times on the order of seconds. However, the treatment can be extended to account for pulses of finite duration leading to corrections in the order of τ/T [36, 37].

The gravity-gradient compensation (GCC) technique proposed in [30] exploits that the gravity gradients introduce phase shifts $\phi_{GG} = \mathbf{k}_{\text{eff}} \cdot \mathbf{a}_{GG} T^2$ (see Eq. (1)), which linearly depend on the initial position and velocity of an atom and may be compensated by introducing a controllable shift with similar dependency. Indeed, the phase expression (3) features a linear dependency on the atom's position $\mathbf{r}$, such that an additional shift at the mirror pulse, $\mathbf{k}_{\text{eff}}^{(2)} = \mathbf{k}_{\text{eff}} + \delta\mathbf{k}_{\text{eff}}$ gives rise to terms proportional to $\delta\mathbf{k}_{\text{eff}}$ and the initial coordinates of the atom. In another picture, this corresponds to closing the interferometer deformed by gravity gradients as depicted in Fig. 1a. It is interesting to note that also higher orders of the gravitational potential (cubic and higher) can be compensated in a similar fashion, as can be shown in a perturbative treatment [36, 38].

Anticipating the application to satellite missions, in which the gravity gradients are temporally varying and couple to rotations of the apparatus, we generalize this idea to the wave vectors

$$\mathbf{k}_{\text{eff}}^{(j)} = \begin{pmatrix} k_{\text{eff},x}^{(j)} \\ k_{\text{eff},y}^{(j)} \\ k_{\text{eff},z}^{(j)} \end{pmatrix} = \begin{pmatrix} k_{\text{eff}}\Delta_{x,j} \\ 0 \\ k_{\text{eff}}(1 + \Delta_{z,j}) \end{pmatrix} \quad (4)$$

for each pulse by introducing controllable shifts $\Delta_{x,j}$ and $\Delta_{z,j}$ for $j = 2,3$, with $\mathbf{k}_{\text{eff}}^{(1)} = (0,0,k_{\text{eff}}) =: \mathbf{k}_{\text{eff}}$. In an experiment, realizing these wave vectors corresponds to

shifting the laser in frequency and tilting it relative to the first pulse, as detailed in Appendix B and illustrated in Fig. 1b and c. For more general applications, one might introduce additional shifts in the y-direction. However, we will focus on satellites that spin in the orbital plane which we set to coincide with the x-z-plane.

In the satellite frame, the Lagrangian describing the free fall of an atom may be written as

$$L = \frac{1}{2}m\left(\dot{\mathbf{r}} + \mathbf{\Omega}_s \times \mathbf{r}\right)^2 + m\mathbf{a}(t)\mathbf{r} + \frac{1}{2}m\mathbf{r}\Gamma(t)\mathbf{r}, \quad (5)$$

where $\mathbf{\Omega}_s$ accounts for the spinning of the satellite, m is the atomic mass and $\Gamma(t)$ denotes the local gravity gradient tensor. Note that under the assumption of the UFF, the Lagrangian is independent of the linear gravitational acceleration in an inertial reference frame. The acceleration term $\mathbf{a}(t)$ needs however to be included in the treatment since it comprises the sensitivity to a possible UFF violation $\eta\mathbf{g}(t) = \mathbf{a}_A(t) - \mathbf{a}_B(t)$ in a differential measurement of two species A and B.

The interferometer phase is obtained by solving the (classical) equations of motion for segment-wise freely falling atoms, with boundary conditions defined by the wave vectors (4). The solution is obtained by virtue of a power-series ansatz [35] for the trajectories. Then, using the Lagrangian (5) the phase can be written as

$$\phi = \phi_{\text{indep.}} + \sum_{i=1}^{3} \alpha_i r_{0,i} + \sum_{i=1}^{3} \beta_i v_{0,i} \quad (6)$$

by collecting the dependencies on the initial position $r_{0,i}$ and velocity $v_{0,i}$ in the coefficients α_i and β_i, respectively, with $i = x,y,z$. ϕ_{indep} comprises all contributions

that are independent of the initial conditions. The coefficients α_i and β_i are, among other experimental parameters, functions of the wave vector shifts $\Delta_{i,j}$ introduced in Eq. (4). Therefore, the unwanted phase dependencies on the initial kinematics are compensated by requiring $\alpha_i = \beta_i = 0$, which yields explicit expressions for $\Delta_{i,j}$.

B. Results

In the case of a stationary ground experiment, in which, to leading order, the gradient tensor is given by $\Gamma = \mathrm{diag}(-\gamma/2, \gamma/2, \gamma)$ with $\gamma = 2GM_E/R_E^2$ (with M_E, R_E being Earth's mass and radius, respectively, and G the gravitational constant), we indeed recover the result $\Delta_{z,2} = \gamma T^2/2$ (the other shifts being zero) of reference [30] when neglecting rotations, $\mathbf{\Omega}_s = 0$. Similarly, for $\Gamma = 0$ and $\mathbf{\Omega}_s = (0, \Omega_y, 0)$, we find $\Delta_{x,2} = -\sin(\Omega_y T)$, $\Delta_{z,2} = -1 + \cos(\Omega_y T)$, $\Delta_{x,2} = -\sin(2\Omega_y T)$ and $\Delta_{z,2} = -1 + \cos(2\Omega_y T)$. This corresponds to counter-rotating the laser (mirror) between two pulses by the angle $\Omega_y T$ to compensate for rotations, a well known result used in ground-based experiments to account for Coriolis forces introduced by the rotation of the Earth [39].

In this study, we focus on the case of a satellite in inertial configuration (i.e. it keeps its orientation with respect to a celestial reference system, $\mathbf{\Omega}_s = 0$) on a circular orbit. The effect of residual rotations $\delta\mathbf{\Omega} \neq 0$, however, is taken into account in the error assessment in Sec. IV. The assumed spherically symmetric gravitational potential of the Earth allows for an analytical calculation. The concepts of this paper, however, can be extended to arbitrary orbits and more sophisticated gravitational potential models in a numerical treatment. An important feature in the system under consideration is the modulation of the gravitational field components in the local frame of the satellite as illustrated in Fig. 1d and detailed in Appendix A. In particular, the values of the gravity gradient tensor are modulated at twice the orbital frequency, which is $\Omega_{\mathrm{orbit}} = \sqrt{GM_E/(R_E + h_{\mathrm{sat}})^3}$ for a circular orbit at altitude h_{sat}. As a consequence, the required compensation shifts $\Delta_{i,j}$ have to be modulated in a similar fashion, as displayed in Fig. 2. Their magnitude is mainly determined by the scale factor $k_{\mathrm{eff}}T^2$ of the interferometer and the value of the local gravity gradients, and they are given by

$$\Delta_{x,2} = \frac{3}{8}\gamma T^2 \sin(2\chi) + \frac{5}{8}\gamma T^3 \Omega_{\mathrm{orbit}} \cos(2\chi) + ...$$
$$\Delta_{z,2} = \frac{1}{8}\gamma T^2 \left(1 + 3\cos(2\chi) - 5T\Omega_{\mathrm{orbit}}\sin(2\chi)\right) + ...$$
$$\Delta_{x,3} = \frac{1}{2}\gamma T^3 \Omega_{\mathrm{orbit}} \cos(2\chi) + ...$$
$$\Delta_{z,3} = -\frac{1}{2}\gamma T^3 \Omega_{\mathrm{orbit}} \sin(2\chi) + ...$$

$$(7)$$

to first order in γT^2, where χ is the angle characterizing the orbital position (see Fig. 1b).
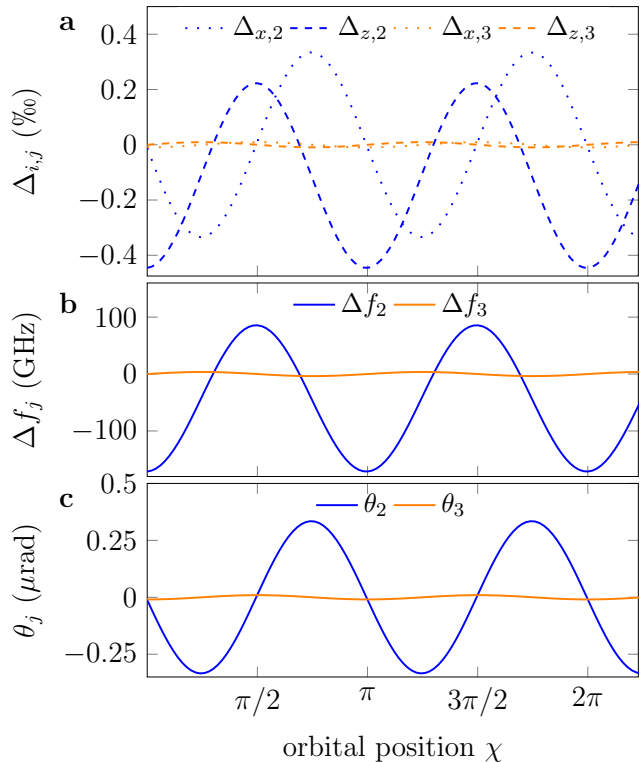
Figure 2. **Parameters for gravity gradient compensation in an inertial satellite mission. a)** Fractional momentum vector shifts in x (dotted) and z (dashed) direction. These shifts are realized by periodically **b)** shifting the laser in frequency and **c)** tilting the setup with respect to the first pulse. In all plots, blue (orange) corresponds to the value at the second (third) pulse, and χ denotes the orbital position when the first pulse is applied. The assumed parameters target $\delta\eta \leq 10^{-17}$ and are stated in Tab. I.

III. SIGNAL DEMODULATION

A decisive advantage of space tests of the UFF is the inherent modulation of the signal. As alluded to in the previous section, the different components of the gravitational field are modulated at different frequencies. The measured differential acceleration signal can hence be decomposed into its frequency components,

$$\Delta a = \eta g_0 \cos(\Omega_m t) + \Delta a_{\mathrm{const}} + \sum_{k=1} \Delta a_{\mathrm{sys}}^k \cos(k\Omega_m t). \quad (8)$$

Here, ηg_0 is the differential acceleration introduced by a possible violation, modulated at a certain frequency Ω_m. This frequency corresponds to the orbital frequency Ω_{orbit} for inertial configurations, or to $\Omega_m = \Omega_{\mathrm{orbit}} + \Omega_s$ for a satellite spinning in the orbital plane by Ω_s. All non-varying contributions or very slow drifts (i.e. varying on time scales $\ll 2\pi/\Omega_m$) are comprised in $\Delta a_{\mathrm{const}}$, for example a differential acceleration caused by a constant magnetic field bias. Finally, we consider systematic contributions $\Delta a_{\mathrm{sys}}^j$ at higher harmonics $j\Omega_m$ of the modulation, with gravity gradients varying at $2\Omega_m$. As in the

previous section, we suppose a simplified scenario with a circular orbit and a spherical gravitational potential for clarity. The following considerations can, however, be extended to continuous frequency spectra [8].

Demodulation of the differential acceleration signal at the target frequency Ω_m, at which the violation is expected, for a duration τ is given by

$$
\begin{aligned}
\frac{2}{\tau} \int_0^\tau \Delta a \cos(\Omega_m t) \ \mathrm{d}t &= (\eta g_0 + \Delta a_{sys}^1) \\
&+ \frac{2}{\tau \Omega_m} \left[\frac{\eta g_0 + \Delta a_{sys}^1}{2} \sin(2\Omega_m \tau) + \Delta a_{const} \sin(\Omega_m \tau) + 2 \sum_{k=2} \Delta a_{sys}^k \left[\frac{\sin([k\Omega_m - \Omega_m]\tau)}{k\Omega_m - \Omega_m} + \frac{\sin([k\Omega_m + \Omega_m]\tau)}{k\Omega_m + \Omega_m} \right] \right] \\
&\leq \left(\eta g_0 + \Delta a_{\mathrm{sys}}^1\right) + \frac{2}{\tau \Omega_m} \left(\frac{\eta g_0}{2} + |\Delta a_{\mathrm{const}}| + \frac{4}{3} \sum_{k=2} \left| \Delta a_{\mathrm{sys}}^{(k)} \right| \right),
\end{aligned}
\tag{9}
$$

where $\Delta a_{\mathrm{sys}}^1$ displays any components of the systematics (only co-location related effects in the scope of this paper), which are modulated at the same frequency as a possible violation signal. In the scenario under consideration, for an inertial mission on a perfectly circular orbit, this contribution is zero. However, any finite ellipticity introduces such a frequency component, as is shown in Appendix A.

The final expression shows that the potential violation signal is demodulated to DC, while the contributions at other frequencies and constant terms are integrated down. Here, the modulation frequency Ω_m determines the rate of integration. With respect to the integration behaviour it may hence be beneficial to spin the satellite in the orbital plane, as for example employed in [8] and along the lines of [24]. However, spinning the satellite introduces fictitious forces which couple to the initial conditions, too. It is possible to compensate them by counter-rotating the mirror [39] by the angle $T\Omega_s$ between two subsequent pulses. This rotation is additionally modulated with the periodic tilt determined in the previous section for gravity gradient compensation. Note that the authors of [40], too, exploit the fact that the gravity gradients are modulated at a different rate than the gravitational acceleration by introducing an artificial modulation by rotating the experimental setup on a gimbal mount. We find, however, that an additional spinning is not required, even for the ambitious scenario under consideration, as will be demonstrated in the next section. Finally, the described integration behaviour displays the worst case scenario, as the final expression (9) is obtained by taking the upper bound of the trigonometric functions in the intermediate step. In fact, the choice of an adequate integration time τ allows to evaluate the signal more efficiently by matching the minima of the expression (c.f. minima in Fig. 3).

IV. UFF TEST SCENARIO

A. Sensitivity to UFF violations

The concurrent operation of two matter-wave interferometers employing different atomic species A and B allows to infer the differential acceleration by simultaneous, individual phase measurements $\phi_\alpha = \mathbf{k}_{\mathrm{eff},\alpha} a_\alpha T_\alpha^2 + \phi_{\mathrm{sys},\alpha}$ with $\alpha = A/B$. The single-shot quantum projection noise (atomic shot noise)

$$
\sigma_{\Delta a}^{(1)} = \sqrt{\left(\frac{1}{C_A k_{\mathrm{eff},A} T_A^2 \sqrt{N_A}} \right)^2 + \left(\frac{1}{C_B k_{\mathrm{eff},B} T_B^2 \sqrt{N_B}} \right)^2}
\tag{10}
$$

given by the number N_α of atoms contributing to the signal, is the intrinsic differential acceleration uncertainty per experimental cycle. The contrast C_α accounts for the visibility of the interference fringes. Such a setup is sensitive to violations of the UFF, with the fundamental statistical uncertainty of the Eötvös-parameter

$$
\sigma_\eta = \frac{\sigma_{\Delta a}^{(1)} \sqrt{2}}{g_0 \sqrt{n}}.
\tag{11}
$$

after $n \gg 1$ measurements. As explained in Appendix B, the factor $\sqrt{2}$ accounts for the sinusoidally varying local value of the gravitational acceleration within a measurement campaign [26, 41]. In the following discussion, we assume the parameters stated in Tab. I for an exemplary UFF test scenario as presented in [26], targeting an accuracy of $\delta\eta \leq 10^{-17}$ involving isotopes of rubidium (Rb) and potassium (K). This analysis is not covering all aspects of a mission proposal but rather demonstrates the mitigation of co-location-related systematics for scenarios far beyond the state-of-the-art [8]. Since the free-fall time T in space-borne atom interferometers is not subject to the same limitations as on ground, it can be assumed to be much larger than in table-top experiments or fountains. Indeed, the coherence and low expansion rate of ultra-cold atomic sources allows to operate on time scales in the order of several seconds [22, 42]. Due to the geometrical constraints in a satellite mission, the magni-

quantity	value	definition
T	20 s	pulse separation time
$k_{\mathrm{eff,Rb}}$	$8\pi/(780\,\mathrm{nm})$	effective wave number (Rb)
$k_{\mathrm{eff,K}}$	$8\pi/(767\,\mathrm{nm})$	effective wave number (K)
N	10^6	number of atoms per shot
T_c	10 s	cycle time
$\boldsymbol{\delta r_{j,0}}$	$\mathbf{1\ \mu m}$	**differential initial position**
$\boldsymbol{\delta v_{j,0}}$	$\mathbf{1\ \mu m/s}$	**differential initial velocity**
h_{sat}	700 km	orbit height
$\delta\Omega$	$0.1\ \mu\mathrm{rad/s}$	residual satellite rotations
$\delta\gamma$	$10^{-10}\ \mathrm{s}^{-2}$	gravity gradient uncertainty
e	10^{-3}	orbit ellipticity
$\delta\theta$	$1\ \mu\mathrm{rad}$	laser tilt angle uncertainty
δf	400 kHz	laser frequency shift uncertainty

Table I. **Assumed parameters for a UFF test mission on an inertial satellite featuring gravity gradient cancellation and signal demodulation.** For the assumed orbit, the maximal value of the gravitational acceleration and gravity gradient tensor are $g_0 = 7.9\,\mathrm{m/s}^2$ and $\gamma = -2\times10^{-6}\,\mathrm{s}^{-2}$, respectively, and the orbital frequency is $\Omega_{\mathrm{orbit}} = 0.17\times2\pi\,\mathrm{mHz}$. The cycle time $T_c = 10\,\mathrm{s}$ can be realized by the concurrent operation of 5 interferometers, assuming 10 s for the preparation of the source. In combination with signal demodulation, the compensation technique allows to reduce the systematic uncertainties linked to gravity gradients by five orders of magnitude for these parameters, which relaxes the requirements on the initial co-location of the species by the same amount.

tude of momentum transfer k_{eff} is, however, limited, and we choose a second-order double diffraction scheme [43] ($k_{\mathrm{eff}} = 4k_L$ with k_L being the laser wave number) in the following, such that the spatial extent of the interferometer is less than 1 m. Moreover, we suppose typical atomic numbers and cycle times for the generation of sufficiently well-engineered quantum sources of Bose-Einstein condensates [22, 44]. Assuming that 10 s are required for the atomic source preparation followed by $2T = 40\,\mathrm{s}$ of interferometry, a cycle time of 10 s can be achieved supposing an interleaved operation of 5 concurrent interferometers [45]. Thanks to the choice of modest momentum transfer and the mitigation of major sources of contrast loss, such as gravity gradients, the contrast can be assumed to be near unity. With these parameters, the shot-noise limited Eötvös parameter is integrated down to 8×10^{-16} after one orbit, such that $\sigma_\eta \leq 10^{-17}$ can be reached within a total of $\tau = 15$ months of integration, corresponding to $n = 4\times10^6$ interferometric measurements.

B. Initial kinematics dependence

As indicated in the introduction, any spurious differential acceleration between the two species can, a priori, not be distinguished from a potential UFF violation signal. Consequently, all systematic error sources have to be controlled at a level better than the target inaccuracy of $\delta\eta = 10^{-17}$, or be modulated at other frequencies than the local projection of **g**. Eq. (1) describes how the

acceleration of each species is linked to its initial mean position and velocity and constrains the interspecies displacement uncertainty to $\delta\mathbf{r}_0 \sim 10\,\mathrm{pm}$ and $\delta\mathbf{v}_0 \sim 1\,\mathrm{pm/s}$ in position and velocity, respectively. The number of verification measurements $\nu \sim 10^8$ (see Eq. (2)) required to ensure the source preparation at this level would exceed the number of realizations of the actual interferometric experiment by far. Even the less ambitious goal of $\delta\eta = 2\times10^{-15}$ as in [22] would necessitate to allocate a significant part of the mission duration to the analysis of this systematic effect.

However, by employing the recipe outlined in Sec. II, we find that for the assumed mission parameters, the gravity gradient induced uncertainties can be compensated by applying the time-dependent momentum vector shifts (7) which corresponds to periodically tilting the laser up to $300\,\mu\mathrm{rad}$ and shifting it in frequency in the order of 150 GHz as displayed in Fig. 2. Indeed, the dependencies on the initial kinematics are largely compensated, such that the major residual contributions to the differential acceleration uncertainty stem from:

- Imperfections in the experimental realization, mainly given by the tilt error $\delta\theta$: $\delta\theta\delta x_0/T^2$ and $\delta\theta\delta v_{x,0}/T$ in the order of $\sim 5\times10^{-14}\ \mathrm{m\ s}^{-2}$.

- Residual satellite rotations $\delta\Omega$: $\delta\Omega\delta v_{x,0}$ and $\delta\Omega\delta v_{y,0}$ in the order of $\sim 10^{-13}\ \mathrm{m\ s}^{-2}$.

- Uncertainties in the knowledge of the local gravity gradient $\delta\gamma$: $\delta\gamma\delta z_0\cos(2\chi)$ and $\delta\gamma\delta v_{z,0}T\cos(2\chi)$ in the order of $10^{-16}\ \mathrm{m\ s}^{-2}$.

More details are found in Appendix B. These relations allow for a trade-off between required control of the experimental background ($\delta\Omega, \delta\theta, \delta\gamma$) and characterization of the source preparation ($\delta\mathbf{r}_0, \delta\mathbf{v_0}$), leading to the numbers in Tab. I. Note that these numbers are conservative as they stem from a linear (rather than quadratic) sum of uncertainties, although many of those uncertainties are expected to be uncorrelated (c.f. Appendix B).

Most importantly, these contributions are either constant or modulated at twice the orbital frequency, which is the modulation frequency of a potential UFF violation in the given setup. As outlined in Sec. III, this allows to distinguish these accelerations by demodulating the signal, which is of great significance as illustrated in Fig. 3. GGC allows for a large reduction of the systematic uncertainties due to the initial kinematics uncertainties, such that $\delta\eta = 10^{-15}$ may be readily achieved within hours of measurement. This overcomes one of the major challenges for missions like STE-QUEST [22] by relaxing the requirements on the source preparation by three orders of magnitude (μm displacement uncertainty instead of nm, similar for velocity). Even more, the systematics are integrated below 10^{-17} within a week and even reach 10^{-18} in a few months. Ultimately, in order to reach these inaccuracies in the Eötvös parameter, the combination of GGC and signal demodulation is indispensable.
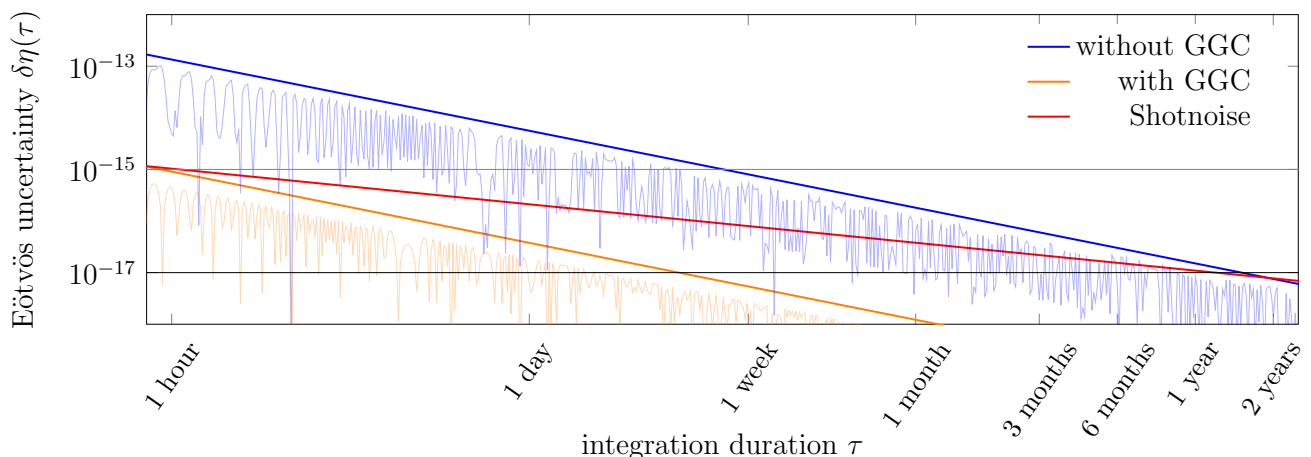
Figure 3. **Integration of systematic uncertainties due to gravity gradients in a UFF test with Rb and K.** GGC significantly reduces the systematic contributions, such that the residual differential acceleration may be attenuated to unprecedented degree through signal demodulation (orange curve). This does not only allow for largely reduced requirements on the source preparation for mission proposals as STE-QUEST [22] but also paves the way for more ambitious mission scenarios [26] targeting $\delta\eta \leq 10^{-17}$ in shot-noise limited operation (red curve). In comparison, although the systematics are integrated down thanks to demodulation, the measurement would be limited by systematics without GGC (blue curve).

C. Co-location feasibility

Atom interferometry for metrological applications has enjoyed a surge of interest in the last years [46, 47]. In particular, parabolic flights [48, 49], drop towers [42, 50, 51], sounding rockets [52] and the international space station [53, 54] enable research on atom optics in microgravity including the demonstration of atom interferometry, BEC production, and BEC interferometry in this environment. In the following, we provide an assessment of the aspects related to the dual-source preparation, in particular the co-location in position and velocity, and evaluate the feasibility of the GGC scheme. A complete error model and other aspects of a full space mission are beyond the scope of this paper and are discussed elsewhere [22, 24, 26].

a. BEC source The production of BECs with 10^6 rubidium atoms in a few seconds are within the capabilities of current devices [52, 55–57]. Magnetic and optical collimation of the matter waves to $100\,\mathrm{pK}$ and below was demonstrated [42, 58, 59], supporting high beam splitting efficiency [58, 60] and extended free evolution times [42, 57]. Mixtures of condensed rubidium and potassium were generated by exploiting Feshbach resonances [61, 62], but reaching sufficient numbers of atoms and collimation of both overlapped ensembles requires additional research efforts [63].

b. Atom interferometry Beam splitters based on double diffraction providing the required momentum transfer were implemented in interferometric measurements [43, 64, 65] and extended free fall times on the order of seconds were utilised to boost the sensitivity [57]. Furthermore, the experimental implementation of the GGC scheme has been shown via adjusting the effective wave vector of the central beam splitting pulse and

rotation of the mirror [21, 25, 31]. In trapped ensembles, Bloch oscillations and the signal of an atom interferometer were observed for total evolution times of up to $20\,\mathrm{s}$, but with a significantly reduced contrast [66, 67]. Although interleaved operation has previously been demonstrated in a rotation sensor using a single species [45], the dual-species, microgravity operation will require adaptations for the transfer to the interferometer zone [68] and for assuring the initial overlap.

c. Requirements on beam splitting light fields imposed by GGC Current tip-tilt mirror technology to adjust the beam pointing appears to fulfill the requirement stated in Tab. I (see Appendix B for details) since it was utilized to compensate for Earth's rotation with a performance of $1\,\mathrm{nrad}/\sqrt{\mathrm{Hz}}$ [57] and repeatable to $\lesssim 1\,\mu\mathrm{rad}$ [39, 69]. The implementation of the GGC scheme will likely require two lasers per species, where each laser provides two frequencies. Here, one laser drives the initial and final beam splitter, the second laser provides the central beam splitting pulse with a different and variable wave vector. In order to ensure the necessary phase stability of the lasers with respect to each other, a reference provided by a frequency comb or a high-finesse transfer cavity is mandatory [70]. A setup based on only a single laser per species might be possible using fiber lasers offering sufficiently large tuning range. As a fallback option, the requirement on the tuning range may be relaxed by trading off free fall time against higher beam splitting order [30].

d. Satellite platform Due to its similarity in scope and technological requirements on the satellite platform, the heritage of MICROSCOPE [8] is essential for the discussion of potential UFF test scenarios. The orbit assumed in this paper is motivated by MICROSCOPE's highly circular orbit at $700\,\mathrm{km}$ resulting from a trade-

off to maximize the local value of **g** and to minimize atmospheric drag. In particular, the mission has demonstrated excellent attitude and satellite position control [71] far beyond the parameter assumptions made here in Tab. I. Even better control has been demonstrated in the context of space-borne gravitational wave detection [72], which is, however, not required for the scenario under consideration.

V. CONCLUSION

In this paper, we have illustrated the co-location problem of the two test species in a space-borne quantum test of the UFF way beyond the state-of-the-art. We particularly presented a dual strategy based on variable wave vector shifts and demodulation to mitigate systematic contributions linked to errors in the source preparation. Whilst an exhaustive discussion of all sources of noise and systematic effects is beyond the scope of this paper, we have demonstrated that those related to initial co-location uncertainties can be reduced to below $\delta\eta = 10^{-17}$ for realistic experimental scenarios and reasonable mission durations. At the same time, the requirements on the initial overlap in position and velocity of the two employed species are reduced by five orders of magnitude. The described methods allow to significantly decrease the required mission duration in proposals like [22] and pave the way for missions with unprecedented accuracy beyond state-of-the-art [26].

[1] C. M. Will, The Confrontation between General Relativity and Experiment, Living Reviews in Relativity **17**, 4 (2014).

[2] V. A. Kostelecký and J. D. Tasson, Matter-gravity couplings and Lorentz violation, Phys. Rev. D **83**, 016013 (2011).

[3] T. Damour, Theoretical aspects of the equivalence principle, Classical Quantum Gravity **29**, 184001 (2012).

[4] L. I. Schiff, On Experimental Tests of the General Theory of Relativity, Am. J. Phys. **28**, 340 (1960).

[5] K. Nordtvedt, Quantitative relationship between clock gravitational "red-shift" violations and nonuniversality of free-fall rates in nonmetric theories of gravity, Phys. Rev. D **11**, 245 (1975).

[6] T. A. Wagner, S. Schlamminger, J. H. Gundlach, and E. G. Adelberger, Torsion-balance tests of the weak equivalence principle, Classical Quantum Gravity **29**, 184002 (2012).

[7] F. Hofmann and J. Müller, Relativistic tests with lunar laser ranging, Classical Quantum Gravity **35**, 035015 (2018).

[8] P. Touboul, G. Métris, M. Rodrigues, *et al.*, MICROSCOPE Mission: First Results of a Space Test of the Equivalence Principle, Phys. Rev. Lett. **119** (2017).

[9] M. A. Hohensee, H. Müller, and R. B. Wiringa, Equivalence Principle and Bound Kinetic Energy, Phys. Rev. Lett. **111** (2013).

[10] C. Lämmerzahl, The search for quantum gravity effects I, Appl. Phys. B: Lasers Opt. **84**, 551 (2006).

[11] M. G. Tarallo, T. Mazzoni, N. Poli, D. V. Sutyrin, X. Zhang, and G. M. Tino, Test of Einstein Equivalence Principle for 0-Spin and Half-Integer-Spin Atoms: Search for Spin-Gravity Coupling Effects, Phys. Rev. Lett. **113** (2014).

[12] G. Rosi, G. D'Amico, L. Cacciapuoti, F. Sorrentino, M. Prevedelli, M. Zych, Č. Brukner, and G. M. Tino, Quantum test of the equivalence principle for atoms in coherent superposition of internal energy states, Nat. Commun. **8**, 15529 (2017).

[13] I. Pikovski, M. Zych, F. Costa, and Č. Brukner, Universal decoherence due to gravitational time dilation, Nat. Phys. **11**, 668 (2015).

[14] A. Roura, Gravitational Redshift in Quantum-Clock Interferometry, Phys. Rev. X **10**, 021014 (2020).

[15] C. Ufrecht, F. Di Pumpo, A. Friedrich, A. Roura, C. Schubert, D. Schlippert, E. M. Rasel, W. P. Schleich, and E. Giese, An atom interferometer testing the universality of free fall and gravitational redshift, arXiv:2001.09754 (2020).

[16] S. Fray, C. A. Diez, T. W. Hänsch, and M. Weitz, Atomic Interferometer with Amplitude Gratings of Light and Its Applications to Atom Based Tests of the Equivalence Principle, Phys. Rev. Lett. **93**, 240404 (2004).

[17] A. Bonnin, N. Zahzam, Y. Bidel, and A. Bresson, Simultaneous dual-species matter-wave accelerometer, Phys. Rev. A **88** (2013).

[18] D. Schlippert, J. Hartwig, H. Albers, L. L. Richardson, C. Schubert, A. Roura, W. P. Schleich, W. Ertmer, and E. M. Rasel, Quantum Test of the Universality of Free Fall, Phys. Rev. Lett. **112** (2014).

[19] L. Zhou *et al.*, United test of the equivalence principle at 10^{-10} level using mass and internal energy specified atoms, arXiv:1904.07096 (2019).

[20] H. Albers *et al.*, Quantum test of the Universality of Free Fall using rubidium and potassium, arXiv:2003.00939 (2020).

[21] P. Asenbaum, C. Overstreet, M. Kim, J. Curti, and M. A. Kasevich, Atom-interferometric test of the equivalence principle at the 10^{-12} level, arXiv:2005.11624 (2020).

[22] D. N. Aguilera *et al.*, STE-QUEST – test of the universality of free fall using cold atom interferometry, Classical Quantum Gravity **31**, 115010 (2014).

[23] J. Hartwig, S. Abend, C. Schubert, D. Schlippert, H. Ahlers, K. Posso-Trujillo, N. Gaaloul, W. Ertmer, and E. M. Rasel, Testing the universality of free fall with rubidium and ytterbium in a very large baseline atom interferometer, New J. Phys. **17**, 035011 (2015).

[24] J. Williams, S.-w. Chiow, N. Yu, and H. Müller, Quantum test of the equivalence principle and space-time aboard the International Space Station, New J. Phys. **18**, 025018 (2016).

[25] C. Overstreet, P. Asenbaum, T. Kovachy, R. Notermans, J. M. Hogan, and M. A. Kasevich, Effective Inertial Frame in an Atom Interferometric Test of the Equivalence Principle, Phys. Rev. Lett. **120**, 183604 (2018).

[26] J. Bergé *et al.*, Exploring the Foundations of the Universe with Space Tests of the Equivalence Principle, arXiv:1908.11785 (2019).

[27] J. P. Blaser, Can the equivalence principle be tested with freely orbiting masses?, Classical Quantum Gravity **18**, 2509 (2001).

[28] Throughout this paper, we will use Δ and δ to denote a difference and an uncertainty, respectively. For example, $\Delta\mathbf{r}_0 = \mathbf{r}_{0,A} - \mathbf{r}_{0,B}$ is the displacement of species A and B, and $\delta\Delta\mathbf{r}_0$ denotes the uncertainty in that quantity.

[29] $\delta\Delta\mathbf{r}_{0,i} = \left(\sigma_{r,0,i,A}^2/N_A + \sigma_{r,0,i,B}^2/N_B\right)^{1/2}/\sqrt{\nu}$. For simplicity, we assume similar values for both clouds, $\sigma_{r,0,i,A} = \sigma_{r,0,i,B} = \sigma_{r,0,i}$ and $N_A = N_B = N$.

[30] A. Roura, Circumventing Heisenberg's Uncertainty Principle in Atom Interferometry Tests of the Equivalence Principle, Phys. Rev. Lett. **118** (2017).

[31] G. D'Amico, G. Rosi, S. Zhan, L. Cacciapuoti, M. Fattori, and G. M. Tino, Canceling the Gravity Gradient Phase Shift in Atom Interferometry, Phys. Rev. Lett. **119** (2017).

[32] M. Kasevich and S. Chu, Atomic interferometry using stimulated Raman transitions, Phys. Rev. Lett. **67**, 181 (1991).

[33] P. Storey and C. Cohen-Tannoudji, The Feynman path integral approach to atomic interferometry. A tutorial, J. Phys. II **4**, 1999 (1994).

[34] C. Antoine and C. J. Bordé, Quantum theory of atomic clocks and gravito-inertial sensors: an update, J. Opt. B: Quantum Semiclassical Opt. **5**, S199 (2003).

[35] Hogan J. M., Johnson D. M. S., and Kasevich M. A., Light-pulse atom interferometry, Proceedings of the International School of Physics "Enrico Fermi" **168**, 411 (2009).

[36] A. Bertoldi, F. Minardi, and M. Prevedelli, Phase shift in atom interferometers: Corrections for nonquadratic potentials and finite-duration laser pulses, Phys. Rev. A **99**, 033619 (2019).

[37] Y.-J. Wang, X.-Y. Lu, Y.-J. Tan, C.-G. Shao, and Z.-K. Hu, Improved frequency-shift gravity-gradient compensation on canceling the Raman-pulse-duration effect in atomic gravimeters, Phys. Rev. A **98**, 053604 (2018).

[38] C. Ufrecht and E. Giese, Perturbative operator approach to high-precision light-pulse atom interferometry, Phys. Rev. A **101**, 053615 (2020).

[39] S.-Y. Lan, P.-C. Kuan, B. Estey, P. Haslinger, and H. Müller, Influence of the Coriolis Force in Atom Interferometry, Phys. Rev. Lett. **108** (2012).

[40] S.-w. Chiow, J. Williams, N. Yu, and H. Müller, Gravity-gradient suppression in spaceborne atomic tests of the equivalence principle, Phys. Rev. A **95** (2017).

[41] C. Schubert *et al.*, Differential atom interferometry with ^{87}Rb and ^{85}Rb for testing the UFF in STE-QUEST, arXiv:1312.5963 (2013).

[42] H. Müntinga *et al.*, Interferometry with Bose-Einstein Condensates in Microgravity, Phys. Rev. Lett. **110**, 093602 (2013).

[43] H. Ahlers *et al.*, Double Bragg Interferometry, Phys. Rev. Lett. **116**, 173601 (2016).

[44] S. Loriani *et al.*, Atomic source selection in space-borne gravitational wave detection, New J. Phys. **21**, 063030 (2019).

[45] D. Savoie, M. Altorio, B. Fang, L. A. Sidorenkov, R. Geiger, and A. Landragin, Interleaved atom interferometry for high-sensitivity inertial measurements, Sci. Adv. **4** (2018).

[46] R. Geiger, A. Landragin, S. Merlet, and F. Pereira Dos Santos, High-accuracy inertial measurements with cold-atom sensors, arXiv:2003.12516 (2020).

[47] K. Bongs, M. Holynski, J. Vovrosh, P. Bouyer, G. Condon, E. Rasel, C. Schubert, W. P. Schleich, and A. Roura, Taking atom interferometric quantum sensors from the laboratory to real-world applications, Nat. Rev. Phys. **1**, 731 (2019).

[48] B. Barrett, L. Antoni-Micollier, L. Chichet, B. Battelier, T. Lévèque, A. Landragin, and P. Bouyer, Dual matter-wave inertial sensors in weightlessness, Nat. Commun. **7**, 13786 (2016).

[49] R. Geiger, V. Ménoret, G. Stern, N. Zahzam, P. Cheinet, B. Battelier, A. Villing, F. Moron, M. Lours, Y. Bidel, A. Bresson, A. Landragin, and P. Bouyer, Detecting inertial effects with airborne matter-wave interferometry, Nat. Commun. **2**, 474 (2011).

[50] C. Vogt, M. Woltmann, S. Herrmann, C. Lämmerzahl, H. Albers, D. Schlippert, and E. M. Rasel (PRIMUS), Evaporative cooling from an optical dipole trap in microgravity, Phys. Rev. A **101**, 013634 (2020).

[51] G. Condon, M. Rabault, B. Barrett, L. Chichet, R. Arguel, H. Eneriz-Imaz, D. Naik, A. Bertoldi, B. Battelier, P. Bouyer, and A. Landragin, All-optical bose-einstein condensates in microgravity, Phys. Rev. Lett. **123**, 240402 (2019).

[52] D. Becker, M. D. Lachmann, S. T. Seidel, *et al.*, Space-borne Bose-Einstein condensation for precision interferometry, Nature **562**, 391 (2018).

[53] K. Frye *et al.*, The Bose-Einstein Condensate and Cold Atom Laboratory, arXiv:1912.04849 (2019).

[54] E. R. Elliott, M. C. Krutzik, J. R. Williams, R. J. Thompson, and D. C. Aveline, NASAs Cold Atom Lab

(CAL): system development and ground test status, npj Microgravity **4**, 1 (2018).

[55] K. S. Hardman *et al.*, Simultaneous Precision Gravimetry and Magnetic Gradiometry with a Bose-Einstein Condensate: A High Precision, Quantum Sensor, Phys. Rev. Lett. **117**, 138501 (2016).

[56] J. Rudolph *et al.*, A high-flux BEC source for mobile atom interferometers, New J. Phys. **17**, 065001 (2015).

[57] S. M. Dickerson, J. M. Hogan, A. Sugarbaker, D. M. S. Johnson, and M. A. Kasevich, Multiaxis Inertial Sensing with Long-Time Point Source Atom Interferometry, Phys. Rev. Lett. **111**, 083001 (2013).

[58] S. Abend *et al.*, Atom-Chip Fountain Gravimeter, Phys. Rev. Lett. **117**, 203003 (2016).

[59] T. Kovachy, J. M. Hogan, A. Sugarbaker, S. M. Dickerson, C. A. Donnelly, C. Overstreet, and M. A. Kasevich, Matter Wave Lensing to Picokelvin Temperatures, Phys. Rev. Lett. **114**, 143004 (2015).

[60] S. S. Szigeti, J. E. Debs, J. J. Hope, N. P. Robins, and J. D. Close, Why momentum width matters for atom interferometry with Bragg pulses, New J. Phys. **14**, 023009 (2012).

[61] G. Thalhammer, G. Barontini, L. De Sarlo, J. Catani, F. Minardi, and M. Inguscio, Double Species Bose-Einstein Condensate with Tunable Interspecies Interactions, Phys. Rev. Lett. **100**, 210402 (2008).

[62] G. Ferrari, M. Inguscio, W. Jastrzebski, G. Modugno, G. Roati, and A. Simoni, Collisional Properties of Ultracold K-Rb Mixtures, Phys. Rev. Lett. **89**, 053202 (2002).

[63] R. Corgier, *Engineered atomic states for precision interferometry*, Ph.D. thesis, Leibniz Universität Hannover (2019).

[64] M. Gebbe *et al.*, Twin-lattice atom interferometry, arXiv:1907.08416 (2019).

[65] T. Lévèque, A. Gauguet, F. Michaud, F. Pereira Dos Santos, and A. Landragin, Enhancing the Area of a Raman Atom Interferometer Using a Versatile Double-Diffraction Technique, Phys. Rev. Lett. **103**, 080405 (2009).

[66] V. Xu, M. Jaffe, C. D. Panda, S. L. Kristensen, L. W. Clark, and H. Müller, Probing gravity by holding atoms for 20 seconds, Science **366**, 745 (2019).

[67] N. Poli, F.-Y. Wang, M. G. Tarallo, A. Alberti, M. Prevedelli, and G. M. Tino, Precision Measurement of Gravity with Cold Atoms in an Optical Lattice and Comparison with a Classical Gravimeter, Phys. Rev. Lett. **106**, 038501 (2011).

[68] A. Trimèche, B. Battelier, D. Becker, A. Bertoldi, P. Bouyer, C. Braxmaier, E. Charron, R. Corgier, M. Cornelius, K. Douch, N. Gaaloul, S. Herrmann, J. Müller, E. Rasel, C. Schubert, H. Wu, and F. P. dos Santos, Concept study and preliminary design of a cold atom interferometer for space gravity gradiometry, Classical Quantum Gravity **36**, 215004 (2019).

[69] M. Hauth, C. Freier, V. Schkolnik, A. Senger, M. Schmidt, and A. Peters, First gravity measurements using the mobile atom interferometer GAIN, Appl. Phys. B **113**, 49 (2013).

[70] A. Resch, *Hochstabiler optischer Resonator im Fallturmbetrieb für Präzisionsmessungen in Schwerelosigkeit*, Ph.D. thesis, Universität Bremen (2016).

[71] P. Touboul, G. Métris, M. Rodrigues, *et al.*, Space test of the equivalence principle: first results of the MICROSCOPE mission, Classical Quantum Gravity **36**, 225006 (2019).

[72] M. Armano *et al.*, LISA Pathfinder platform stability and drag-free performance, Phys. Rev. D **99**, 082001 (2019).

[73] N. K. Pavlis, S. A. Holmes, S. C. Kenyon, and J. K. Factor, The development and evaluation of the Earth Gravitational Model 2008 (EGM2008), J. Geophys. Res.: Solid Earth **117** (2012).

[74] O. Montenbruck and E. Gill, *Satellite orbits: models, methods, and applications* (Springer, Berlin, 2012).

Appendix A: Gravity model

For Lagrangians up to quadratic order in $\mathbf{r}$ and $\dot{\mathbf{r}}$, the interferometer phases may be inferred by a semi-classical model, in which the classical trajectories of the atoms are computed and inserted into the phase expression (3). Throughout this manuscript, we suppose

$$L = \frac{1}{2}m\left(\dot{\mathbf{r}} + \mathbf{\Omega}_s \times \mathbf{r}\right)^2 + \frac{1}{2}m\mathbf{r}\Gamma(t)\mathbf{r}, \qquad (A1)$$

to describe the free motion of the atoms in the satellite reference frame. The local gravity gradient tensor $\Gamma(t)$ depends on the the satellite position and attitude and is therefore a function of time. $\mathbf{\Omega}_s$ incorporates rotations of the satellite, i.e. spinning around its own axis. To this end, we expand the gravitational potential of the Earth for coordinates $\mathbf{r}$ much smaller than the satellite position $\mathbf{R}$,

$$\phi(\mathbf{R} + \mathbf{r}) \approx \phi(\mathbf{R}) + \partial_{R_i}\phi(\mathbf{R})r_i + \frac{1}{2!}\partial_{R_i}\partial_{R_j}\phi(\mathbf{R})r_ir_j + ...$$

$$= \phi(\mathbf{R}) + \mathbf{g} \cdot \mathbf{r} + \frac{1}{2!}\mathbf{r}\Gamma\mathbf{r} + ...$$
$$(A2)$$

with

$$\Gamma_\chi = \begin{pmatrix} T_{xx} & 0 & T_{xz} \\ 0 & T_{yy} & 0 \\ T_{xz} & 0 & T_{zz} \end{pmatrix}, \qquad (A3)$$

supposing the orbital motion to be restricted to the x-z-plane. This approximates the potential for the order-of-magnitude assessment performed in this work. A concise mission analysis would involve a realistic gravitational model such as [73]. For the Newtonian gravitational potential, the gradient components are given by

$$T_{ij} = \frac{3Gm_E}{|\mathbf{R}|^5}R_iR_j - \frac{Gm_E}{|\mathbf{R}|^3}\delta_{i,j}. \qquad (A4)$$

The parameter $0 \leq \chi < 2\pi$, which parametrizes the satellite position on the orbit, is chosen such that the initial position

$$\mathbf{R}(\chi = 0) = (0, 0, R_0) \qquad (A5)$$

is aligned with the z-axis and the initial gradient tensor reads

$$\Gamma_0 = \begin{pmatrix} -\gamma/2 & 0 & 0 \\ 0 & -\gamma/2 & 0 \\ 0 & 0 & \gamma \end{pmatrix}, \qquad (A6)$$

with $\gamma = 2GM/R_0^3$. The way how the time dependent tensor components T_{ij} relate to those of the initial gradient tensor Γ_0 depends on the shape of the orbit. For a circular orbit (index c), where the satellite position is given by

$$\mathbf{R}^{\mathrm{e}}(\chi) = \begin{pmatrix} R_0 \sin \chi \\ 0 \\ R_0 \cos \chi \end{pmatrix}, \qquad (A7)$$

the explicit relations are

$$T_{xx}^{\mathrm{c}} = \frac{1}{4}\gamma\left(1 - 3\cos(2\chi)\right)$$
$$T_{zz}^{\mathrm{c}} = \frac{1}{4}\gamma\left(1 + 3\cos(2\chi)\right). \qquad (A8)$$
$$T_{xz}^{\mathrm{c}} = \frac{3}{4}\gamma\sin(2\chi)$$

It is important to note that the modulation of the components is at twice the orbital frequency. In the case of a circular orbit, we can describe the time evolution of the gradient tensor during the interferometer sequence by another rotation, such that it is given by

$$\Gamma(t) = D(\Omega_m t)\Gamma_\chi D^T(\Omega_m t) \qquad (A9)$$

at time t after the measurement has been started at orbital position χ. $D(\theta)$ is the 3D-rotation matrix by an angle θ around the y-axis. For an orbit featuring an eccentricity e and semi-major axis a, the satellite position is given by [74]

$$\mathbf{R}^{\mathrm{e}}(\chi) = \begin{pmatrix} R_0\sqrt{1-e^2}\sin\chi \\ 0 \\ R_0(\cos\chi - e). \end{pmatrix} \qquad (A10)$$

Note that the initial position coincides with perigee, $R_0 = a(1-e)$ in the coordinate system fixed to center of the Earth. With the help of (A4), we readily obtain

$$T_{xx}^{\mathrm{e}} = -\frac{1 - 4e^2 + 4e\cos(\chi) + (2e^2 - 3)\cos(2\chi)}{4|1 - e\cos\chi|^5/|1 - e|^3}\,\gamma$$
$$T_{zz}^{\mathrm{e}} = -\frac{1 - 3e^2 + 4e\cos(\chi) + (e^2 - 3)\cos^2\chi}{2|1 - e\cos\chi|^5/|1 - e|^3}\,\gamma$$
$$T_{xz}^{\mathrm{e}} = -\frac{3\sqrt{1-e^2}(\cos\chi - e)\sin\chi}{2|1 - e\cos\chi|^5/|1 - e|^3}\,\gamma$$
$$\qquad (A11)$$

A series expansion to first order in the ellipticity yields

$$T_{xx}^{\mathrm{e}} = T_{xx}^{\mathrm{c}} + \frac{3}{8}\gamma\left[-2 + \cos(\chi) + 6\cos(2\chi) - 5\cos(3\chi)\right]e$$
$$T_{zz}^{\mathrm{e}} = T_{zz}^{\mathrm{c}} + \frac{3}{8}\gamma\left[-2 + 3\cos(\chi) - 6\cos(2\chi) + 5\cos(3\chi)\right]e$$
$$T_{xz}^{\mathrm{e}} = T_{xz}^{\mathrm{c}} + \frac{3}{8}\gamma\left[\sin(\chi) - 6\sin(2\chi) + 5\cos(3\chi)\right]e$$
$$\qquad (A12)$$

which shows that the ellipticity introduces an additional modulation of the gradient components at different frequencies compared to the circular orbit (A8). In particular, it features a component at the orbital frequency,

which leads to a systematic contribution even after demodulation ($\Delta a_{\mathrm{sys}}^1$ in Eq. (9)), since is modulated at the same frequency as a possible UFF violation signal. However, it is suppressed by e and can be accounted for with the compensation technique of section II. Similarly, higher orders in the expansion of the gravitational potential (A2) feature frequency components at the orbital frequency. However, the associated acceleration uncertainties are suppressed with respect to the gravity gradient terms discussed in this paper by a factor of $\Delta r/|\mathbf{R}| \sim 10^{-12}$.

Appendix B: Implementation and feasibility of the compensation method

1. Experimental method

The shifts $\Delta_{x,j}$, $\Delta_{z,j}$ in the wave vector of the j-th pulse, required to compensate the gravity gradient induced acceleration uncertainties as outlined in section II in the main text, are realized by tilting the laser by an angle θ_j and shifting it in frequency by Δf_j. We find the relations

$$\theta_j = \arctan\left(\frac{\Delta_{x,j}}{1 + \Delta_{z,j}}\right)$$
$$\Delta f_j = \frac{ck_{\mathrm{eff}}}{8\pi} \times \left[-1 + \sqrt{(\Delta_{x,j})^2 + (1 + \Delta_{z,j})^2}\right], \qquad (B1)$$

where the factor 8 accounts for two-photon transitions employed to realize the beam splitters and the second order diffraction process. c is the speed of light and $k_{\mathrm{eff}} = |\mathbf{k}_{\mathrm{eff}}| = 4k_L$ the effective total momentum transferred by the pulses, with k_L being the wave number of the light.

2. Treatment of residual rotations

The employed Lagrangian (5) with $\mathbf{\Omega}_s = \mathbf{0}$ describes the perfectly inertial case, i.e. the constant rotation of the gravity gradient tensor by an angle $\Omega_{\mathrm{orbit}}t$. Residual rotations of the satellite, however, modify the Lagrangian in two ways. In the following we assume the same rotation uncertainty $\delta\Omega$ for all three directions which gives rise to

$$L_{\delta\Omega} = \frac{1}{2}m\left(\dot{\mathbf{r}} + (\delta\Omega, \delta\Omega, \delta\Omega) \times \mathbf{r}\right)^2 + \frac{1}{2}m\mathbf{r}D_{\delta\Omega}^T\Gamma_\chi D_{\delta\Omega}\mathbf{r}, \qquad (B2)$$

where $D_{\delta\Omega}$ is the matrix that rotates the gradient tensor under consideration of the orbital motion and residual rotations. Under the assumption that $\delta\Omega t << 1$ (the case here), for an arbitrary permutation $D_p = [D_{\delta\Omega,x}D_{\delta\Omega,y}D_{\delta\Omega,z}D_{\Omega_{\mathrm{orbit}},y}]$ of these four rotations (three small residual rotations, one comparably large orbital rotation), the relative deviation of the term $D_p^T\Gamma_\chi D_p$ from $D_{\Omega_{\mathrm{orbit}}}^T\Gamma_\chi D_{\Omega_{\mathrm{orbit}}}$ is smaller than 10^{-6} for the parameters of interest. Therefore, neglecting the residual rotations results in an error of less than $10^{-11}\,\mathrm{s}^{-2}$ in the value of

the gradient tensor components, which is well in line with the assumptions. As a consequence, the impact of residual rotations on the modulation of the gradient tensor can be safely neglected, and the Lagrangian

$$L_{\delta\Omega} = \frac{1}{2}m\left(\dot{\mathbf{r}} + \delta\boldsymbol{\Omega} \times \mathbf{r}\right)^2 + \frac{1}{2}m\mathbf{r}D_{\Omega_{\text{orbit}}}^T\Gamma_\chi D_{\Omega_{\text{orbit}}}\mathbf{r} \quad \text{(B3)}$$

with $\delta\boldsymbol{\Omega} = (\delta\Omega, \delta\Omega, \delta\Omega)$ captures the relevant influence of residual rotations on the system.

3. Uncertainty assessment

Due to the linear dependence on the initial kinematics, the differential acceleration between two species A and B,

$$\Delta a = a_A - a_B = \Delta a_{\text{indep}} + \sum_{i=1}^3 \left(\alpha_i' r_{0,i} + \beta_i' v_{0,i}\right), \quad \text{(B4)}$$

can be directly obtained from the phase expression (6) after division by the respective scale factor $k_{\text{eff},\alpha}T_\alpha^2$ of species α, i.e. $\alpha_i' = \alpha_{i,A}/k_{\text{eff},A}T_A^2 - \alpha_{i,B}/k_{\text{eff},B}T_B^2$ (analogous for β_i'). The total differential acceleration uncertainty is given by the absolute sum

$$\begin{aligned}\delta\Delta a = &|\delta\Delta a_{\text{indep}}| \\ &+ \sum_{i=1}^3 \Big(|\delta\alpha_i'|\Delta r_{0,i} + (|\alpha_i'| + |\delta\alpha_i'|)\delta\Delta r_{0,i} \\ &\quad |\delta\beta_i'|\Delta v_{0,i} + (|\beta_i'| + |\delta\beta_i'|)\delta\Delta v_{0,i}\Big),\end{aligned} \quad \text{(B5)}$$

where δ indicates the uncertainty of a term. For example, $\delta\Delta r_{0,i}$ is the uncertainty in the initial displacement $\Delta r_{0,i}$. The error in the coefficients α_i' is computed via

$$\delta\alpha_i' = \sum_{j=1}^N \left|\frac{\partial\alpha_i'}{\partial Q_j}\delta Q_j\right|, \quad \text{(B6)}$$

with $Q_j \in \{\gamma, T, \boldsymbol{\Omega}_s, \Delta_{2,x}, \Delta_{2,z}, \Delta_{3,x}, \Delta_{3,z}\}$ and δQ_j being the corresponding uncertainty (analogous for β_i'). Note that this is a conservative treatment, since most of these contributions are uncorrelated such that the favourable quadratic sum would be sufficient. To first order, $\Delta_{x,j} \sim \theta_j$ and $\Delta_{z,j} \sim \Delta f_j/f$ such that their uncertainties are given by $\delta\Delta_{x,j} \sim \delta\theta_j$ and $\delta\Delta_{z,j} \sim \delta f_j/f$, respectively.

The differential acceleration uncertainty of a measurement without the compensation technique is obtained from (B5) with $\Delta_{i,j} = \delta\Delta_{i,j} = 0$. By construction, application of the compensation shifts $\Delta_{i,j}$ derived in Sec. II

leads to $\alpha_i' = \beta_i' = 0$ in Eq. (B5), i.e.

$$\begin{aligned}\delta\Delta a_{\text{GGC}}(t) = &|\delta a_{\text{indep}}| \\ &+ \sum_{i=1}^3 \Big(|\delta\alpha_i'|\left(\Delta r_{0,i} + \delta\Delta r_{0,i}\right) \\ &\quad + |\delta\beta_i'|\left(\Delta v_{0,i} + \delta\Delta v_{0,i}\right)\Big).\end{aligned} \quad \text{(B7)}$$

As discussed in Sec. III, the integrated uncertainty is then given by

$$\delta a(\tau) = \frac{2}{\tau}\int_0^\tau \delta\Delta a_{\text{GGC}}(t)\cos(\Omega_{\text{orbit}}t)\,\mathrm{d}t. \quad \text{(B8)}$$

4. Demodulation of a discrete sample

In order to account for the finite sampling of the data due to the experimental cycle time T_c, the averaging expression (B8) needs to be discretized,

$$\delta a(n) = \frac{2}{n}\sum_{m=1}^n \delta\Delta a_{\text{GGC}}(mT_c)\cos(\Omega_{\text{orbit}}mT_c). \quad \text{(B9)}$$

The total integration time corresponding to n measurements is consequently given by $\tau = nT_c$.

5. Noise

The integration of noise is modified in the presence of a modulated signal. For an order-of-magnitude assessment, we refer to a simplified model in which the time signal of a differential measurement is given by

$$\Delta a = \eta g_0 \cos(\Omega_{\text{orbit}}t) + \sigma_a, \quad \text{(B10)}$$

with σ_a being the atomic shot noise. The covariance of η after n measurements is quantified by

$$\text{cov}(\eta) = \sigma^2\left(\mathbf{X}^T\mathbf{X}\right)^{-1}, \quad \text{(B11)}$$

where $X_m = g_0\cos(\Omega_{\text{orbit}}mT_c)$ captures the modulated local value of the gravitational acceleration in the mth measurement, T_c is the cycle time. Consequently, the statistical uncertainty due to shot noise in the determination of η is given by

$$\begin{aligned}\sigma_\eta(n) &= \sqrt{\text{cov}(\eta)} \\ &= \frac{\sigma}{g_0}\left(\sum_m^n \cos^2(\Omega_{\text{orbit}}mT_c)\right)^{-1} \\ &\to \frac{\sigma\sqrt{2}}{g_0\sqrt{n}}\end{aligned} \quad \text{(B12)}$$

in the limit of many measurements, $\tau = nT_c \gg T_c$.

Interference of clocks: A quantum twin paradox

Sina Loriani[1]*, Alexander Friedrich[2]*[†], Christian Ufrecht[2], Fabio Di Pumpo[2], Stephan Kleinert[2], Sven Abend[1], Naceur Gaaloul[1], Christian Meiners[1], Christian Schubert[1], Dorothee Tell[1], Étienne Wodey[1], Magdalena Zych[3], Wolfgang Ertmer[1], Albert Roura[2], Dennis Schlippert[1], Wolfgang P. Schleich[2,4,5], Ernst M. Rasel[1], Enno Giese[2]

The phase of matter waves depends on proper time and is therefore susceptible to special-relativistic (kinematic) and gravitational (redshift) time dilation. Hence, it is conceivable that atom interferometers measure general-relativistic time-dilation effects. In contrast to this intuition, we show that (i) closed light-pulse interferometers without clock transitions during the pulse sequence are not sensitive to gravitational time dilation in a linear potential. (ii) They can constitute a quantum version of the special-relativistic twin paradox. (iii) Our proposed experimental geometry for a quantum-clock interferometer isolates this effect.

INTRODUCTION

Proper time is operationally defined (*1*) as the quantity measured by an ideal clock (*2*) moving through spacetime. As the passage of time itself is relative, the comparison of two clocks that traveled along different world lines gives rise to the twin paradox (*3*). Whereas this key feature of relativity relies on clocks localized on world lines, today's clocks are based on atoms that can be in a superposition of different trajectories. This nature of quantum objects is exploited by matter-wave interferometers, which create superpositions at macroscopic spatial separations (*4*). One can therefore envision a single quantum clock such as a two-level atom in a superposition of two different world lines, suggesting a twin paradox, in principle susceptible to any form of time dilation (*5–7*). We demonstrate which atom interferometers implement a quantum twin paradox, how quantum clocks interfere, and their sensitivity to different types of time dilation.

The astonishing consequences of time dilation can be illustrated by the story of two twins (*3*), depicted in Fig. 1A: Initially at the same position, one of them decides to go on a journey through space and leaves his brother behind. Because of their relative motion, he experiences time dilation and, upon meeting his twin again after the voyage, has aged slower than his brother who remained at the same position. Although this difference in age is notable by itself, the twin who traveled could argue that, from his perspective, his brother has moved away and returned, making the same argument. This twin paradox can be resolved in the context of relativity, where it becomes apparent that not both twins are in an inertial system for the whole duration. In the presence of gravity, two twins that separate and reunite experience additional time dilation depending on the gravitational potential during their travel. The experimental verifications of the effect that leads to the difference in age, namely, special-relativistic and gravitational time dilation, were milestones in the development of modern physics and have, for instance, been performed by the comparison of two atomic

clocks (*8–10*). Atomic clocks, as used in these experiments, are based on microwave and optical transitions between electronic states and define the state of the art in time keeping (*11*).

In analogy to optical interferometry, atom interferometers measure the relative phase of a matter wave accumulated during the propagation by interfering different modes. Although it is possible to generate these interferometers through different techniques, we focus here on light-pulse atom interferometers like the one of Kasevich and Chu (*12*) with two distinct spatially separated branches, where the matter waves are manipulated through absorption and emission of photons that induce a recoil to the atom. Conventionally, these interferometers consist of a series of light pulses that coherently drive atoms into a superposition of motional states, leading to the spatial separation. The branches are then redirected and finally recombined such that the probability to find atoms in a specific momentum state displays an interference pattern and depends on the phase difference Δφ accumulated between the branches that is susceptible to inertial forces. Hence, light-pulse atom interferometers do not only provide high-precision inertial sensors (*13, 14*) with applications in tests of the foundations of physics (*15–21*) but also constitute a powerful technique to manipulate atoms and generate spatial superpositions.

Atom interferometry, in conjunction with atomic clocks, has led to the idea of using time dilation between two branches of an atom interferometer as a which-way marker to measure effects like the gravitational redshift through the visibility of the interference signal (*5, 6*). However, no specific geometry for an atom interferometer was proposed and no physical process for the manipulation of the matter waves was discussed. The geometry as well as the protocols used for coherent manipulation crucially determine whether and how the interferometer phase depends on proper time (*22*). Therefore, the question of whether the effects connected to time dilation can be observed in light-pulse atom interferometers is still missing a conclusive answer.

In this work, we study a quantum version of the twin paradox, where a single twin is in a superposition of two different world lines, aging simultaneously at different rates, illustrated in Fig. 1B. We show that light-pulse atom interferometers can implement the scenario where time dilation is due to special-relativistic effects but are insensitive to gravitational time dilation. To this end, we establish a relation between special-relativistic time dilation and kinematic asymmetry of closed atom interferometers, taking the form of recoil measurements (*15, 21, 23, 24*). For these geometries, a single atomic clock in a superposition of two different trajectories undergoes special-relativistic time

[1]Institut für Quantenoptik, Leibniz Universität Hannover, Welfengarten 1, D-30167 Hannover, Germany. [2]Institut für Quantenphysik and Center for Integrated Quantum Science and Technology (IQST), Universität Ulm, Albert-Einstein-Allee 11, D-89069 Ulm, Germany. [3]Centre for Engineered Quantum Systems, School of Mathematics and Physics, The University of Queensland, St Lucia, QLD 4072, Australia. [4]Hagler Institute for Advanced Study and Department of Physics and Astronomy, Institute for Quantum Science and Engineering (IQSE), Texas A&M AgriLife Research, Texas A&M University, College Station, TX 77843-4242, USA. [5]Institute of Quantum Technologies, German Aerospace Center (DLR), D-89069 Ulm, Germany.
*These authors contributed equally to this work.
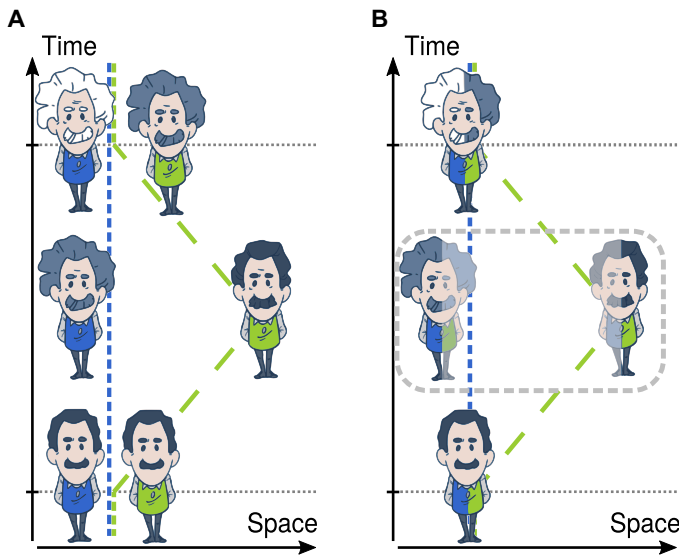†Corresponding author. Email: alexander.friedrich@uni-ulm.de

Fig. 1. Twin paradox and its quantum version. (**A**) As a consequence of relativity, two initially co-located twins experience time dilation when traveling along different world lines. Upon reunion, they find that they aged differently due to the relative motion between them. (**B**) In a quantum version of this gedankenexperiment, a single individual is traveling along two paths in superposition, serving as his own twin and aging at two different rates simultaneously.

dilation. The induced distinguishability leads to a loss of visibility upon interference such that the proposed experiment represents a realization of the twin paradox in quantum-clock interferometry.

In general relativity, the proper time along a world line $z = z(t)$ is invariant under coordinate transformations and can be approximated as

$$\tau = \int \mathrm{d}\tau \cong \int \mathrm{d}t [1 - (\dot{z}/c)^2/2 + U/c^2] \qquad (1)$$

where c denotes the speed of light. Here, $\dot{z} = \mathrm{d}z/\mathrm{d}t$ is the velocity of the particle and $U(z)$ is the Newtonian gravitational potential along the trajectory. This classical quantity is connected to the phase

$$\varphi = -\omega_C \tau + S_{em}/\hbar \qquad (2)$$

acquired by a first-quantized matter wave, assuming that it is sufficiently localized such that it can be associated with this trajectory. Here, $\omega_C = mc^2/\hbar$ denotes the Compton frequency of a particle of mass m and

$$S_{em} = -\int \mathrm{d}t \ V_{em} \qquad (3)$$

is the classical action arising from the interaction of the matter wave with electromagnetic fields described by the potential $V_{em}(z, t)$ evaluated along the trajectory. For instance, if the electromagnetic fields generate optical gratings, then this potential can transfer momentum to the matter wave, thus changing its trajectory, which, in turn, affects proper time.

Light-pulse interferometers (12) use this concept of pulsed optical gratings to manipulate matter waves. In case of interferometers closed in phase space (25) and for potentials up to the second order in z, the phase difference $\Delta\varphi$ can be calculated from Eq. 2 by integrating along the classical trajectories.

RESULTS

Time dilation and gravito-kick action

Because the light pulses act differently on the two branches of the interferometer, we add superscripts $\alpha = 1,2$ to the potential $V_{em}^{(\alpha)}$. Moreover, we separate $V_{em}^{(\alpha)} = V_k^{(\alpha)} + V_p^{(\alpha)}$ into a contribution $V_k^{(\alpha)}$ causing momentum transfer and $V_p^{(\alpha)}$ imprinting the phase of the light pulse without affecting the motional state (26). Consequently, we find that the motion $z^{(\alpha)} = z_g + z_k^{(\alpha)}$ along one branch can also be divided into two contributions: z_g caused by the gravitational potential and $z_k^{(\alpha)}$ determined by the momentum transferred by the light pulses on branch α.

For a linear gravitational potential, the proper-time difference between both branches takes the form

$$\Delta\tau = \int \mathrm{d}t \left[\ddot{z}_k^{(1)} z_k^{(1)} - \ddot{z}_k^{(2)} z_k^{(2)} \right] / (2c^2) \qquad (4)$$

(see Materials and Methods). It is explicitly independent of z_g as well as of the particular interferometer geometry, which is a consequence of the phase of a matter wave being invariant under coordinate transformations. When transforming to a freely falling frame, both trajectories reduce to the kick-dependent contribution $z_k^{(\alpha)}$ and the proper-time difference $\Delta\tau$ is thus independent of gravity (22). Accordingly, closed light-pulse interferometers are insensitive to gravitational time dilation. Our result implies that time dilation in these interferometer configurations constitutes a purely special-relativistic effect caused by the momentum transferred through the light pulses.

Our model of atom-light interaction assumes instantaneous momentum transfer and neglects the propagation time of the light pulses. A potential V_k linear in z, where the temporal pulse shape of the light is described by a delta function, that is $\ddot{z}_k \propto \delta(t - t_\ell)$, reflects exactly such a transfer. For such a potential, we find the differential action

$$\Delta S_{em} = 2\hbar\omega_C \Delta\tau + \Delta S_{gk} + \Delta S_p \qquad (5)$$

(see Materials and Methods), which can be interpreted (27) as the laser pulses sampling the position of the atoms $z = z_k + z_g$. The first contribution has the form of the proper-time difference, which highlights that the action of the laser can never be separated from proper time in a phase measurement in the limit given by Eq. 2. It arises solely from the interaction with the laser, and in the case of instantaneous acceleration $\ddot{z}_k$, these kicks read out the recoil part of the motion z_k according to Eq. 4. Similarly, the second contribution in Eq. 5 is the action that arises from the acceleration $\ddot{z}_k$ measuring the gravitational part z_g of the motion and takes the form

$$\Delta S_{gk} = m \int \mathrm{d}t \ \Delta\ddot{z}_k z_g \qquad (6)$$

where we define the difference $\Delta\ddot{z}_k = \ddot{z}_k^{(1)} - \ddot{z}_k^{(2)}$ between branch-dependent accelerations. Although this contribution is caused by the interaction with the light, the position of the atom still depends on gravity and is caused by the combination of both the momentum transfers and gravity. Hence, we refer to it as gravito-kick action. Last, the lasers imprint the laser phase action

$$\Delta S_p = -\int \mathrm{d}t \ \Delta V_p \qquad (7)$$

with $\Delta V_p = V_p^{(1)} - V_p^{(2)}$.

So far, we have not specified the interaction with the light but merely assumed that the potential V_k is linear in z. In the context of our discussion, beam splitters and mirrors are generated through optical gratings made from two counter-propagating light beams that diffract the atoms (12). In a series of light pulses, the periodicity of the ℓth grating is parameterized by an effective wave vector k_ℓ. Depending on the branch and the momentum of the incoming atom, the latter receives a recoil $\pm\hbar k_\ell$ in agreement with momentum and energy conservation. At the same time, the phase difference of the light beams is imprinted to the diffracted atoms.

To describe this process, we use the branch-dependent potential $V_k^{(\alpha)} = -\sum_\ell \hbar k_\ell^{(\alpha)} z^{(\alpha)} \delta(t - t_\ell)$ for the momentum transfer $\hbar k_\ell^{(\alpha)}$ of the ℓth laser pulse at time t_ℓ and the potential $V_p^{(\alpha)} = -\sum_\ell \hbar \phi_\ell^{(\alpha)} \delta(t - t_\ell)$ to describe the phase $\phi_\ell^{(\alpha)}$ imprinted by the light pulses (26). Because the phases imprinted by the lasers can be evaluated trivially and are independent of z, we exclude the discussion of $V_p^{(\alpha)}$ from the study of different interferometer geometries and set it to zero in the following.

Atom-interferometric twin paradox

The Kasevich-Chu–type (12) Mach-Zehnder interferometer (MZI) has been at the center of a vivid discussion about gravitational redshift in atom interferometers (26–28). It has been demonstrated that its sensitivity to the gravitational acceleration g stems entirely from the interaction with the light, i.e., ΔS_{gk}, while the proper time vanishes (26, 27). It is hence insensitive to gravitational time dilation, which, a priori, is not necessarily true for arbitrary interferometer geometries.

Such an MZI consists of a sequence of pulses coherently creating, redirecting, and finally recombining the two branches. The three pulses are separated by equal time intervals of duration T. We show

the spacetime diagram of the two branches $z_k^{(\alpha)}$, the light-pulse–induced acceleration $\ddot{z}_k^{(\alpha)}$ as a sequence in time, and the gravitationally induced trajectory z_g in Fig. 2 on the left. The contributions $z_k^{(\alpha)}$ are branch dependent, while z_g is common for both arms of the interferometer. From these quantities and with the help of Eqs. 4 and 6, we obtain the phase contributions shown at the bottom of Fig. 2 (see Materials and Methods). The phase takes the familiar form $\Delta\varphi = -kgT^2$ and has no proper-time contribution, but is solely determined by the gravito-kick action originating in the interaction with the light pulses (26, 27).

The vanishing proper-time difference can be explained by the light-pulse–induced acceleration $\ddot{z}_k^{(\alpha)}$ that acts symmetrically on both branches. We draw on the classical twin paradox to illustrate the effect: At some time, one twin starts to move away from his brother and undergoes special-relativistic time dilation, as shown by hypothetical ticking rates in the spacetime diagram (the dashing periods in Fig. 2). After a time T, he stops and his brother starts moving toward him. Because his velocity corresponds to the one that caused the separation, he undergoes exactly the same time dilation his brother experienced previously. Hence, when both twins meet after another time interval T, their clocks are synchronized and no proper-time difference arises. In an MZI, we find the quantum analog of this configuration, where a single atom moves in a superposition of two different world lines like the quantum twin of Fig. 1B. However, because of the symmetry of the light-pulse–induced acceleration, no proper-time difference is accumulated between the branches of the interferometer.

A similar observation is made for the symmetric Ramsey-Bordé interferometer (RBI), where the atom separates for a time T, then stops on one branch for a time T' before the other branch is redirected. We show the spacetime diagrams and the light-pulse–induced acceleration
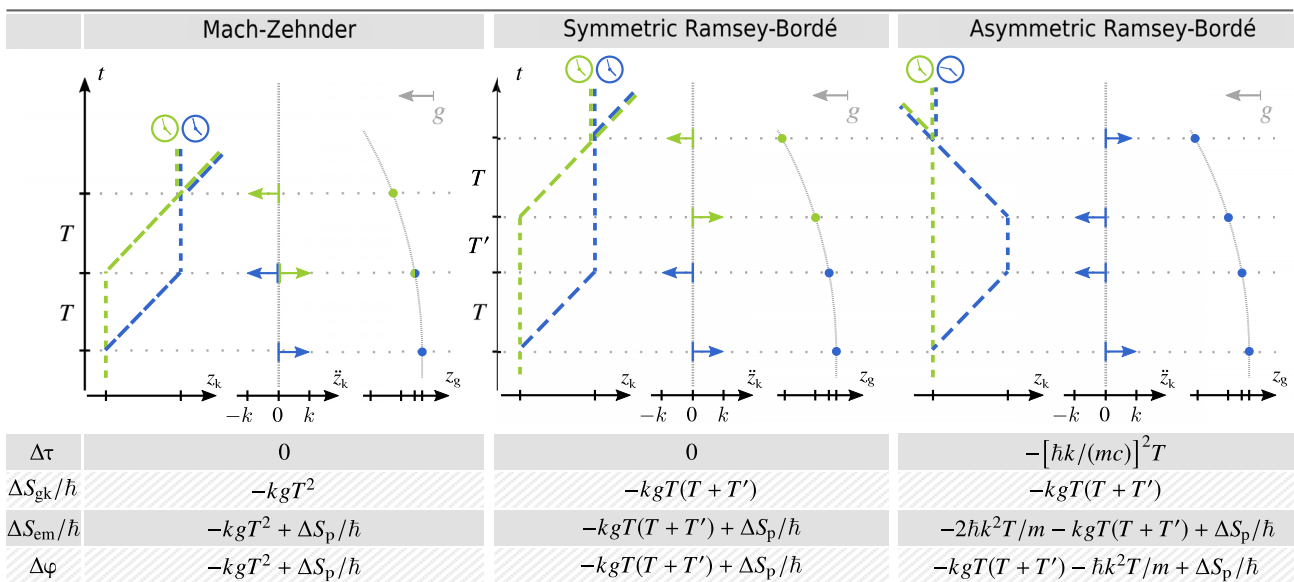

Fig. 2. Time dilation in different interferometer geometries. Spacetime diagrams for the light-pulse and gravitationally induced trajectories z_k and z_g, as well as the accelerations $\ddot{z}_k$ caused by the light pulses, together with the proper-time difference $\Delta\tau$, the gravito-kick action ΔS_{gk}, the electromagnetic contribution $\Delta S_{em}/\hbar$, and the total phase difference $\Delta\varphi$ of an MZI (left), a symmetric RBI (center), and an asymmetric RBI (right). The first two geometries display a symmetric momentum transfer between the two branches, leading to vanishing proper-time differences. However, the asymmetric RBI features a proper-time difference that has the form of a recoil term. The spacetime diagrams also illustrate the connection to the twin paradox by displaying ticking rates (the dashes) of the two twins traveling along the two branches. Both quantum twins in the MZI and symmetric RBI experience the same time dilation, whereas in the asymmetric RBI, one twin stays at rest and the other one leaves and returns so that their proper times are different. The arrows in the plot of $\ddot{z}_k$ denote the amplitude of the delta functions that scale with $\pm\hbar k/m$. Because of the instantaneous nature of $\ddot{z}_k$, the integration over time in Eqs. 4 and 6 reduces to a sampling of the positions z_k and z_g at the time of the pulses such that the respective phase contributions can be inferred directly from the figure.

	Mach-Zehnder	Symmetric Ramsey-Bordé	Asymmetric Ramsey-Bordé
$\Delta\tau$	0	0	$-\left[\hbar k/(mc)\right]^2 T$
$\Delta S_{gk}/\hbar$	$-kgT^2$	$-kgT(T+T')$	$-kgT(T+T')$
$\Delta S_{em}/\hbar$	$-kgT^2 + \Delta S_p/\hbar$	$-kgT(T+T') + \Delta S_p/\hbar$	$-2\hbar k^2 T/m - kgT(T+T') + \Delta S_p/\hbar$
$\Delta\varphi$	$-kgT^2 + \Delta S_p/\hbar$	$-kgT(T+T') + \Delta S_p/\hbar$	$-kgT(T+T') - \hbar k^2 T/m + \Delta S_p/\hbar$

$\ddot{z}_k$ in the center of Fig. 2 with the phase contributions below. The two light pulses in the middle of the symmetric RBI are also beam-splitting pulses that introduce a symmetric loss of atoms. As for the MZI, the proper-time difference between both branches vanishes and the phase is determined solely by the laser contribution and the gravito-kick phase, as shown by the ticking rates in the spacetime diagram. The only difference with respect to the MZI is that the two branches travel in parallel for a time T' during which proper time elapses identically for both of them.

The situation changes substantially when we consider an asymmetric RBI, where one branch is completely unaffected by the two central pulses, as shown on the right of Fig. 2. Specifically, the twin that moved away from his initial position experiences a second time dilation on his way back so that there is a proper-time difference when both twins meet at the final pulse. It is therefore the kinematic asymmetry that causes a nonvanishing proper-time difference, as indicated in the figure by the ticking rates. The proper-time difference

$$\Delta\tau_{\text{aRBI}} = -(\hbar k/mc)^2 T \quad (8)$$

is proportional to a kinetic term (23) that depends on the momentum transfer $\hbar k$, as already implied by Eq. 4. With the light-pulse–induced acceleration $\ddot{z}_k^{(\alpha)}$ as well as the gravitationally induced trajectory z_g also shown on the right of the figure, we find the same contribution for ΔS_{gk} given in Fig. 2 as for the symmetric RBI. The other contribution of $\Delta S_{\text{em}}/\hbar$ has the form $2\omega_C\Delta\tau_{\text{aRBI}}$, and all of them together contribute to the phase difference $\Delta\varphi$.

Clocks in spatial superposition

While the twin paradox is helpful in gaining intuitive understanding and insight into the phase contributions, the dashing length of the world lines in Fig. 2 only indicates the ticking rate of a hypothetical co-moving clock. The atoms are in a stationary internal state during propagation, whereas the concept of a clock requires a periodic evolution between two states. As a consequence, the atom interferometer can be sensitive to special-relativistic time dilation but lacks the notion of a clock. In a debate (28) about whether the latter is accounted for by the Compton frequency ω_C as the prefactor to the proper-time difference in Eq. 2, an additional superposition of internal states (5, 6) was proposed. This idea leads to an experiment where a single clock is in superposition of different branches, measuring the elapsed proper time along each branch. In contrast to these discussions that raised questions about the role of gravitational time dilation in quantum-clock interferometry and where no specific model for the coherent manipulation of the atoms was explored (6), we have demonstrated in this article that light-pulse atom interferometers are only susceptible to special-relativistic time dilation. In a different context, a spatial superposition of a clock has been experimentally realized, however, through an MZI geometry that is insensitive to time-dilation effects (29). The implementation of a twin-paradox–type experiment with an electron in superposition of different states of a Penning trap has been proposed, where the role of internal states is played by the spin (30). Furthermore, quantum teleportation and entanglement between two two-level systems moving in a twin-paradox geometry was considered in the framework of Unruh-DeWitt detectors (31).

To illustrate the effect of different internal states, we introduce an effective model for an atomic clock that moves along branch $\alpha = 1,2$ in an interferometer. In this framework (7, 32), the Hamiltonian

$$\hat{H}_j^{(\alpha)} = m_j c^2 + \frac{\hat{p}^2}{2m_j} + m_j g\hat{z} + V_{\text{em}}^{(\alpha)}(\hat{z}, t) \text{ with } j \in \{a, b\} \quad (9)$$

describes a single internal state of energy $E_j = m_j c^2$ with an effective potential $V_{\text{em}}^{(\alpha)}$, which models the momentum transfer (see Materials and Methods). Mass-energy equivalence in relativity implies that different internal states are associated with different energies and therefore correspond to different masses m_j. To connect with our previous discussion, we take the limit of instantaneous pulses neglecting the delay of the light front propagating from the laser to the atoms. With these considerations, the Hamiltonian for a clock consisting of an excited state $|a\rangle$ and a ground state $|b\rangle$, both forced by Bragg pulses that do not change the internal state (33) on two branches $\alpha = 1,2$, reads

$$\hat{H}^{(\alpha)} = \hat{H}_a^{(\alpha)} |a\rangle\langle a| + \hat{H}_b^{(\alpha)} |b\rangle\langle b| \quad (10)$$

Because the Hamiltonian is diagonal in the internal states, we write the time evolution along branch α as $\hat{U}^{(\alpha)} = \hat{U}_a^{(\alpha)} |a\rangle\langle a| + \hat{U}_b^{(\alpha)} |b\rangle\langle b|$, where $\hat{U}_j^{(\alpha)}$ is the time-evolution operator that arises from the Hamiltonian $\hat{H}_j^{(\alpha)}$. For an atom initially in a state $|j\rangle$ with $j = a, b$, the output state is determined by the superposition $\hat{U}_j^{(1)} + \hat{U}_j^{(2)}$ and leads to an interference pattern $P_j = (1 + \cos \Delta\varphi_j)/2$, where the phase difference $\Delta\varphi_j$ depends on the internal state.

In the case of quantum-clock interferometry, the initial state for the interferometer is a superposition of both internal states $(|a\rangle + |b\rangle)/\sqrt{2}$, which form a clock that moves along both branches in superposition. The outlined formalism shows that such a superposition leads to the sum of two interference patterns, that is, $P = (P_a + P_b)/2$. The sum of the probabilities $P_{a/b}$ with slightly different phases, which corresponds to the concurrent operation of two independent interferometers for the individual states, leads to a beating of the total signal and an apparent modulation of the visibility. Expressing the masses of the individual states by their mass difference Δm, i.e., $m_{a/b} = m \pm \Delta m/2$, and identifying the energy difference $\Delta E = \Delta mc^2 = \hbar\Omega$ lead to the interference pattern

$$P = \frac{1}{2}\left[1 + \cos\left(\eta\frac{\Omega\Delta\tau}{2}\right)\cos\left(\eta\omega_C\Delta\tau + \frac{\Delta S_{\text{gk}} + \Delta S_{\text{p}}}{\hbar}\right)\right] \quad (11)$$

where the scaling factor $\eta = 1/[1 - \Delta m^2/(2m)^2]$ depends on the energy difference of the two states. In this form, the first cosine can be interpreted as a slow but periodic change of the effective visibility of the signal. To first order in $\Delta m/m$, we find that $\eta = 1$ so that the effective visibility $\cos(\Omega\Delta\tau/2)$ corresponds to the signal of a clock measuring the proper-time difference. In this picture, the loss of contrast can be seen as a consequence of distinguishability (6): Because a superposition of internal states travels along each branch, the system can be viewed as a clock with frequency Ω traveling in a spatial superposition. On each branch, the clock measures proper time and by that contains which-way information, leading to a loss of visibility as a direct consequence of complementarity.

We illustrate this effect in Fig. 3A using an asymmetric double-loop RBI, where the gravito-kick action vanishes, i.e., $\Delta S_{\text{gk}} = 0$, because it is insensitive to linear accelerations like other symmetric double-loop geometries that are routinely used to measure rotations and gravity gradients (34). The measured phase takes the form $\Delta\varphi = 2\omega_C\tau_{\text{aRBI}} =$
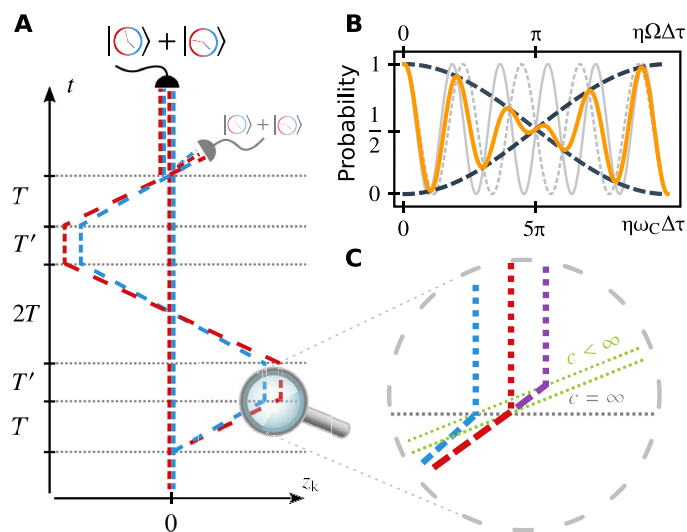
Fig. 3. Interference of quantum clocks. (**A**) Spacetime diagram of a double-loop RBI in superposition of two different internal states (red and blue) and detection at the zero-momentum output port. We indicate the effect of different recoil velocities due to different rest masses of the internal states by slightly diverging trajectories. The different ticking rates of co-moving clocks on the trajectories are indicated by the frequency of the dashing. The dotted gray lines correspond to the light pulses used to redirect the atoms. (**B**) The output signal P (solid orange) shows a visibility modulation (dashed black), which can be interpreted as the beating of the individual signals $P_{a/b}$ of the two internal states (solid and dashed gray). To highlight the effect, we have chosen $\Delta m/m = 0.2$ in Eq. 11. The visibility of the signal vanishes at $\eta\Omega\Delta\tau = \pi$. (**C**) Interaction of a light pulse with the excited and ground states (blue and red). Because the states follow slightly different world lines and the speed of light is finite, the light pulse will not interact simultaneously with both. Our assumption of instantaneous interaction is shown by the red and blue lines. In the case of finite pulse propagation speed, indicated by the slightly tilted dotted green lines, the interaction is not simultaneous and the red line for the ground state becomes the outermost purple line.

$-2\hbar k^2 T/m$. Although this expression is proportional to a term that has the form of proper time, it also comprises contributions from the interaction with the laser pulses (see the first term of Eq. 5). The two internal states, denoted by the blue and red ticking rates, travel along both branches such that each twin carries its own clock, leading to distinguishability when they meet. This distinguishability depends on the frequency Ω of the clock and implies a loss of visibility, as shown in Fig. 3B. However, because each internal state experiences a slightly different recoil velocity $\hbar k/m_{a/b}$, it can be associated with a slightly different trajectory, displayed in red and blue in Fig. 3A. The interpretation as a clock traveling along one particular branch is therefore only valid to lowest order in $\Delta m/m$.

In another interpretation, the quantum twin experiment is performed for each state independently. The trajectories are different for each state, and the proper-time difference as well as the Compton frequency are mass dependent so that the interferometer phase depends explicitly on the mass. The loss of visibility can therefore be explained by the beating of the two different interference signals, which is caused by the mass difference $\Delta m = \hbar\Omega/c^2$. In the spacetime diagram of Fig. 3A, the finite speed of light pulses causing the momentum transfers is not taken into account. However, to illustrate the neglected effects induced by the propagation time, Fig. 3C magnifies such an interaction and showcases the assumption we made in our calculation:

Both internal states interact simultaneously and instantaneously with the light pulse, although they might be spatially separated. For feasible recoil velocities, as well as interferometer and pulse durations, this approximation is reasonable as detailed in Materials and Methods on the light-matter interaction.

DISCUSSION

A realization of quantum-clock interferometry in a twin experiment requires atomic species that feature a large internal energy splitting, suggesting typical clock atoms like strontium (Sr) with optical frequencies Ω in the order of hundreds of terahertz. The proper-time difference is a property of the interferometer geometry and is enhanced for large splitting times T and effective momentum transfers $\hbar k$. Besides large-momentum transfer techniques (4, 21), this calls for atomic fountains in the order of meters (20, 35, 36) and more or the operation in microgravity (18, 37).

To observe a full drop in visibility and its revival, the accumulated time dilation in the experiment needs to be on the order of femtoseconds. In the example of Sr, this can be achieved for $T = 350$ ms and $k = 1200\,k_m$, where $k_m = 1.5 \times 10^7$ m^{-1} is the effective wave number of the magic two-photon Bragg transition. At the magic wavelength (38) of 813 nm, the differential ac-Stark shift of the two clock states vanishes to first order such that the beam splitters act equally on the two internal states and hence leave the clock unaffected. Increasing T and by that $\Delta\tau$, one should observe a quadratic loss of visibility as a signature of which-path information, assuming that this loss can be distinguished from other deleterious effects. Times up to $T = 350$ ms and $k = 580\,k_m$ induce a visibility reduction of 10%.

Although they do not use the same species, large atomic fountains (20) already realize long free evolution times and large momentum transfer with hundreds of recoil momenta has been demonstrated (4, 21). Techniques to compensate the impact of gravity gradients (25) and rotations (39) have already proven to be successful (20, 35, 40). The main challenge in implementing quantum-clock interferometers as described above lies in the concurrent manipulation of the two clock states (29), requiring a transfer of concepts and technologies well established for alkaline atoms to alkaline earth species. Besides magic Bragg diffraction, other mechanisms like simultaneous single-photon transitions between the clock states (41) are also conceivable and relax the requirements on laser power. In view of possible applications to gravitational wave detection (42), atom interferometry based on single-photon transitions is already becoming a major line of research. To this end, the first steps toward quantum-clock interferometry have been demonstrated by driving clock transitions of Sr to generate MZI geometries (32).

Because the effect can be interpreted as a beating of the signal of two atomic species (defined through their internal state), one can also determine the phase for each state independently and infer their difference in the data analysis. A differential phase of 1 mrad assuming $T = 60$ ms and $k = 70\,k_m$ may already be resolved in a table-top setup in a few hundred shots with 10^6 atoms, supposing shot-noise limited measurements of the two internal states. Equation 4 shows that proper-time differences in our setting arise only from special-relativistic effects caused by the momentum transfer. Such an experiment is equivalent to the comparison of two recoil measurements (15, 21) performed independently but simultaneously to suppress common-mode noise. Beyond recoil spectroscopy, state resolving measurements can be of particular interest for a doubly differential

measurement scheme that, in contrast to the setup discussed above, does not rely on an initial superposition of two internal states. Instead, the superposition of internal states is generated during the interferometer (41) such that these setups can be used to measure the time dilation caused by a gravitational redshift. In contrast, our discussion highlights the relevance of special-relativistic time dilation for the interference of quantum clocks in conventional interferometers without internal transitions.

In summary, we have shown that, for an interferometer that does not change the internal state during the sequence, the measured proper-time difference is in lowest order independent of gravity and is nonvanishing only in recoil measurements, connecting matter-wave interferometry to the special-relativistic twin paradox. As a consequence of this independence, these light-pulse atom interferometers are insensitive to gravitational time dilation.

The light pulses creating the interferometer cause a contribution to its phase that is of the same form as the special-relativistic proper-time difference and depends on the position of the branches in a freely falling frame, which can be associated with the world line of a quantum twin. Because these trajectories and thus proper time depend on the recoil velocity that is slightly different for different internal states, an initial superposition causes a beating of two interference patterns. In such a quantum version of the twin paradox, a clock is in a spatial superposition of different world lines, leading to a genuine implementation of quantum-clock interferometry but based on special-relativistic time dilation only.

MATERIALS AND METHODS
Recoil terms and proper time
In this section, we show that, for light pulses acting instantaneously on both branches and gravitational potentials up to linear order, the proper time consists only of recoil terms. We provide the explicit expressions for the proper-time difference and find a compact form for the action of the electromagnetic potential describing pulsed optical gratings that contributes to the phase of the atom interferometer.

As already implied by the decomposition from Eq. 3, the interaction of an atom with a light pulse transfers momentum and imprints a phase on the atom (26). Because the latter contribution does not modify the motion of the atom, we find $\partial V_p / \partial z = 0$. Consequently, the classical equations of motion can be written as $m\ddot{z} = -\partial(mU)/\partial z - \partial V_k / \partial z = m\ddot{z}_g + m\ddot{z}_k$. The integration of these equations leads to the trajectory $z = z(t)$ that can be decomposed into two contributions associated with these accelerations, i.e., $z = z_g + z_k$, where we collect the initial conditions in z_g.

Proper time takes in lowest order expansion in c^{-2}, i.e., for weak fields and low velocities, according to Eq. 1 for a linear gravitational potential the form

$$c^2 \tau = \int dt (c^2 - \dot{z}^2/2 - \ddot{z}_g z) \qquad (12)$$

We simplify this expression by integrating the kinetic term $\dot{z}^2/2$ by parts and make the substitution $z = z_g + z_k$ in the remaining integral so that we find

$$c^2 \tau = -\frac{\dot{z}z}{2} \Big| + \int dt \left(c^2 + \frac{\ddot{z}_k z_k}{2} - \frac{\ddot{z}_g z_g}{2} + \frac{\ddot{z}_k z_g - \ddot{z}_g z_k}{2} \right) \qquad (13)$$

for the proper time. Partial integration of the last term in the integral leads to the compact form

$$c^2 \tau = \frac{\dot{z}_k z_g - \dot{z}_g z_k - \dot{z}z}{2} \Big| + \int dt \left(c^2 - \frac{\ddot{z}_g z_g}{2} + \frac{\ddot{z}_k z_k}{2} \right) \qquad (14)$$

that explicitly depends on the initial and final positions and velocities.

In a light-pulse atom interferometer, light pulses act independently through the potentials $V_k^{(\alpha)}$ on the two branches $\alpha = 1,2$ and give rise to the light-pulse–induced trajectories $z_k^{(\alpha)}$. In turn, these branch-dependent potentials lead to a proper-time difference $\Delta\tau = \tau^{(1)} - \tau^{(2)}$ between the upper and lower branch of the interferometer and cause a phase contribution to the interference pattern. In an interferometer closed in phase space, the initial and final positions as well as velocities are the same for both branches, and thus, the first term in Eq. 14 vanishes. Because z_g is branch independent, the first two terms in the integral also cancel and we are left with

$$\Delta\tau = \int dt \left[\ddot{z}_k^{(1)} z_k^{(1)} - \ddot{z}_k^{(2)} z_k^{(2)} \right] / (2c^2) \qquad (15)$$

for the lowest order of the proper-time difference of an atom interferometer in a linear gravitational potential. Hence, the proper-time difference in a closed interferometer is independent of gravity and constitutes a special-relativistic effect. This result can also be derived for a time-dependent gravitational acceleration $g(t)$.

Because proper time is invariant under coordinate transformations, the proper-time difference of a closed atom interferometer is independent of the gravitational acceleration by considering the common freely falling frame. In this frame, the trajectories are straight lines and correspond to $z_k^{(\alpha)}$, as implied by Fig. 2, so that the proper-time difference is of special-relativistic origin. Hence, Eq. 15 can also be interpreted as a direct consequence of transforming to a freely falling frame in a homogeneous gravitational field.

The laser contribution to the phase can be calculated from Eq. 3, and we write the classical action in the form of

$$S_{em} = -\int dt \, (V_k + V_p) = m \int dt \, \ddot{z}_k z - \int dt \, V_p \qquad (16)$$

where we assumed that $V_k = -m\ddot{z}_k z$ is linear in z. When we again use the decomposition of the position $z = z_g + z_k$ into a part induced by gravity and a part induced by the light pulses, we find

$$S_{em} = m \int dt \, \ddot{z}_k z_k + m \int dt \, \ddot{z}_k z_g - \int dt \, V_p \qquad (17)$$

for the action. Because z_g is branch independent in contrast to z_k, the difference

$$\Delta S_{em} = m \int dt \left[\ddot{z}_k^{(1)} z_k^{(1)} - \ddot{z}_k^{(2)} z_k^{(2)} \right] + m \int dt \, \Delta\ddot{z}_k z_g - \int dt \, \Delta V_p \qquad (18)$$

between upper and lower branch depends on $\Delta\ddot{z}_k = \ddot{z}_k^{(1)} - \ddot{z}_k^{(2)}$ and $\Delta V_p = V_p^{(1)} - V_p^{(2)}$. With the expression for the proper time from Eq. 4, the gravito-kick action from Eq. 6, and the laser phase action from Eq. 7,

we arrive at the form of Eq. 5 for the action of the interaction with the electromagnetic field such as pulsed optical gratings.

For the specific form of the phase contributions and proper time, we first calculate the trajectory that arises from $\ddot{z}_g = -g$ and find by simple integration that

$$z_g(t) = z(0) + \dot{z}(0)\, t - gt^2/2 \tag{19}$$

which is branch independent. For the specific form of the phase contributions and proper time, we calculate the trajectories that arise from the atom-light interaction. To this end, we assume the potential $V_k^{(\alpha)} = -\sum_\ell \hbar k_\ell^{(\alpha)} z^{(\alpha)} \delta(t - t_\ell)$ that causes the momentum transfer $m\ddot{z}_k^{(\alpha)} = \sum_\ell \hbar k_\ell^{(\alpha)} \delta(t - t_\ell)$. Integrating the acceleration leads to the two branches of the interferometer given by the two trajectories

$$z_k^{(\alpha)}(t) = \sum_{\ell=1}^{n} (t - t_\ell) \hbar k_\ell^{(\alpha)}/m \tag{20}$$

for $t_{n+1} > t > t_n$.

Using the expression for $\ddot{z}_k^{(\alpha)}$, the gravito-kick phase from Eq. 6 takes the explicit form

$$\Delta S_{gk}/\hbar = \sum_\ell \Delta k_\ell z_g(t_\ell) \tag{21}$$

where we evaluate the gravitationally induced trajectory from Eq. 19 at the times of the pulses. Note that we defined the differential momentum transfer $\Delta k_\ell = k_\ell^{(1)} - k_\ell^{(2)}$ of the ℓth laser pulse.

With the branch-dependent trajectory from Eq. 20 and $\ddot{z}_k^{(\alpha)}$, we perform the integration in Eq. 15 to arrive at the expression

$$\omega_C \Delta\tau = \frac{\hbar}{2m} \sum_{n=1}^{M} \sum_{\ell=1}^{n} \left[k_n^{(1)} k_\ell^{(1)} - k_n^{(2)} k_\ell^{(2)} \right] (t_n - t_\ell) \tag{22}$$

where M is the total number of light-matter interaction points. This phase difference is proportional to $\hbar/m$ and includes a combination of the transferred momenta and separation between the laser pulses.

Post-Galilean bound systems in a Newtonian gravitational field

We consider a static spacetime with a line element of the form

$$ds^2 = g_{\mu\nu}(x) dx^\mu dx^\nu = -N(\vec{x})(c dt)^2 + B_{ij}(\vec{x}) dx^i dx^j \tag{23}$$

where $g_{\mu\nu}$ is the metric with Greek indices running from 0 to 3, N is the lapse function, and B_{ij} is the three-metric with Latin indices from 1 to 3. In the limit of Newtonian gravity, the lapse function becomes $N(\vec{x}) = 1 + 2U(\vec{x})/c^2$, with U being the Newtonian gravitational potential and $B_{ij} = [1 - 2U(\vec{x})/c^2] \delta_{ij}$, where δ_{ij} is the Kronecker symbol. The post-Newtonian correction to the spatial part of the metric decomposition only needs to be considered for the electromagnetic field but not for the atoms inside a light-pulse atom interferometer.

To model atomic multilevel systems inside such a background metric including effects that arise from special-relativistic and general-relativistic corrections due to the lapse function of the metric to the bound state energies, one can resort to a quantum field theoretical treatment (43) and perform the appropriate limit to a first-quantized theory afterward. In this approach, one first performs the second quan-

tization of the respective interacting field theory in the classical background metric provided by Eq. 23 and derives the bound state energies as well as possible spin states of, e.g., hydrogen-like systems. For each pair of energy and corresponding internal state, one can take the limit of a first-quantized theory and Newtonian gravity. Expanding the Newtonian gravitational potential up to second order leads to a Hamiltonian

$$\hat{H}_{0,j} = m_j c^2 + \frac{\hat{\vec{p}}^2}{2m_j} + m_j \left(\vec{g}^\top \hat{\vec{x}} + \frac{1}{2} \hat{\vec{x}}^\top \Gamma \hat{\vec{x}} \right) \tag{24}$$

Here, $E_j = m_j c^2$ is the energy corresponding to the energy eigenstate $|j\rangle$; $\hat{\vec{p}}$ and $\hat{\vec{x}}$ are the momentum and position operator, respectively; $\vec{g}$ is the (local) gravitational acceleration vector; and Γ is the (local) gravity gradient tensor. This Hamiltonian includes special-relativistic and possibly post-Newtonian contributions to its internal energies as indicated by the different masses m_j of the individual internal states, which is a direct manifestation of the mass-energy equivalence. In principle, terms proportional to $\hat{\vec{p}}^4$ and $\hat{\vec{p}}^\top \left(\vec{g}^\top \hat{\vec{x}} + \frac{1}{2} \hat{\vec{x}}^\top \Gamma \hat{\vec{x}} \right) \hat{\vec{p}}$ appear as a correction to the center-of-mass Hamiltonian. However, because these terms are state independent to order $1/c^2$, they leave the beating in Eq. 11 unaffected and will therefore be disregarded. The third addend in Eq. 24 is the Newtonian gravitational potential energy, which we denote by $V_g(\hat{\vec{x}})$. The fact that each state couples separately to the (expanded) gravitational potential with its respective mass m_j directly highlights the weak equivalence principle. The full Hamiltonian of an atomic system with multiple internal states labeled by the index j is thus $\hat{H}_0 = \sum_j \hat{H}_{0,j} |j\rangle\langle j|$. This Hamiltonian is diagonal with respect to different internal states, and gravity induces no cross-coupling between the states of freely moving atoms.

Light-matter interaction and total Hamiltonian

In typical light-pulse atom interferometers, the light-matter interaction is only switched on during the beam-splitting pulses. Hence, the propagation of the atoms through an interferometer can be partitioned into periods of free propagation and periods where the lasers are acting on the atoms. In particular, the light-matter interaction including post-Newtonian corrections to the atoms' bound state energies (44, 45) in the low-velocity, dipole approximation limit reduces to

$$\hat{\mathcal{V}}_{em}(\hat{\vec{x}}, t) = -\hat{\vec{\wp}} \cdot \vec{E}(\hat{\vec{x}}, t) + \hat{\mathcal{V}}_R(\hat{\vec{x}}, t; \hat{\wp}) \tag{25}$$

where $\hat{\vec{\wp}}$ is the electric dipole moment operator, $\vec{E}$ is the external electric field, and $\hat{\mathcal{V}}_R$ is the Röntgen contribution to the interaction Hamiltonian. The information about special-relativistic corrections to the energies is included in the definition of the dipole moments. Moreover, because the light-matter coupling is of the usual form, we can apply the standard framework of quantum optics to derive effective models for the interaction.

However, before proceeding, we simplify our model by only considering unidirectional motion in the z-direction and an acceleration g anti-parallel to it so that the Hamiltonian for the full interferometer becomes

$$\begin{aligned} \hat{H}(\hat{z}, t) &= \sum_j \left[m_j c^2 + \frac{\hat{p}^2}{2m_j} + m_j \left(g\hat{z} + \frac{\Gamma}{2} \hat{z}^2 \right) \right] |j\rangle\langle j| \\ &\quad + \sum_{i \neq j} \mathcal{V}_{em,ij}(\hat{z}, t) |i\rangle\langle j| \end{aligned} \tag{26}$$

where $\mathcal{V}_{\mathrm{em},ij}$ are the time-dependent matrix elements of the light-matter coupling, which include the switch on/off of the lasers. On the basis of this model, we can derive an effective potential description, for example, two-photon Raman or Bragg transitions, inside an interferometer. In particular, for magic Bragg diffraction, we consider pairs of one relevant state $|j\rangle$ and one ancilla state out of the atomic state manifold, each interacting with two light fields. After applying the rotating wave approximation, adiabatic elimination, and two-photon resonance conditions (33) and taking the limit of instantaneous pulses, we can replace the electromagnetic interaction by the effective potential

$$\hat{V}_{\mathrm{em}} = -\hbar\sum_j (k_\ell \hat{z} + \phi_\ell)\delta(t - t_\ell)\,|j\rangle\langle j| \qquad (27)$$

Here, we evaluate the effective momentum transfer $\hbar k_\ell$ as well as the phase ϕ_ℓ of the electromagnetic field at time t_ℓ of the pulse. Although we have written the state dependence explicitly in Eq. 27, the effective interaction $\hat{V}_{\mathrm{em}}$ becomes state independent because the sum over the relevant states $|j\rangle$ corresponds to unity in case of magic Bragg diffraction.

During a typical light-pulse atom interferometer sequence, one usually has multiple wave-packet components centered on different trajectories, each of which constitutes an individual branch of the interferometer. In this case, the previously defined interaction can be applied (25) on each branch individually. Hence, the effective interaction Hamiltonian in the case of instantaneous Bragg pulses becomes

$$\hat{V}_{\mathrm{em}}^{(\alpha)} = -\hbar\sum_\ell \left(k_\ell^{(\alpha)}\hat{z} + \phi_\ell^{(\alpha)}\right)\delta(t - t_\ell) \qquad (28)$$

where the superscript α labels the individual branch. A perturbative treatment shows that the approximation of instantaneous pulses is appropriate if the interaction time of the laser pulses with the atoms is sufficiently short compared to the duration of the interferometer (46). Furthermore, the propagation delay of the lightfront between wave-packet components introduces a further phase contribution. However, this phase is suppressed in the differential measurement by an additional factor of $\hbar k/(m_{a/b}c)$ compared to the phases of interest; it is thus of order $1/c^3$ and can be neglected.

Branch-dependent light-pulse atom interferometry
As shown above, the momentum transfer caused by light pulses can be described by an effective potential that generally depends on the classical trajectory of the particle. In our limit, this dependence reduces to a mere dependence on the two branches of an atom interferometer. Because our description is diagonal in the different internal states and we assume that, throughout the free propagation inside the interferometer, the internal state of the atoms does not change, the time evolution along branch $\alpha = 1,2$ takes the form

$$\hat{U}^{(\alpha)} = \hat{U}_a^{(\alpha)}\,|a\rangle\langle a| + \hat{U}_b^{(\alpha)}\,|b\rangle\langle b| \qquad (29)$$

where $\hat{U}_j^{(\alpha)}$ is the time-evolution operator for state $|j\rangle$ along path α ending in one particular exit port. We limit our discussion to one excited state and one ground state; hence, we use the labels $j = a, b$. If $|\psi_j(0)\rangle$ describes the initial external degree of freedom of the atoms in state $|j\rangle$ and we project onto the internal state when we perform

the measurement, the postselected state in one of the output ports of the interferometer is a superposition of the two branches, i.e., $|\psi_j\rangle = (\hat{U}_j^{(1)} + \hat{U}_j^{(2)})\,|\psi_j(0)\rangle/2$, leading to the interference pattern

$$P_j = \langle\psi_j|\psi_j\rangle = \frac{1}{2}\left(1 + \frac{1}{2}\langle\psi_j(0)|\,\hat{U}_j^{(2)\dagger}\hat{U}_j^{(1)}\,|\psi_j(0)\rangle + \mathrm{c.c.}\right) \qquad (30)$$

The calculation of the inner product can now be performed using the explicit form of the branch-dependent potentials. For a closed geometry and potentials up to linear order, the calculation reduces to the description outlined in the main part of the article (26). This treatment is also exact in the presence of gravity gradients and rotations but will lead in general to open geometries, which can be closed through suitable techniques (25). When we introduce the state-dependent Compton frequency $\omega_j = m_j c^2/\hbar$ and proper-time difference $\Delta\tau_j$ where m has to be replaced by m_j, we find $P_j = (1 + \cos\Delta\varphi_j)/2$ and the phase difference

$$\Delta\varphi_j = -\omega_j\Delta\tau_j + 2\omega_j\Delta\tau_j + \Delta S_{\mathrm{gk}}/\hbar + \Delta S_{\mathrm{p}}/\hbar \qquad (31)$$

Here, we used the fact that both ΔS_{gk} and ΔS_{p} do not depend on the internal state in accordance with the weak equivalence principle. Moreover, the phases are degenerate if the proper-time difference vanishes.

If the atoms are initially in a superposition of the two internal states, i.e., $(|a\rangle + |b\rangle)/\sqrt{2}$, the exit port probability without postselection on one internal state is $P = (P_a + P_b)/2$, which corresponds to the sum of the two interference patterns. After some trigonometry, we find

$$P = \frac{1}{2}\left[1 + \cos\left(\frac{\Delta\varphi_a - \Delta\varphi_b}{2}\right)\cos\left(\frac{\Delta\varphi_a + \Delta\varphi_b}{2}\right)\right] \qquad (32)$$

so that the two interference patterns beat. The first term, i.e., the difference of the phases of the individual states, can be interpreted as a visibility modulation of the concurrent measurement. Because the two masses $m_{a/b} = m \pm \Delta m/2$ are connected to the energy difference $\Delta E = \hbar\Omega = \Delta mc^2$ between the excited and ground state, the frequency Ω determines the beating.

Connection to clock Hamiltonians
We discuss in the main body of the article that, in an expansion of the phase difference in orders of $\Delta m/m$, the beating effect can be interpreted as a loss of contrast due to the distinguishability of two internal clock states. In this section, we show the connection of the Hamiltonian from Eq. 26 to a clock Hamiltonian (6)

$$\hat{H}_{\mathrm{int}} = \left(mc^2 - \frac{\hbar\Omega}{2}\right)|b\rangle\langle b| + \left(mc^2 + \frac{\hbar\Omega}{2}\right)|a\rangle\langle a| \qquad (33)$$

Expanding Eq. 10 up to the linear order of $\Delta m/m$, we find the expression

$$\hat{H}^{(\alpha)} = \hat{H}_{\mathrm{int}} + \frac{\hat{p}^2}{2m} + mg\hat{z} + \hat{V}_{\mathrm{em}}^{(\alpha)} + \left(-\frac{\hat{p}^2}{2m} + mg\hat{z}\right)\frac{\hat{H}_{\mathrm{int}}}{mc^2} \qquad (34)$$

with the help of Eq. 33. In this form, the coupling of the internal dynamics to the external degrees of freedom is prominent and leads to the interference signal from Eq. 11 with $\eta = 1$. Hence, the Hamiltonian describes a moving clock experiencing time dilation (6).

REFERENCES AND NOTES

1. A. Einstein, Zur Elektrodynamik bewegter Körper. *Ann. Phys.* **322**, 891–921 (1905).
2. C. Møller, The ideal standard clocks in the general theory of relativity. *Helv. Phys. Acta* **4**, 54–57 (1956).
3. A. Einstein, Dialog über Einwände gegen die Relativitätstheorie. *Naturwissenschaften* **6**, 697–702 (1918).
4. T. Kovachy, P. Asenbaum, C. Overstreet, C. A. Donnelly, S. M. Dickerson, A. Sugarbaker, J. M. Hogan, M. A. Kasevich, Quantum superposition at the half-metre scale. *Nature* **528**, 530–533 (2015).
5. S. Sinha, J. Samuel, Atom interferometry and the gravitational redshift. *Class. Quant. Grav.* **28**, 145018 (2011).
6. M. Zych, F. Costa, I. Pikovski, Č. Brukner, Quantum interferometric visibility as a witness of general relativistic proper time. *Nat. Commun.* **2**, 505 (2011).
7. M. Zych, *Quantum Systems Under Gravitational Time Dilation* (Springer, 2017).
8. J. C. Hafele, R. E. Keating, Around-the-world atomic clocks: Observed relativistic time gains. *Science* **177**, 168–170 (1972).
9. R. F. C. Vessot, M. W. Levine, E. M. Mattison, E. L. Blomberg, T. E. Hoffman, G. U. Nystrom, B. F. Farrel, R. Decher, P. B. Eby, C. R. Baugher, J. W. Watts, D. L. Teuber, F. D. Wills, Test of relativistic gravitation with a space-borne hydrogen maser. *Phys. Rev. Lett.* **45**, 2081–2084 (1980).
10. C. W. Chou, D. B. Hume, T. Rosenband, D. J. Wineland, Optical clocks and relativity. *Science* **329**, 1630–1633 (2010).
11. T. L. Nicholson, S. L. Campbell, R. B. Hutson, G. E. Marti, B. J. Bloom, R. L. McNally, W. Zhang, M. D. Barrett, M. S. Safronova, G. F. Strouse, W. L. Tew, J. Ye, Systematic evaluation of an atomic clock at 2×10^{-18} total uncertainty. *Nat. Commun.* **6**, 6896 (2015).
12. M. Kasevich, S. Chu, Atomic interferometry using stimulated Raman transitions. *Phys. Rev. Lett.* **67**, 181–184 (1991).
13. C. Freier, M. Hauth, V. Schkolnik, B. Leykauf, M. Schilling, H. Wziontek, H.-G. Scherneck, J. Müller, A. Peters, Mobile quantum gravity sensor with unprecedented stability. *J. Phys. Conf. Ser.* **723**, 012050 (2015).
14. D. Savoie, M. Altorio, B. Fang, L. A. Sidorenkov, R. Geiger, A. Landragin, Interleaved atom interferometry for high-sensitivity inertial measurements. *Sci. Adv.* **4**, eaau7948 (2018).
15. R. Bouchendira, P. Cladé, S. Guellati-Khélifa, F. Nez, F. Biraben, New determination of the fine structure constant and test of the quantum electrodynamics. *Phys. Rev. Lett.* **106**, 080801 (2011).
16. D. Schlippert, J. Hartwig, H. Albers, L. L. Richardson, C. Schubert, A. Roura, W. P. Schleich, W. Ertmer, E. M. Rasel, Quantum test of the universality of free fall. *Phys. Rev. Lett.* **112**, 203002 (2014).
17. L. Zhou, S. Long, B. Tang, X. Chen, F. Gao, W. Peng, W. Duan, J. Zhong, Z. Xiong, J. Wang, Y. Zhang, M. Zhan, Test of equivalence principle at 10^{-8} level by a dual-species double-diffraction Raman atom interferometer. *Phys. Rev. Lett.* **115**, 013004 (2015).
18. B. Barrett, L. Antoni-Micollier, L. Chichet, B. Battelier, T. Lévèque, A. Landragin, P. Bouyer, Dual matter-wave inertial sensors in weightlessness. *Nat. Commun.* **7**, 13786 (2016).
19. G. Rosi, F. Sorrentino, L. Cacciapuoti, M. Prevedelli, G. M. Tino, Precision measurement of the Newtonian gravitational constant using cold atoms. *Nature* **510**, 518–521 (2014).
20. C. Overstreet, P. Asenbaum, T. Kovachy, R. Notermans, J. M. Hogan, M. A. Kasevich, Effective inertial frame in an atom interferometric test of the equivalence principle. *Phys. Rev. Lett.* **120**, 183604 (2018).
21. R. H. Parker, C. Yu, W. Zhong, B. Estey, H. Müller, Measurement of the fine-structure constant as a test of the Standard Model. *Science* **360**, 191–195 (2018).
22. E. Giese, A. Friedrich, F. Di Pumpo, A. Roura, W. P. Schleich, D. M. Greenberger, E. M. Rasel, Proper time in atom interferometers: Diffractive versus specular mirrors. *Phys. Rev. A* **99**, 013627 (2019).
23. S.-Y. Lan, P.-C. Kuan, B. Estey, D. English, J. M. Brown, M. A. Hohensee, H. Müller, A clock directly linking time to a particle's mass. *Science* **339**, 554–557 (2013).
24. C. J. Bordé, M. Weitz, T. W. Hänsch, New optical atomic interferometers for precise measurements of recoil shifts. Application to atomic hydrogen. *AIP Conf. Proc.* **290**, 76–78 (1993).
25. A. Roura, Circumventing Heisenberg's uncertainty principle in atom interferometry tests of the equivalence principle. *Phys. Rev. Lett.* **118**, 160401 (2017).
26. W. P. Schleich, D. M. Greenberger, E. M. Rasel, Redshift controversy in atom interferometry: Representation dependence of the origin of phase shift. *Phys. Rev. Lett.* **110**, 010401 (2013).
27. P. Wolf, L. Blanchet, C. J. Bordé, S. Reynaud, C. Salomon, C. Cohen-Tannoudji, Does an atom interferometer test the gravitational redshift at the Compton frequency? *Class. Quant. Grav.* **28**, 145017 (2011).
28. H. Müller, A. Peters, S. Chu, A precision measurement of the gravitational redshift by the interference of matter waves. *Nature* **463**, 926–929 (2010).
29. G. Rosi, G. D'Amico, L. Cacciapuoti, F. Sorrentino, M. Prevedelli, M. Zych, Č. Brukner, G. M. Tino, Quantum test of the equivalence principle for atoms in coherent superposition of internal energy states. *Nat. Commun.* **8**, 15529 (2017).
30. P. A. Bushev, J. H. Cole, D. Sholokhov, N. Kukharchyk, M. Zych, Single electron relativistic clock interferometer. *New J. Phys.* **18**, 093050 (2016).
31. S.-Y. Lin, K. Shiokawa, C.-H. Chou, B. L. Hu, Quantum teleportation between moving detectors in a quantum field. *Phys. Rev. D* **91**, 084063 (2015).
32. L. Hu, N. Poli, L. Salvi, G. M. Tino, Atom interferometry with the Sr optical clock transition. *Phys. Rev. Lett.* **119**, 263601 (2017).
33. E. Giese, A. Roura, G. Tackmann, E. M. Rasel, W. P. Schleich, Double Bragg diffraction: A tool for atom optics. *Phys. Rev. A* **88**, 053608 (2013).
34. K.-P. Marzlin, J. Audretsch, State independence in atom interferometry and insensitivity to acceleration and rotation. *Phys. Rev. A* **53**, 312–318 (1996).
35. S. M. Dickerson, J. M. Hogan, A. Sugarbaker, D. M. S. Johnson, M. A. Kasevich, Multiaxis inertial sensing with long-time point source atom interferometry. *Phys. Rev. Lett.* **111**, 083001 (2013).
36. J. Hartwig, S. Abend, C. Schubert, D. Schlippert, H. Ahlers, K. Posso-Trujillo, N. Gaaloul, W. Ertmer, E. M. Rasel, Testing the universality of free fall with rubidium and ytterbium in a very large baseline atom interferometer. *New J. Phys.* **17**, 035011 (2015).
37. D. Becker, M. D. Lachmann, S. T. Seidel, H. Ahlers, A. N. Dinkelaker, J. Grosse, O. Hellmig, H. Müntinga, V. Schkolnik, T. Wendrich, A. Wenzlawski, B. Weps, R. Corgier, T. Franz, N. Gaaloul, W. Herr, D. Lüdtke, M. Popp, S. Amri, H. Duncker, M. Erbe, A. Kohfeldt, A. Kubelka-Lange, C. Braxmaier, E. Charron, W. Ertmer, M. Krutzik, C. Lämmerzahl, A. Peters, W. P. Schleich, K. Sengstock, R. Walser, A. Wicht, P. Windpassinger, E. M. Rasel, Space-borne Bose-Einstein condensation for precision interferometry. *Nature* **562**, 391–395 (2018).
38. H. Katori, M. Takamoto, V. G. Pal'chikov, V. D. Ovsiannikov, Ultrastable optical clock with neutral atoms in an engineered light shift trap. *Phys. Rev. Lett.* **91**, 173005 (2003).
39. J. M. Hogan, D. M. S. Johnson, M. A. Kasevich, Light-pulse atom interferometry, in *Atom Optics and Space Physics: Proceedings of the International School of Physics "Enrico Fermi", Course CLXVIII*, E. Arimondo, W. Ertmer, E. M. Rasel, W. Schleich, Eds. (IOS Press, 2008).
40. S.-Y. Lan, P.-C. Kuan, B. Estey, P. Haslinger, H. Müller, Influence of the Coriolis force in atom interferometry. *Phys. Rev. Lett.* **108**, 090402 (2012).
41. A. Roura, Gravitational redshift in quantum-clock interferometry. arXiv:1810.06744 [physics.atom-ph] (15 October 2018).
42. P. W. Graham, J. M. Hogan, M. A. Kasevich, S. Rajendran, Resonant mode for gravitational wave detectors based on atom interferometry. *Phys. Rev. D* **94**, 104022 (2016).
43. C. Anastopoulos, B. L. Hu, Equivalence principle for quantum systems: Dephasing and phase shift of free-falling particles. *Class. Quant. Grav.* **35**, 035011 (2018).
44. K.-P. Marzlin, Dipole coupling of atoms and light in gravitational fields. *Phys. Rev. A* **51**, 625–631 (1995).
45. M. Sonnleitner, S. M. Barnett, Mass-energy and anomalous friction in quantum optics. *Phys. Rev. A* **98**, 042106 (2018).
46. A. Bertoldi, F. Minardi, M. Prevedelli, Phase shift in atom interferometers: Corrections for nonquadratic potentials and finite-duration laser pulses. *Phys. Rev. A* **99**, 033619 (2019).

Citation: S. Loriani, A. Friedrich, C. Ufrecht, F. Di Pumpo, S. Kleinert, S. Abend, N. Gaaloul, C. Meiners, C. Schubert, D. Tell, É. Wodey, M. Zych, W. Ertmer, A. Roura, D. Schlippert, W. P. Schleich, E. M. Rasel, E. Giese, Interference of clocks: A quantum twin paradox. *Sci. Adv.* **5**, eaax8966 (2019).

Science Advances

Interference of clocks: A quantum twin paradox

Sina Loriani, Alexander Friedrich, Christian Ufrecht, Fabio Di Pumpo, Stephan Kleinert, Sven Abend, Naceur Gaaloul,
Christian Meiners, Christian Schubert, Dorothee Tell, Étienne Wodey, Magdalena Zych, Wolfgang Ertmer, Albert Roura,
Dennis Schlippert, Wolfgang P. Schleich, Ernst M. Rasel and Enno Giese

ARTICLE TOOLS	http://advances.sciencemag.org/content/5/10/eaax8966
REFERENCES	This article cites 43 articles, 5 of which you can access for free http://advances.sciencemag.org/content/5/10/eaax8966#BIBL
PERMISSIONS	http://www.sciencemag.org/help/reprints-and-permissions

Use of this article is subject to the Terms of Service

PAPER • OPEN ACCESS

Atomic source selection in space-borne gravitational wave detection

To cite this article: S Loriani *et al* 2019 *New J. Phys.* **21** 063030

View the article online for updates and enhancements.

New Journal of Physics

The open access journal at the forefront of physics

CrossMark

PAPER

Atomic source selection in space-borne gravitational wave detection

S Loriani[1] ⬥ , D Schlippert[1] , C Schubert[1] , S Abend[1] , H Ahlers[1] , W Ertmer[1] , J Rudolph[2] , J M Hogan[2] ⬥ ,
M A Kasevich[2] , E M Rasel[1] and N Gaaloul[1] ⬥

[1] Institut für Quantenoptik and Centre for Quantum Engineering and Space-Time Research (QUEST), Leibniz Universität Hannover, Welfengarten 1, D-30167 Hannover, Germany
[2] Department of Physics, Stanford University, Stanford, CA 94305, United States of America

E-mail: gaaloul@iqo.uni-hannover.de

Keywords: atom interferometry, gravitational wave detection, inertial sensors, quantum gases, space physics, general relativity
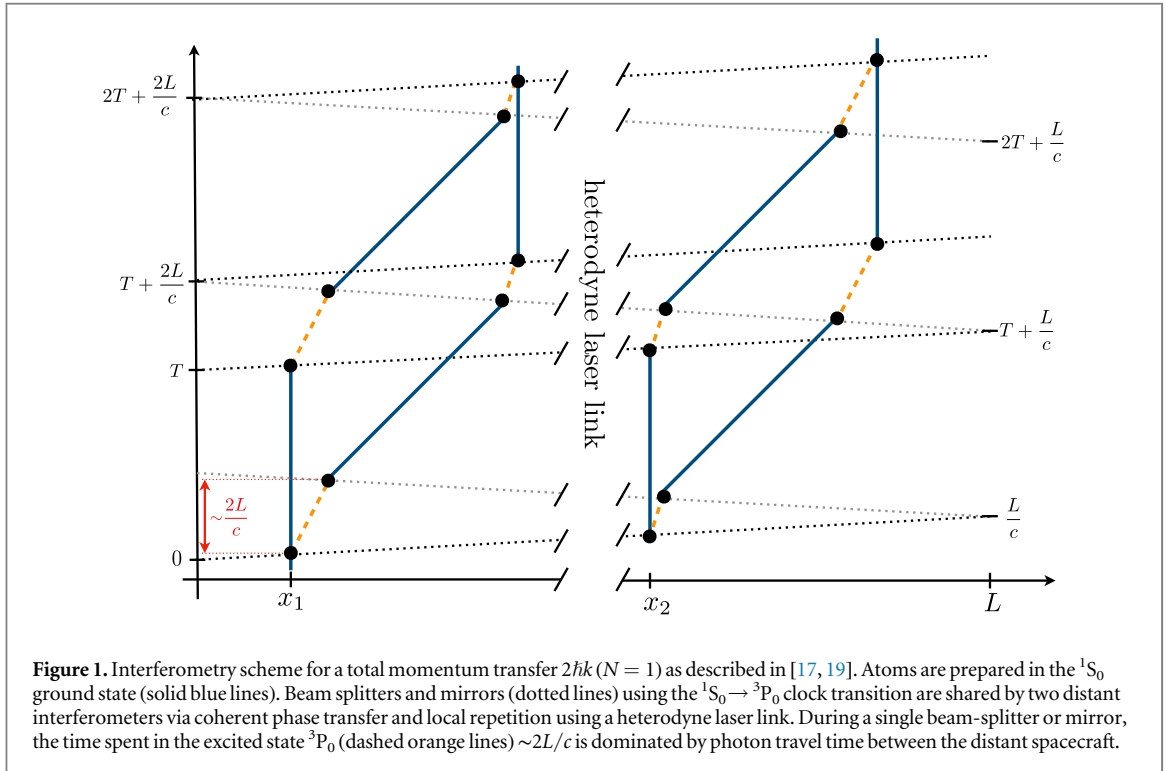
Abstract

Recent proposals for space-borne gravitational wave detectors based on atom interferometry rely on extremely narrow single-photon transition lines as featured by alkaline-earth metals or atomic species with similar electronic configuration. Despite their similarity, these species differ in key parameters such as abundance of isotopes, atomic flux, density and temperature regimes, achievable expansion rates, density limitations set by interactions, as well as technological and operational requirements. In this study, we compare viable candidates for gravitational wave detection with atom interferometry, contrast the most promising atomic species, identify the relevant technological milestones and investigate potential source concepts towards a future gravitational wave detector in space.

1. Introduction

The first detection of gravitational waves [1], predicted by Einstein's theory of general relativity one hundred years ago, is without any doubt among the most exciting developments at the forefront of modern physics and holds the potential of routinely using gravitational wave antennas as an observational tool [2]. Beyond its significance as confirmation of general relativity predictions, the progress in establishing a network of gravitational wave observatories opens the path towards novel tools in astronomy. Indeed, it will enable the observation of previously undetectable phenomena [1], help gain insight into their event rates, correlate data analysis in multi-messenger astronomy campaigns [3], and allow for novel tests of the Einstein equivalence principle [4].

Ground-based laser interferometer detectors such as advanced VIRGO [5], advanced LIGO [6], GEO-600 [7], and others are designed to detect relatively weak, transient sources of gravitational waves such as coalescing black holes, supernovae, and pulsars in the frequency range of tens of Hz up to a few kHz. While significantly longer-lived and stronger sources such as galactic binaries, supermassive black hole binaries, and extreme mass ratio inspirals, emit gravitational waves at frequencies below 10Hz, these signals are masked on Earth by seismic and Newtonian noise when using state-of-the-art optical interferometers. Over the last decades, this has motivated the drive for space missions such as LISA pathfinder [8] and LISA [9] to perform millihertz-gravitational wave detection circumventing ground limits. Low-frequency gravitational waves below 10 Hz could be accessed in a terrestrial detector using freely falling atoms as test masses, that are decoupled from vibrational noise [10–14]. Gravity-gradient noise compensation concepts, using multiple atomic ensembles along a single baseline, can open up even lower frequency bands [15]. However, ground-based atom interferometers are also ultimately limited at frequencies approaching a fraction of a Hz and space-borne detectors are vital to probe the lowest frequencies [16].

In this article, we discuss methods for gravitational wave detection using matter-wave interferometry in space, assuming an experimental outline similar to the one recently reported in [17]. The scenario, which is based on the use of atom interferometry utilizing single-photon transitions [18–21], is assessed in view of available atomic species, demands on the atomic source, systematic effects, and the required environmental

Figure 1. Interferometry scheme for a total momentum transfer $2\hbar k$ ($N = 1$) as described in [17, 19]. Atoms are prepared in the $^1S_0$ ground state (solid blue lines). Beam splitters and mirrors (dotted lines) using the $^1S_0 \rightarrow {}^3P_0$ clock transition are shared by two distant interferometers via coherent phase transfer and local repetition using a heterodyne laser link. During a single beam-splitter or mirror, the time spent in the excited state $^3P_0$ (dashed orange lines) $\sim 2L/c$ is dominated by photon travel time between the distant spacecraft.

control. A detailed trade-off study focusing on atomic source aspects as input for gravitational wave detectors has as of yet been missing.

2. Mission summary

The proposed sensor for low-frequency gravitational radiation exploits the differential phase shift of two inertially-sensitive atom interferometers on two spacecraft, separated by a baseline L. Such an atom interferometer scheme is proposed in [17, 19] and depicted in figure 1. The sequential absorption and stimulated emission of single photons on the $^1S_0 \rightarrow {}^3P_0$ clock transition (frequency ω_a) of a two-electron system allows the realization of effective $2\hbar k$ beam splitters. N sequentially applied beam splitters can address higher momentum states. The phase difference accumulated between the two interferometers under the influence of a passing gravitational wave with strain h, initial phase ϕ_0, and frequency ω reads

$$\Delta\phi = \frac{4N\omega_a}{c}\, h\, L \sin^2\left(\frac{\omega T}{2}\right) \sin(\phi_0 + \omega T), \tag{1}$$

growing linearly with increasing baseline as known from operation of gravity-gradiometers.

Laser phase noise requirements are mitigated in a differential measurement, since both gravimeters are operated with the same light, hence allowing for single baseline operation. In contrast to earlier proposals [19], a heterodyne laser link between the spacecraft allows to overcome previous limitations of the baseline L imposed by finite optical power and requirements on the link's collimation [17]. By locally repeating an incoming optical pulse and thus coherently transferring the interferometer phase over very large distances, baselines as suggested for LISA-like missions become accessible. The feasibility of the two scenarios proposed in [17] for different atomic sources is assessed in the following sections. The experimental arrangement consists in a baseline of $L = 2 \times 10^9$ m (6×10^8 m) with a maximum interrogation time $T = 160$ s (75 s) and beam splitting order $N = 1$ (6) yielding an expected maximum strain sensitivity of $< 10^{-19}$ Hz$^{-1/2}$ ($< 10^{-20}$ Hz$^{-1/2}$) around 10 mHz, meeting or even surpassing the expected LISA strain sensitivity.

3. Species assessment

3.1. Trade-off criteria
In this section we define and apply the criteria to identify an optimal species choice for the envisioned experiment. Desired properties can be summarized in the following three categories.

(i) *Electronic structure and narrow line transitions*—As the sensitivity of the proposed gravitational wave detector scales linearly with the effective wave number linked to the momentum ($\propto N\omega_a$) transferred onto the atomic wave packet, large transition frequencies are desired. Unlike the case of a small-scale experiment, the proposed single-photon beam splitting scheme studied here implies that the wave packets spend a non-negligible time, on the order of seconds, in the excited state (see figure 1). Consequently, this state has to have a lifetime significantly larger than $2L/c$ to overcome spontaneous emission, loss of coherence and deterioration of the output signal [22]. The obvious species considered here are typical optical clock atoms. Their two valence electrons can align parallel or anti-parallel, thus giving rise to a singlet and a triplet system. Naturally, dipole selection rules render electronic intercombination transitions forbidden and these transitions have narrow linewidths. In strontium e.g. this makes $^1S_0 \rightarrow {}^3P_1$ a favorable cooling transition due to the intimately related low Doppler cooling limit. The even further suppressed $^1S_0 \rightarrow {}^3P_0$ transition is consequently used in many optical atomic clocks, where spectroscopy on a mHz or narrower transition at a THz frequency is performed.

(ii) *Coherent excitation and ultra-low expansion rates*—Efficiently addressing an optical transition implies maintaining a good spatial mode overlap of the driving laser beam with the corresponding atomic ensemble. The Rabi frequency when driving a transition with linewidth Γ and saturation intensity $I_{\text{sat}} = 2\pi^2 \hbar c \Gamma / 3\lambda^3$ reads

$$\Omega = \Gamma \sqrt{\frac{I}{2I_{\text{sat}}}}. \tag{2}$$

Since the available laser intensity I is always finite, and especially limited on a spacecraft, small laser mode diameters and correspondingly even smaller atomic wave packet diameters are desired. The detector's frequency band of interest lies in the range of tens of millihertz, and hence the resulting evolution time T for maximum sensitivity is on the order of hundreds of seconds (equation (1)). During an interferometer time scale $2T$, the thermal expansion of an ensemble of strontium atoms at a temperature of 1 μK yields a cloud radius on the order of meters. As a direct consequence, cooling techniques to prepare atomic ensembles with the lowest possible expansion rates are required and heavier nuclei are in favor. Moreover, matter-wave collimation as realized in [23–25] is an indispensable tool to engineer the required weak expansion energies. Throughout the manuscript, we express this expansion energy in units of temperature and refer to it as the effective temperature T_{eff}. For the purpose of this study, it lies typically in the picokelvin regime, which corresponds to few tens of μm s^{-1} of expansion velocity.

(iii) *Available technology and demonstration experiments*—Finally, any heritage from demonstration experiments is of importance when designing the sensor, especially in the scope of a space mission. Similarly, the availability of easy-to-handle reliable high-power laser sources with perspectives to develop space-proof systems are important criteria in the selection of an atomic species. As an example, laser wavelengths far-off the visible range should be avoided for the sake of simplicity, robustness, and mission lifetime.

In table 1, we provide an overview of available atomic species. While usually not occurring in atomic clocks, the proposed experimental arrangement requires the metastable state to be populated over time scales on the order of seconds or more. Within a single pair of sequential single-photon beam splitters, the time an atom spends in the excited state is $\sim 2L/c$ (dashed lines in figure 1), dominated by the light travel time between the two spacecraft. With an excited clock state decay rate Γ_0, a baseline L, and diffraction order N the remaining fraction of atoms in the interferometer reads

$$P_r = \exp\left[-\frac{4 L \cdot N}{c} \cdot \Gamma_0 \right]. \tag{3}$$

This loss of atoms by spontaneous emission[3] causes an increase in quantum projection noise by a factor of $1/\sqrt{P_r}$. In order to keep up the device's single-shot sensitivity, the atomic flux has to be increased accordingly or non-classical correlations have to be utilized to compensate for these losses. Similarly, when mitigating spontaneous losses via reduction of the instrument baseline or the beam splitting order, the linearly reduced sensitivity needs to be recovered with a quadratically larger atomic flux. As a result of their nuclear spins ($I \neq 0$), the electronic structure of fermionic species is subject to hyperfine interactions and has significantly larger clock linewidths than their bosonic counterparts [39]. Consequently, losses due to finite excited state lifetimes can significantly attenuate the signal for some species. Remaining atomic fractions after a full interferometer cycle for several fermionic isotopes are stated in table 2.

---

[3] Given the long pulse separation times on the order of hundreds of seconds, spontaneously decaying atoms will mostly drift away and not participate in the detection signal which can thus be expected to be near unity.

Table 1. Overview of possible two-electron systems featuring clock transitions. The isotopes treated in detail in this article are printed in boldface.

| | Mass in u | $^1S_0 \rightarrow {}^3P_0$ linewidth $\Gamma_0/2\pi$ in Hz | Nat. abund. | $^1S_0 \rightarrow$ | | | References |
| | | | | $^1P_1$ | $^3P_1$ | $^3P_0$ | |
					in nm		
Fermions							
Mg	25	70×10^{-6}	10%	285	457	458	[26]
Ca	43	350×10^{-6}	0.1%	423	657	659	[26, 27]
Sr	**87**	1.5×10^{-3}	7%	461	689	698	[28]
Cd	111	5×10^{-3a}	13%	228	325	332	[29]
Yb	**171**	8×10^{-3}	14%	399	556	578	[30]
Hg	199	100×10^{-3}	17%	185	254	266	[31]
Bosons							
Mg	24	403×10^{-9b}	79%	285	458	457	[32]
Ca	40	355×10^{-9b}	97%	423	657	659	[33]
Sr	**84**	459×10^{-9b}	0.6%	461	689	698	[34]
Cd	114	c	29%	228	325	332	[35]
Yb	**174**	833×10^{-9b}	32%	399	556	578	[36]
Hg	202	c	30%	185	254	266	[37]

Notes.

[a] Linewidth estimation [29].

[b] Linewidth achievable with external magnetic field as described below; Calculated using equation (5) and [38] assuming $B = 100$ G, $P = 1$ W, laser waist $w = 4\sigma_r$, atomic ensemble radius $\sigma_r = 6$ mm and expansion rate $T_{eff} = 10$ pK.

[c] Necessary coefficients for the calculation unknown to the authors.

Table 2. Fraction of remaining atoms after an interferometric cycle for the different fermionic isotopes under consideration.

Baseline L	Diffraction order N	^{25}Mg	^{43}Ca	^{87}Sr	^{111}Cd	^{171}Yb	^{199}Hg
2×10^9 m	1	0.99	0.94	0.78	0.43	0.26	5×10^{-8}
6×10^8 m	6	0.98	0.90	0.64	0.22	0.09	8×10^{-14}

3.2. Single-pulse excitation rates

Using bosonic isotopes with theoretical lifetimes of thousands of years in the metastable state $^3P_0$ circumvents the losses described above but requires different experimental efforts. Indeed, unlike fermionic candidates, single-photon clock transitions in bosonic species are not weakly allowed through spin-orbit-induced and hyperfine interaction mixing [39] and the excited state lifetime is limited by two-photon $E1M1$-decay processes, hence typically lying in the range of picohertz [34, 39].

Accordingly, efficient manipulation on the clock transition for beam splitting depends on induced state-mixing by magnetic-field induced spectroscopy [38]. For example, such a magnetic quench allows to weakly mix the triplet states $^3P_0$ and $^3P_1$ and thus increases the clock transition probability. Using the formalism described in [38], which holds for linear polarizations, it is possible to infer Rabi frequencies

$$\Omega_0 = \alpha \cdot \sqrt{I} \cdot B, \tag{4}$$

and corresponding effective clock linewidths

$$\Gamma_{0,\text{eff}} = \gamma \frac{\Omega_L^2/4 + \Omega_B^2}{\Delta_{32}^2}, \tag{5}$$

under the assumption that the external magnetic field is colinear to the laser polarization[4]. Here, γ denotes the decay rate of $^3P_1$, Δ_{32} is the splitting between the triplet states and Ω_L and Ω_B are the coupling Rabi frequencies induced by the laser and the static magnetic field, respectively. Supporting the concept of concurrent operation of multiple interferometers [17], the external fields can be limited in terms of spatial extent to distinct interaction zones.

---

[4] This field configuration deviates from the case generally used in two-photon interferometers where the quantization axis is parallel to the beam splitting axis.

Table 3. Compared single-pulse excitation probability of fermionic and bosonic strontium for different sizes of the atomic ensemble, assuming an expansion energy of $T_{\text{eff}} = 10$ pK, a clock laser power of $P = 1$ W with optimized beam waist, and an external magnetic field of $B = 100$ G in the bosonic case.

	^{84}Sr	^{87}Sr	^{84}Sr	^{87}Sr	^{84}Sr	^{87}Sr
Ensemble size (mm)		1		10		20
Rabi frequency (2π Hz)	111.0	780.3	17.2	148.7	8.6	106.5
Excited fraction	0.79	0.99	0.19	0.87	0.1	0.73

In order to induce homogeneous Rabi frequencies over the spatial extent of the atomic ensemble, a reasonable spatial overlap between the exciting beam and the atomic cloud is required. Given the long drift times in the order of seconds, the clouds reach sizes in the order of millimeters, necessitating even larger beam waists. In view of limited laser power in a space mission, the resulting low intensities lead to Rabi frequencies in the few hundred Hz range for fermions. Assuming a magnetic field of 100 G, the corresponding Rabi frequencies are in the order of a few Hz for bosons. Table 3 illustrates the orders of magnitude for the two isotopes of strontium. Generally, smaller cloud sizes are advantageous, favoring the use of colder, i.e. slowly expanding sources.

The excitation probability is intimately connected to the phase space properties of the atomic cloud. An intensity profile of the exciting beam that varies over the spatial extent of the ensemble induces a space-dependent Rabi frequency except when the laser beam is shaped to be spatially uniform [40, 41]. One can overcome it by an increased beam waist leading to a homogeneous but smaller Rabi frequency. On the other hand, the effective Rabi frequency associated to a beam splitting light of wave number k being $\Omega_{\text{eff}}(r, v) = \sqrt{\Omega_0^2(r) + (k \cdot v)^2}$, large waists (at limited power) would cause the Doppler detuning $(k \cdot v)^2$ to become the dominant term in $\Omega_{\text{eff}}(r, v)$ thereby making the process very sensitive to the velocity distribution of the atomic ensemble. A trade-off to find the optimal waist maximizing the number of excited atoms throughout the full sequence is made in each scenario presented in this study. The respective excitation probability is calculated [42] as

$$P_{exc} = 2\pi \int \int r\, f(v)\, n(r, t) \left(\frac{\Omega_0(r)}{\Omega_{\text{eff}}(r, v)} \right)^2 \sin^2 \left(\frac{\Omega_{\text{eff}}(r, v)}{2} t \right) \mathrm{d}r\mathrm{d}v, \tag{6}$$
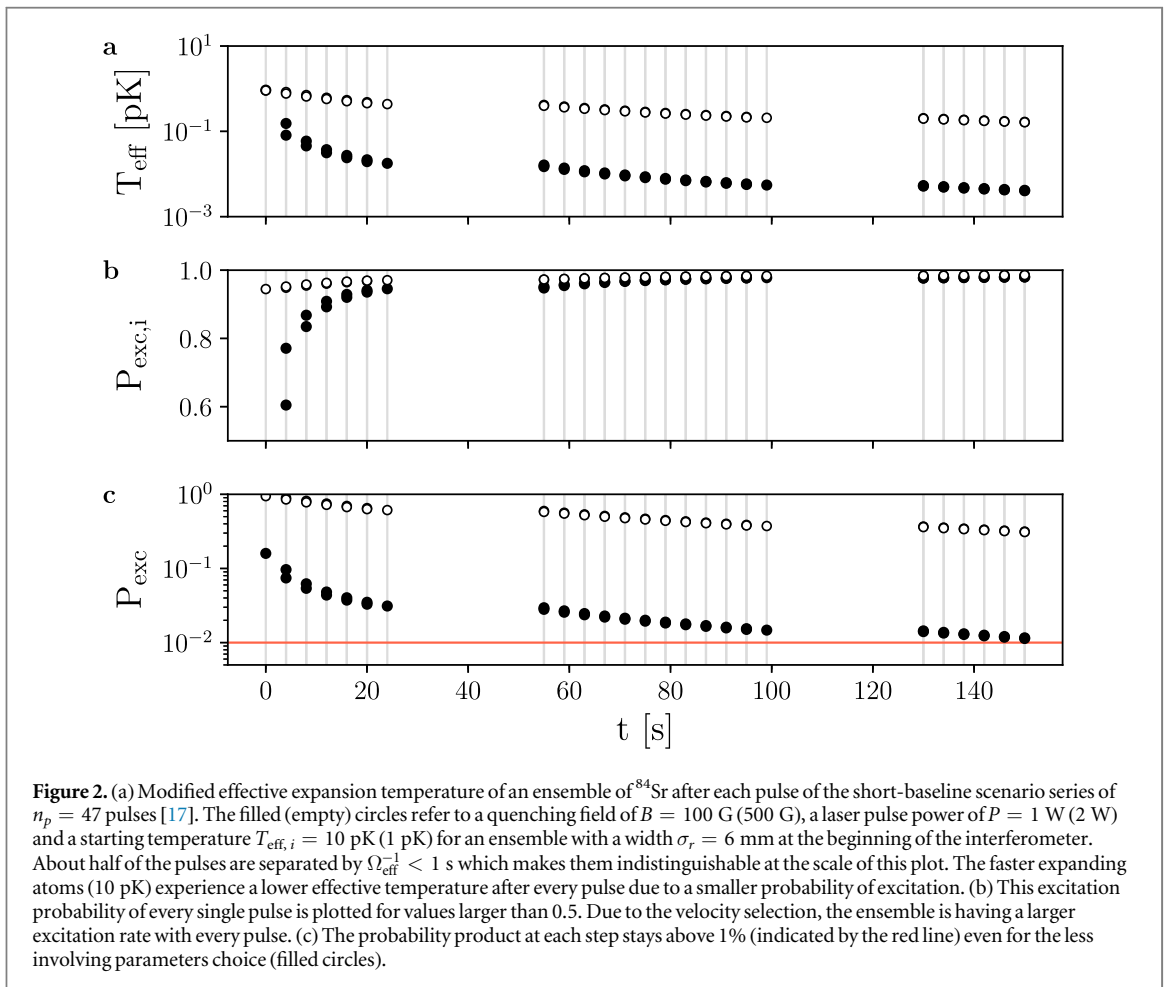
where $f(v)$ is the longitudinal velocity distribution, $\Omega_0(r)$ is the spatially-dependent Rabi frequency and $n(r, t)$ is the transverse atomic density distribution. The resulting excited fraction for typical parameters of this study and for one pulse can be found in table 3.

3.3. Full interferometer excitation rates
In order to calculate the total fraction of atoms left at the detected state at the end of the interferometric sequence, one has to successively evaluate the integral (6) for each pulse. Indeed, the first light pulse selects a certain area in the ensemble's phase space distribution. The resulting longitudinal velocity distribution $f_{\text{new}}(v)$ is computed and will constitute the input of the integral (6) relative to the next pulse. This treatment is iterated over the full pulses sequence of the considered scenarios. The long baseline scenario comprises $n_p = 7$ pulses while the short baseline scenario is realized by a sequence of $n_p = 47$ pulses. We illustrate, in figure 2, the short baseline case by showing, after each pulse, the new effective expansion temperature calculated after the new velocity width σ_{v_i}, the individual-pulse excitation rate $P_{\text{exc},i}$ and the overall excitation probability at that point, given by the product of all previous pulses.

3.4. Residual detected atomic fraction
The total number of atoms detected at the interferometer ports is given, for each isotope, by evaluating the product of the excitation and the lifetime probabilities. In figure 3, we compile the outcome of these two studied aspects for the species considered in table 1. Assuming parameters that are well in line with state-of-the-art technology (filled symbols), i.e. an excitation field with $B = 100$ G, $P = 1$ W as well as an effective expansion temperature $T_{\text{eff}} = 10$ pK and $\sigma_r = 6$ mm at the time of the matter wave lens, the plot suggests a preliminary trade-off. Although the bosons benefit from their small transition linewidths rendering them resilient to spontaneous decay, they all can only be weakly excited in the order of a few % or less (lower right corner of the figure). For clarity reasons, the isotopes that lie under an excitation probability of less than 0.5% are not represented. Heavier fermions, such as cadmium, mercury and ytterbium are subject to particularly large losses due to their broad linewidths (see table 2) in spite of very promising previous demonstration work in the case of ^{171}Yb [43]. It turns out that fermionic strontium and ytterbium are the most promising candidates, with a total fraction of around 12% of the atoms contributing to the interferometric signal in the long baseline scenario (circles), and around 10% in the case of strontium in the short baseline scenario (squares). Pushing the
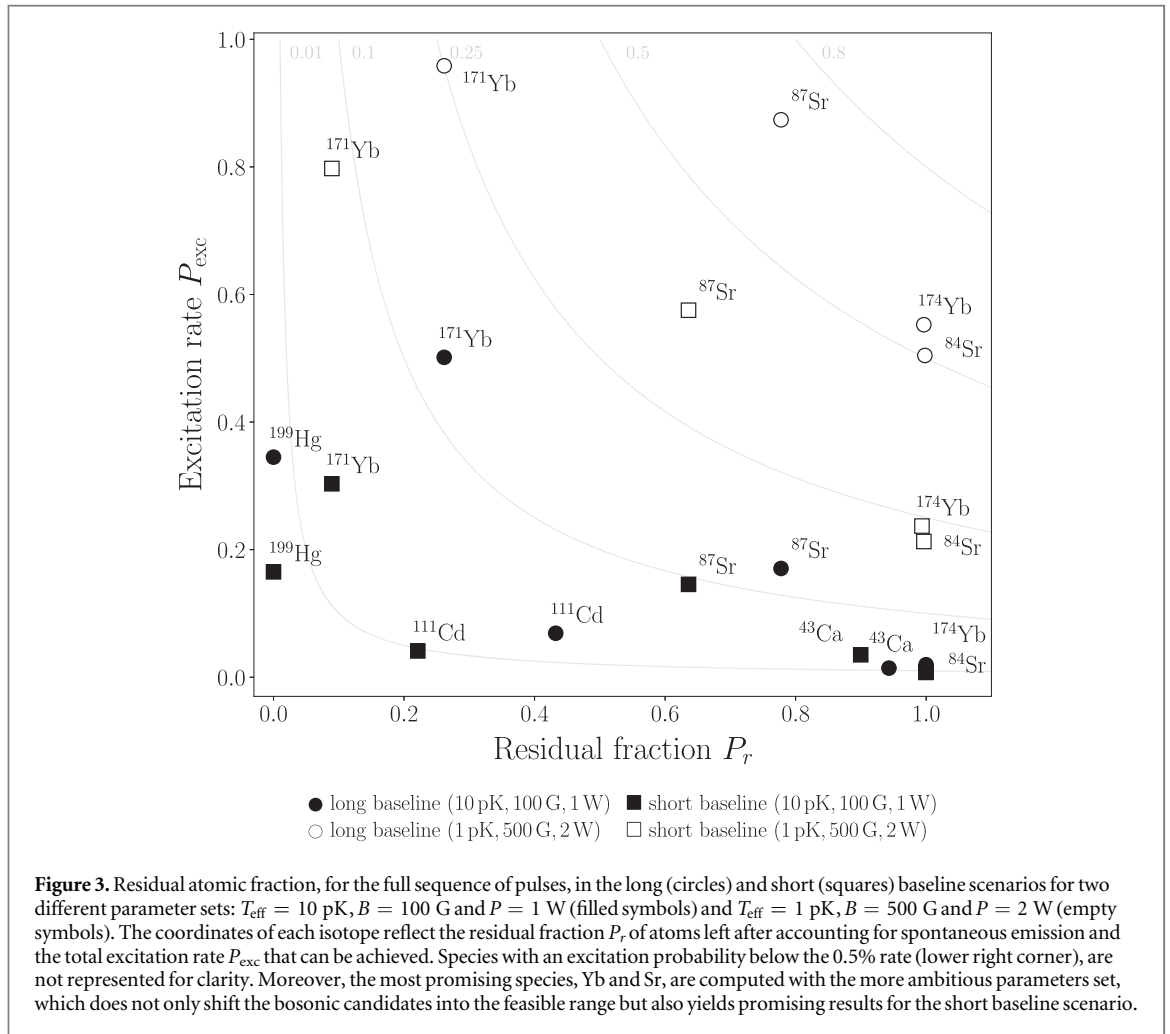
Figure 2. (a) Modified effective expansion temperature of an ensemble of ^{84}Sr after each pulse of the short-baseline scenario series of $n_p = 47$ pulses [17]. The filled (empty) circles refer to a quenching field of $B = 100$ G (500 G), a laser pulse power of $P = 1$ W (2 W) and a starting temperature $T_{eff,\,i} = 10$ pK (1 pK) for an ensemble with a width $\sigma_r = 6$ mm at the beginning of the interferometer. About half of the pulses are separated by $\Omega_{eff}^{-1} < 1$ s which makes them indistinguishable at the scale of this plot. The faster expanding atoms (10 pK) experience a lower effective temperature after every pulse due to a smaller probability of excitation. (b) This excitation probability of every single pulse is plotted for values larger than 0.5. Due to the velocity selection, the ensemble is having a larger excitation rate with every pulse. (c) The probability product at each step stays above 1% (indicated by the red line) even for the less involving parameters choice (filled circles).

parameters to more ambitious values of $B = 500$ G, $P = 2$ W and $T_{eff} = 1$ pK, improves the results significantly. In bosonic ytterbium and both isotopes of strontium, more than half of the atoms are left at the end of the pulse sequence of the long baseline scenario, and decent excitation rates are reached even in the short baseline configuration. Overall, ^{87}Sr turns out to be the most favorable isotope in this comparison.

3.5. Heritage

The worldwide efforts on demonstration experiments towards using the narrow clock transitions in Sr as a future frequency standard [28, 44] promises additional advantages of this choice through technological advances and research. In contrast, fermionic magnesium is difficult to address due to the ultraviolet singlet line, the weak cooling force of the $^1S_0 \rightarrow {}^3P_1$ transition [45] and quantum degeneracy not being demonstrated thus far. Likewise, trapping of fermionic calcium has only sparsely been demonstrated [27] and the intercombination cooling force is almost as weak as in the case of magnesium. Cooling techniques can be applied to all candidate bosons and finite clock transition linewidths can be achieved through magnetic field induced state mixing. A selection of a bosonic species would thus be motivated by previous demonstration experiments despite the weak excitation probability. In contrast, magnesium and calcium isotopes are missing simple paths to quantum degeneracy as a starting point for picokelvin kinetic energies. Although Bose–Einstein condensation has been shown for ^{40}Ca [33], the scheme is not particularly robust and the scattering length of 440 a_0 inhibits long-lived Bose–Einstein condensates (BEC). For cadmium, only magneto-optical trapping has been demonstrated [35]. Next to missing pathways to quantum degeneracy, its transition lines lie in the ultraviolet range. Mercury atoms can be ruled out for the same reason, although significant experience is available [37]. Additional candidates with convincing heritage are ^{174}Yb [46, 47] and ^{84}Sr, which has been brought to quantum degeneracy with large atom numbers in spite of its low abundance [48].

To conclude this section, we remark that the bosonic and fermionic isotopes of Yb and Sr are the most favorable when it comes to the number of atoms involved in the interferometric measurement. This holds for all scenarii considered: short and long baselines, modest and ambitious parameters and their combinations. We, therefore, pursue this trade-off focusing on these elements. We analyze their suitability for the use in the

Figure 3. Residual atomic fraction, for the full sequence of pulses, in the long (circles) and short (squares) baseline scenarios for two different parameter sets: $T_{\text{eff}} = 10$ pK, $B = 100$ G and $P = 1$ W (filled symbols) and $T_{\text{eff}} = 1$ pK, $B = 500$ G and $P = 2$ W (empty symbols). The coordinates of each isotope reflect the residual fraction P_r of atoms left after accounting for spontaneous emission and the total excitation rate P_{exc} that can be achieved. Species with an excitation probability below the 0.5% rate (lower right corner), are not represented for clarity. Moreover, the most promising species, Yb and Sr, are computed with the more ambitious parameters set, which does not only shift the bosonic candidates into the feasible range but also yields promising results for the short baseline scenario.

proposed gravitational wave detector by considering the respective laser sources requirements and the necessary environmental control to constrain systematic effects.

4. Available laser sources

In this section, we discuss the technological feasibility to use the four most promising isotopes ^{84}Sr, ^{87}Sr, ^{171}Yb and ^{174}Yb in the proposed mission scheme. In terms of available laser technology, both elements are commonly used as sources in laboratory grade optical clocks, as well as considered to be interesting candidates for use in space missions with optical clocks [49]. Concerning the laser sources necessary to cool and manipulate both species, previous work has been performed for space qualification, mostly relying on diode laser systems [50]. Beyond the scope of this previous work, we want to discuss the possibilities for lattice-based atomic transport to isolate the preparation and detection zones from the interferometry region. The laser lines for the cooling transitions and their properties are listed in table 4.

In the laboratory environment, Zeeman slowers are routinely employed and a commercial compact source was recently presented for strontium [51], whose design can be adapted to ytterbium as well. For pre-cooling on the singlet transition at the UV wavelength 461 nm (399 nm) for Sr (Yb), fully free space coupled diode laser systems exist [49–51]. A possible alternative would be higher-harmonics generation of mid-IR fiber laser systems, which are robust and benefit from a large selection of commercially available sources.

To generate the 399 nm wavelength, a fiber laser for ytterbium would need two doubling stages starting from the infrared and thus requires high laser power in the IR. While the required fundamental wavelength for such a system is only slightly out of range of commercial fiber lasers, the strontium singlet line lies in an unsuitable range for second or even fourth harmonic generation with fiber lasers. As an alternative, tapered amplifiers are available at both fundamental frequencies to amplify the laser light.

The triplet transition for strontium at 689 nm can also be addressed by diode lasers [49]. While one does not require large power on this line due to its narrow linewidth in the kilohertz regime, the laser frequency needs to be stabilized using a stable optical cavity and a modulation scheme as well as a second 'stirring' laser are

Table 4. Laser lines and their properties for ^{84}Sr, ^{87}Sr, ^{171}Yb and ^{174}Yb as well as possible wavelengths for an optical dipole trap (ODT).

Laser line	^{84}Sr and ^{87}Sr			^{171}Yb and ^{174}Yb		
	λ	$\Gamma/2\pi$	I_{sat}	λ	$\Gamma/2\pi$	I_{sat}
Singlet	461 nm	30 MHz	10 mW cm^{-2}	399 nm	25 MHz	66 mW cm^{-2}
Triplet	689 nm	7.4 kHz	3 μW cm^{-2}	556 nm	182 kHz	0.14 mW cm^{-2}
Clock	698 nm	see section 3.1		578 nm	see section 3.1	
ODT	1 μm, 1.5 μm or 2 μm					

commonly used [52]. The required stability is relaxed for the triplet line for ytterbium lying at 556 nm due to the factor of 20 larger linewidth. It is accessible using frequency-doubled fiber laser systems, which have been developed for space applications [50, 53]. For trapping, evaporative cooling to quantum degeneracy, and matter wave lensing, fiber laser systems in the mid-IR, e.g. erbium-doped fiber lasers at 1 μm [54] or thulium-doped fiber lasers at 2 μm [55], can be employed.

More stringent requirements on the lasers are set by beam splitting on the clock transitions as discussed in the previous section. The same laser technology as for the triplet transitions is available for driving the clock transitions of both species at 698 nm and 578 nm, respectively, as their wavelengths only differ from the triplet transition by a few tens of nanometers. The suitable laser power on the order of 1 W is more demanding than for cooling applications, but feasible by either tapered amplifiers or frequency doubled fiber amplifiers. Larger laser powers can be reached by combining a high power fiber amplifier and a resonant doubling cavity, which might further increase the attainable Rabi frequencies. The necessary linewidth for single photon excitation scales with the effective Rabi frequency [19]. In our case, according to table 3 this requires Hz to sub-Hz linewidths, which is feasible for robust and transportable state-of-the-art cavities with already Hz linewidths [56, 57].

The transport of atoms from the preparation zone onto the interferometry axis and into the detection region will be realized via coherent momentum transfer using Bloch oscillations in an optical lattice [58, 59]. This technique is well established and enables the efficient transfer of a large number of photon momenta by two-photon scattering, employed for example in recoil measurements [60] or to realize fountain geometries on ground [61, 62]. Bloch oscillations can be driven by coupling to an arbitrary optical transition already discussed for cooling. Two main loss mechanisms have to be considered during the transport in an optical lattice, namely spontaneous emission and Landau–Zehner tunneling. To suppress spontaneous scattering, a laser detuning Δ with respect to the single-photon transition on the order of $10^4-10^5\,\Gamma$ is needed. The larger detuning Δ will lead to reduced transfer efficiencies unless the laser power is increased. This requires additional amplification stages, which due to their broad bandwidth might be shared with the cooling lasers. An optical lattice coupling to the narrower triplet line for ytterbium would yield a factor of three reduction in needed laser power at constant detuning Δ compared to the singlet transition. In contrast, the needed laser power to address both lines in strontium is rather similar and even 20% smaller for the singlet transition.

5. Error budget and source requirements

Source parameters such as the number of atoms and residual expansion do not only affect the shot noise as defined in section 3.1, but can also introduce an additional noise contribution which is not common to the interferometers on the two satellites. Consequently, additional requirements have to be derived to maintain the anticipated performance in a given environment and are consolidated in table 5. The discussion in this section is based on the following assumptions: The strain sensitivity shall be comparable to the LISA scenario with a free evolution time $2T = 320$ s and an effective wave vector corresponding to two photon recoil momenta [17, 19]. The two satellites are trailing behind earth and are nadir pointing with respect to the Sun which corresponds to a rotation rate of the satellites of 2×10^{-7} rad s^{-1}. This rotation rate implies a maximum allowed velocity fluctuation of the center of the cloud. In order to constrain residual rotation contributions below 1 mrad/Hz$^{1/2}$ for example, a maximum expansion rate of $T_{\text{eff}} = 10$ pK is allowed in the case of 4×10^7 atoms s^{-1}, when shot-noise-limited fluctuations are assumed. Spatial and velocity distributions are assumed to be isotropic and gaussian. The requirement on the initial rms-width of $\sigma_r = 6$ mm of the wave packet is defined by the necessity for a low density to suppress collisional shifts given an uncertainty of the first beam splitter of 0.1% [63]. Subsequently, the maximum gravity gradient is derived. The atom interferometer operates in the point source limit [61, 64] enabling the read-out of fringe patterns in the interferometer output ports due to gravity gradients. We approximate the interferometer geometry for short pulses when calculating the phase shifts [65, 66]. This does not strictly hold for the given scenario but gives the correct order of magnitude nonetheless.

Table 5. Requirements to reach phase noise contributions of 1 mrad/Hz$^{1/2}$ individually. Motion and position noise, $\sigma_v / \sqrt{N_a}$ and $\sigma_r / \sqrt{N_a}$, respectively, are considered to be shot-noise-limited.

	^{84}Sr	^{174}Yb
Initial radius σ_r	< 6 mm	< 6 mm
Temperature equivalent T_{eff}	< 10 pK	< 10 pK
Final radius	< 16 mm	< 13 mm
Residual rotations Ω	<2.2 × 10^{-7} rad s^{-1}	<2.6 × 10^{-7} rad s^{-1}
Gravity gradients $\gamma_{\parallel}$ + velocity	<2.7 × 10^{-9} 1/s^2	<3.3 × 10^{-9} 1/s^2
Gravity gradients $\gamma_{\parallel}$ + position	<2.3 × 10^{-9} 1/s^2	<1.9 × 10^{-9} 1/s^2
Gravity gradients $\gamma_{\perp}$ + velocity	<1.6 × 10^{-5} 1/s^2	<1.7 × 10^{-5} 1/s^2
Gravity gradients $\gamma_{\perp}$ + position	<7.8 × 10^{-6} 1/s^2	<5.7 × 10^{-6} 1/s^2
Maximum wave front fluctuation σ_R	< 20% · 54 km	< 12% · 54 km

Residual rotations Ω coupled to a velocity uncertainty of the cloud $\sigma_v / \sqrt{N_a} = \sqrt{k_{\text{B}} T_{\text{eff}} / m} / \sqrt{N_a}$ with Boltzmann's constant k_{B}, atomic mass m, and number N_a induce a phase fluctuation $\sigma_{\phi_{\text{rot}}} = 2\, k\, \sigma_v\, \Omega\, T^2 / \sqrt{N_a}$. A temperature equivalent of 10 pK leads to a shot noise limited cloud velocity uncertainty below 5 nm s^{-1} which is compatible with the anticipated noise limit.

The atoms mostly reside in the ground state (see figure 1), allowing for a straightforward estimation of the phase noise contribution due to collisions. The scattering length of the ground state of ^{174}Yb (^{84}Sr) is 105 a_0 (123 a_0) where a_0 is the Bohr radius [47, 48]. Any imperfection of the initial beam splitter induces a differential density between the two interferometer arms and consequently induces a noise contribution if fluctuating [63]. With an isotropic rms-width of 6 mm at the time of the first beam splitter, an uncertainty in the beam splitting ratio of 0.1%, and an isotropic expansion corresponding to 10 pK, the phase uncertainty stays within a few 0.1 mrad.

Gravity gradients parallel to the sensitive axis $\gamma_{\parallel}$ and a center of mass velocity jitter induce a phase noise according to the formula $\sigma_{\phi_{v,\gamma,\parallel}} = k\, \gamma_{\parallel}\, \sigma_v\, T^3 / \sqrt{N_a}$. Thus, the gravity gradient has to fulfill the condition $\gamma_{\parallel} < 2 \times 10^{-9}$ s^{-2}. A similar requirement is derived, when considering the cloud's shot noise limited position uncertainty $\sigma_r / \sqrt{N_a}$ using $\sigma_{\phi_{r,\gamma,\parallel}} = k\, \gamma_{\parallel}\, \sigma_r\, T^2 / \sqrt{N_a}$.

Gravity gradients $\gamma_{\perp}$ perpendicular to the sensitive axis couple to the center of wave packet motion as well if a rotation is present. With the orbital frequency and the stated uncertainties in position and velocity, the maximum compatible gradient of $\sim 6 \times 10^{-6}$ s^{-2} is deduced from $\sigma_{\phi_{v,\gamma,\perp}} = 14/3\, k\, \sigma_v\, \gamma_{\perp}\, \Omega\, T^4 / \sqrt{N_a}$ and $\sigma_{\phi_{r,\gamma,\perp}} = 8\, k\, \sigma_r\, \gamma_{\perp}\, \Omega\, T^3 / \sqrt{N_a}$.

A properly designed mass distribution will be necessary to reach this target and a distance to Earth of at least 7×10^7 m is required to keep Earth's gravity gradient below the threshold of $\sim 2 \times 10^{-9}$ s^{-2} [17].

Finally, the finite expansion rate σ_v couples to the effective wave front curvature radius which induces the phase shift $\phi_{wf} = k\, T^2\, \sigma_v^2 / R$ [67, 68]. Consequently, instabilities in the effective temperature $\sigma_{T_{\text{eff}}}$ and effective wave front curvature radius σ_R lead to a phase noise of $\sigma_{\phi_{wf}, T} = kT^2\, k_{\text{B}} / (m\, R) \cdot \sigma_{T_{\text{eff}}}$ and $\sigma_{\phi_{wf}, R} = k\, T^2\, k_{\text{B}}\, T_{\text{eff}} / (m\, R^2) \cdot \sigma_R$, respectively[5]. Assuming an effective wavefront curvature radius $R = 54$ km corresponding to a peak-to-valley of $\lambda/30$ across a beam with a diameter of 10 cm, the fluctuations for ytterbium (strontium) have to be limited to $\sigma_{T_{\text{eff}}} < T_{\text{eff}} \cdot 20\% \, (\sigma_{T_{\text{eff}}} < T_{\text{eff}} \cdot 10\%)$ and $\sigma_R < R \cdot 20\% \, (\sigma_R < R \cdot 12\%)$.

6. Regimes of temperature and density

6.1. Expansion dynamics

The error model devised in the previous section assumes a different size of the atomic cloud at different steps of the experimental sequence. The expansion dynamics relies decisively on the temperature and densities considered. Depending on these parameters, bosonic gases, assumed to be confined in harmonic trapping potentials, are found in different possible regimes. Here, we treat Bose–Einstein condensed gases as well as non-degenerate ensembles in all collisional regimes ranging from the collisionless (thermal) to the hydrodynamic limit. We comment on the analogy with fermions later in this section.

The phase-space behavior of ensembles above the critical temperature of condensation is well described by the Boltzmann–Vlasov equation in the collisionless and hydrodynamic regimes [69, 70], whereas the mean-field dynamics of a degenerate gas are captured by the time-dependent Gross–Pitaevskii equation [71]. However, gases released from a harmonic confinement, experience a free expansion that can conveniently be rendered by

---

[5] $\sigma_{T_{\text{eff}}}$ effectively denotes the instability in the expansion rate σ_v.

simple scaling theories. In this approach, the gas is assumed to merely experience a dilation after release with an unchanged shape but a size $L_i(t)$ evolving according to

$$L_i(t) = b_i(t)L_i(0), \tag{7}$$

with $L_i(0)$ being the initial (in-trap) size and i denoting the spatial coordinate x, y or z. The dynamics in time are accounted for by the scaling parameters $b_i(t)$, which interpolate between all collisional regimes of non-degenerate (bosonic[6]) gases in reference [70] and for degenerate gases of bosons in [72, 73]. The initial size $L_i(0)$ depends on the interaction and temperature regime of the gas.

In the thermal non-interacting case, the initial size corresponds to the rms-width $\sigma_i^{\mathrm{th}}(0) = \sqrt{k_B T_a / m\omega_i^2}$ of the Gaussian density distribution trapped with the angular frequency ω_i in the direction i at a temperature T_a [74], the atomic mass m and the Boltzmann constant k_B. Considering elastic interactions, the initial size is a correction of the collisionless rms-width with a modified trapping frequency $\tilde{\omega}_i^2 = \omega_i^2(1 - \xi)$ accounting for the mean-field E_{mf} via the parameter $\xi = E_{\mathrm{mf}}/(E_{\mathrm{mf}} + k_B T_a)$ [75]. In the bosonic case, E_{mf} equals $2gn$, with the density of the cloud n and the interaction strength $g = 4\pi\hbar^2 a_s/m$ for an s-wave scattering length a_s and the the modified Planck constant $\hbar$. BECs are, on the other hand, well represented with a parabolic shape in the Thomas–Fermi regime for a large number of particles (the study case here). Their size is hence parametrized with the Thomas–Fermi-radius $R_i(0) = \sqrt{2\mu/m\omega_i^2}$, where μ is the chemical potential of the degenerate gas [71]. Although the physical origin is different, trapped Fermions display a similar density distribution as the interacting bosons. The Thomas–Fermi radii $R_i(0) = \sqrt{2E_F/m\omega_i^2}$ are determined by the Fermi-energy E_F [76].

6.2. Delta-kick collimation

Having defined the initial sizes for the different regimes of interest, we obtain the size at time t by solving the differential equations for the scaling parameters $b_i(t)$ following the treatment in [72, 73] for condensed and in [70] for non-degenerate gases in all collisional regimes. The result is illustrated in figures 4(a) and (c) in the case of ^{84}Sr and ^{87}Sr. The free expansion of the cloud in the different regimes is in each case plotted for times smaller than t_{DKC} denoting the application time of a delta-kick collimation (DKC) pulse. This pulse consists in re-flashing the initial trap causing a collimation of the atomic cloud [23, 24]. In the case of fermionic atoms populating a single-spin state, the cloud's expansion behavior is similar to that of a non-interacting (thermal) bosonic ensemble [76]. However, for a superposition of hyperfine states, s-wave scattering interactions are possible and the phase diagram of such gases is very rich leading to different expansion laws ranging from collisionless to hydrodynamic, BCS or unitary behavior [77]. DKC of molecular BECs [78] would give results similar to the atomic BEC case. For simplicity, we restrict the dynamics study (expansion and DKC) to the bosonic and single-spin-component fermionic cases keeping in mind that similar results can be retrieved for a superposition of hyperfine states in a fermionic ensemble. Different considerations in this study would therefore be more decisive for the bosons/fermions trade-off.

In the absence of interactions, the physics of an expanding cloud is captured by the Liouville's theorem (phase-space density conservation) and reads

$$\sigma_{v_{f,i}}\sigma_{f,i} = \sigma_{v_{0,i}}\sigma_{0,i}, \tag{8}$$

$\sigma_{0,i} = \sigma_i^{\mathrm{th}}{}_i(0)$ and $\sigma_{v_{0,i}} = \sqrt{k_B T_a/m}$ being the initial size and velocity widths of a thermal cloud, respectively, and $\sigma_{f,i} = \sigma_i^{\mathrm{th}}{}_i(t_{\mathrm{DKC}})$ is the size when the lens is applied. Evaluating this expression thus yields the minimum cloud size required at the delta-kick to achieve a certain target temperature performance T_{eff}. However, interactions affect the free expansion of the cloud (hence the time of free expansion needed to reach the required size at the kick) and the residual velocity width after application of the lens. For non-degenerate gases we account for this by choosing the following ansatz for the phase-space distribution f of the ensemble:
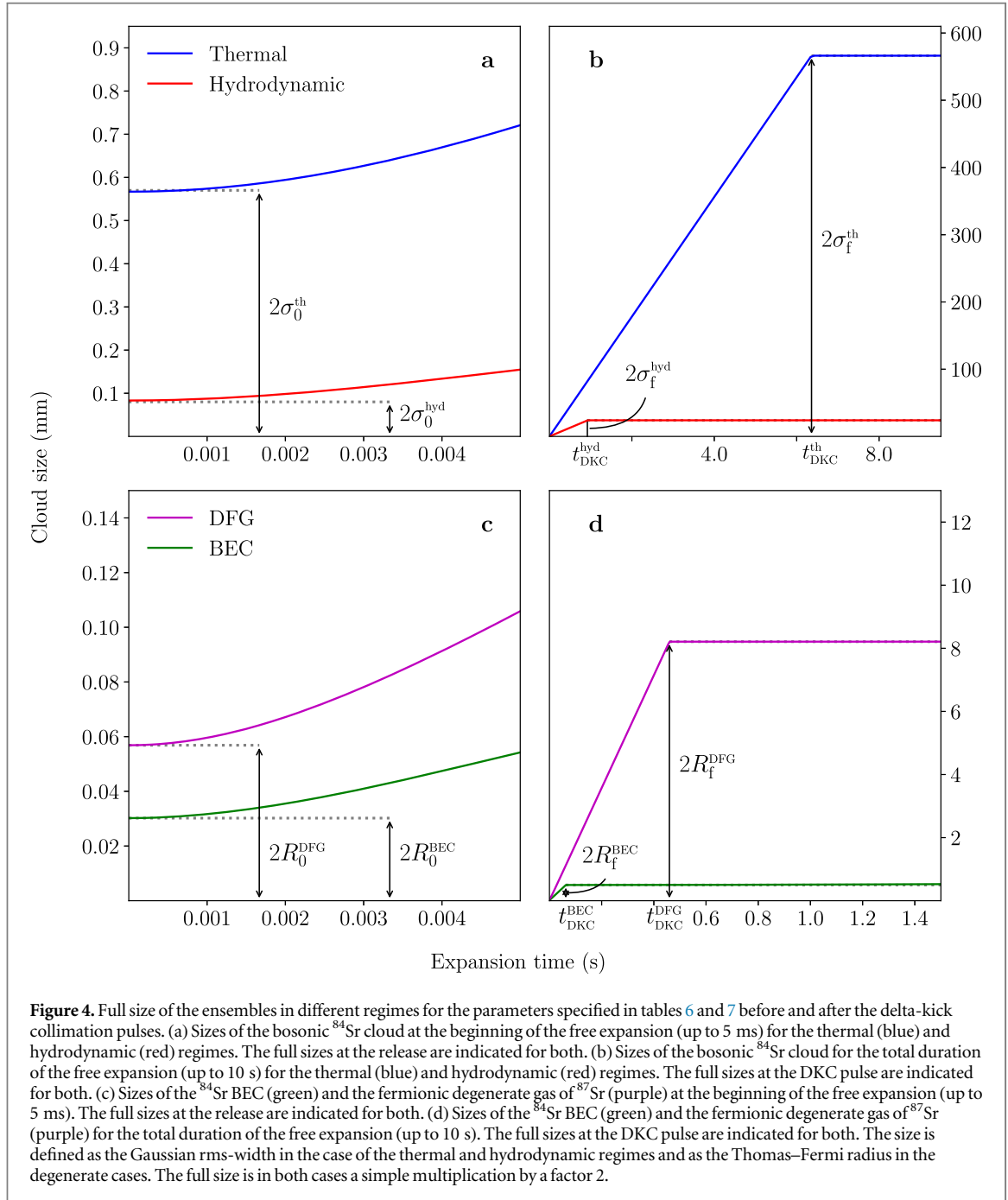
$$f(t_{\mathrm{DKC}} + \tau, x_i, v_i) = f(t_{\mathrm{DKC}}, x_i, v_i - \omega_i^2\tau x_i). \tag{9}$$

This approach, which is inspired by the treatment in [79], assumes that the duration τ of the lens is very small compared to the time of free expansion, such that the spatial distribution is left unchanged while the momentum is changed instantaneously by $\delta p_i = -m\omega_i^2\tau x_i$ when the harmonic lens potential is applied. This, combined with the free expansion of interacting, non-degenerate gases [70], gives rise to the momentum width

$$\sigma_{v_{f,i}} = \sigma_{v_{0,i}}\theta_i^{1/2}(t_{\mathrm{DKC}}) \tag{10}$$

after a lens which satisfies the condition $\dot{b}_i(t_{\mathrm{DKC}}) = \tau\omega_i^2 b_i(t_{\mathrm{DKC}})$. The scaling parameters θ_i are the time-evolved effective temperatures in each direction and are determined, similarly to the spatial scaling parameters b_i, by solving the differential equations in [70]. It is worth noticing that this general treatment leads to equation (8) in the non-interacting case, which we also use to assess the delta-kick performance of a degenerate Fermi gas in one spin state (where interactions are absent [76]).

---

[6] In fact, they are also valid for a Fermi gas in its normal phase.

Figure 4. Full size of the ensembles in different regimes for the parameters specified in tables 6 and 7 before and after the delta-kick collimation pulses. (a) Sizes of the bosonic ^{84}Sr cloud at the beginning of the free expansion (up to 5 ms) for the thermal (blue) and hydrodynamic (red) regimes. The full sizes at the release are indicated for both. (b) Sizes of the bosonic ^{84}Sr cloud for the total duration of the free expansion (up to 10 s) for the thermal (blue) and hydrodynamic (red) regimes. The full sizes at the DKC pulse are indicated for both. (c) Sizes of the ^{84}Sr BEC (green) and the fermionic degenerate gas of ^{87}Sr (purple) at the beginning of the free expansion (up to 5 ms). The full sizes at the release are indicated for both. (d) Sizes of the ^{84}Sr BEC (green) and the fermionic degenerate gas of ^{87}Sr (purple) for the total duration of the free expansion (up to 10 s). The full sizes at the DKC pulse are indicated for both. The size is defined as the Gaussian rms-width in the case of the thermal and hydrodynamic regimes and as the Thomas–Fermi radius in the degenerate cases. The full size is in both cases a simple multiplication by a factor 2.

For BECs at zero temperature, the previous models can not be applied anymore. We employ, instead, an energy conservation model which assumes that the energy due to repulsive atomic interactions converts into kinetic energy during free expansion at a first stage. The asymptotic three-dimensional expansion rate Δv_f after the delta-kick, in this model, stems from the residual mean-field energy and a Heisenberg term $\propto \hbar^2/mR_f^2$, which dominates for larger time of flights when the mean-field energy has dissipated. It reads

$$\Delta v_f = \left(\frac{5N_a g}{2m\pi R_f^3} + \frac{14\hbar^2}{3mR_f^2} \right)^{1/2}, \tag{11}$$

with N_a being the number of atoms and $R_f = R(t_{\mathrm{DKC}})$ being the size at lens [71]. We relate this expansion rate to an effective temperature via $\frac{3}{2}k_B T_{\mathrm{eff}} = \frac{m}{2}(\Delta v_f/\sqrt{7})^2$ [25, 80] and restrict ourselves to the isotropic case for simplicity.

After the application of the delta-kick pulse, we assume a linear expansion during the interferometry sequence lasting $2T$. The full size $L(2T)$ of the cloud at the end of the sequence is then given in all regimes by

Table 6. Ensembles sizes compatible with the 10 pK expansion rate requirement for classical gases in the collisionless and hydrodynamic regimes. The characteristics of the considered experimental arrangement are stated in the six first rows of the table. The computed resulting sizes are given, after the treatment of section 6.2, in the next rows. Of particular importance for the trade-off performed in this paper, are the sizes at lens (bold) and the final detected sizes for several interferometry times $2T$. The larger these sizes, the harsher the requirements are on the DKC and interferometry pulses.

3D expansion rate $T_{\text{eff}} = 10$ pK	Collisionless		Hydrodynamic	
	^{174}Yb	^{84}Sr	^{174}Yb	^{84}Sr
Number of atoms	5×10^8		5×10^7	
Trapping frequency (2π Hz)	25		50	
Initial temperature (μK)	10		0.83	
Initial size $2\sigma_0$ (μm)	393.77	566.91	58.03	83.22
Knudsen number [75]	0.28	0.42	0.06	0.09
Phase space density	$< 10^{-3}$		0.6	
Pre-DKC expansion time (t_{DKC}) (ms)	6359		924	
Size at lens $2\sigma(t_{\text{DKC}})$ (mm)	**393.32**	**566.27**	**16.73**	**23.99**
Final size $2\sigma(t_{\text{DKC}} + 2T)$ (mm)				
$T = 40$ s	393.34	566.29	17.09	24.51
$T = 100$ s	393.42	566.41	18.88	27.09
$T = 160$ s	393.57	566.63	21.81	31.33

Table 7. Ensembles sizes compatible with the 10 pK expansion rate requirement for quantum degenerate regimes. The entries of the table are the same than 6. For BECs and DFGs the computed sizes are dramatically smaller than the thermal counterparts.

3D expansion rate $T_{\text{eff}} = 10$ pK	BEC		DFG	
	^{174}Yb	^{84}Sr	^{171}Yb	^{87}Sr
Number of atoms	7×10^6		7×10^6	
Trapping frequency (2π Hz)	50		50	
Critical temperature (μK)	0.431		0.834	
Initial size $2R_0$ (μm)	30.2	41.8	56.86	81.86
Pre-DKC expansion time (t_{DKC}) (ms)	63	61	460	460
Size at lens $2R(t_{\text{DKC}})$ (mm)	**0.50**	**0.67**	**8.21**	**11.82**
Final size $2R(t_{\text{DKC}} + 2T)$ (mm)				
$T = 40$ s	9.27	13.34	12.86	18.51
$T = 100$ s	23.15	33.32	26.07	37.53
$T = 160$ s	37.03	53.31	40.43	58.20

$$L(2T) = 2\sqrt{L_f^2 + (2T\Delta v)^2}, \tag{12}$$

with $L_f = \sigma_f$, $\Delta v = \sigma_{v_f}$ in the non-degenerate regimes and $L_f = R_f$, $\Delta v = \Delta v_f$ for condensed ensembles. In what follows, indices relative to spatial directions are left since we, for simplicity, chose to treat isotropic cases. With the models adopted above, we show in the tables 6 (non-degenerate gases) and 7 (quantum degenerate ensembles) the characteristic figures for the various regimes for a given asymptotic target expansion temperature of 10 pK. The minimum required cloud sizes are printed in bold and are depicted in figures 4(b) and (d), along with the size at the end of the interferometric sequence. The extent over which state-of-the art magnetic and optical potentials can be considered harmonic is typically limited to a few mm in the best case. This operating range is a decisive criterion for the choice of the initial cloud temperature and density configuration.

As a conclusion to this section with respect to the required size at lens, we find out that degenerate ensembles thanks to their point-like initial extension are largely favored. The availability of traps with significantly larger harmonic extent could eventually make the use of a non-degenerate gas in the hydrodynamic regime feasible in the future. Another possibility in to use classical gases through a velocity selection stage, which, however, is always accompanied by a substantial loss of atoms and typically reduces the velocity spread in one dimension only.

7. Conclusion

In this paper, we have exposed the necessary criteria for choosing the atomic source of a space-borne gravitational wave observatory mission scenario [17]. In that scenario, featuring a baseline $L = 2 \times 10^9$ m (6×10^8 m) and a maximum interrogation time $T = 160$ s (75 s), the use of beam splitting order $N = 1$ (6) yields a maximum strain sensitivity of $< 10^{-19}$ Hz$^{-1/2}$ ($< 10^{-20}$ Hz$^{-1/2}$) around 10 mHz, comparable to the expected LISA strain sensitivity. ^{87}Sr, ^{84}Sr, ^{174}Yb and ^{171}Yb seem to be the most promising candidates in light of their fundamental properties, technical feasibility, and availability of laser sources. Further atomic losses due to the finite excitation rates will have to be mitigated by either enhancing the field parameters through increased laser power and/or stronger static magnetic fields in the case of the bosons or by optimizing the source by achieving even lower expansion rates with longer free expansion time prior to the atomic lens. We constrained the implementation parameters by an error model incorporating source expansion dynamics and interferometric phase shifts. Looking closer at the atomic source properties, it is shown that by the appropriate choice of a quantum-degenerate expansion regime, the assumed expansion performance of 10 pK can be met after a DKC treatment. While further experimental development is necessary to meet the atomic flux requirements of 4×10^7 atoms s^{-1}, recent robust BEC production in microgravity [81] and space [82] demonstrate important steps towards meeting this goal. In general, the exploration of cold atom technologies in microgravity [23, 83, 84] and in space [85, 86] is a promising and rapidly progressing field of research.

ORCID iDs

S Loriani ● https://orcid.org/0000-0001-6660-960X
J M Hogan ● https://orcid.org/0000-0003-1218-2692
N Gaaloul ● https://orcid.org/0000-0001-8233-5848

References

[1] Abbott B P *et al* 2016 *Phys. Rev. Lett.* **116** 061102
[2] Abbott B P *et al* 2016 *Phys. Rev. Lett.* **116** 241103
[3] Nissanke S, Kasliwal M and Georgieva A 2013 *Astrophys. J.* **767** 124
[4] Wu X F, Gao H, Wei J J, Mészáros P, Zhang B, Dai Z G, Zhang S N and Zhu Z H 2016 *Phys. Rev. D* **94** 024061
[5] Acernese F *et al* 2015 *Class. Quantum Grav.* **32** 024001
[6] Aasi J *et al* 2015 *Class. Quantum Grav.* **32** 074001
[7] Affeldt C *et al* 2014 *Class. Quantum Grav.* **31** 224002
[8] Armano M *et al* 2016 *Phys. Rev. Lett.* **116** 231101
[9] Danzmann K *et al* 2011 *ESA Report No. ESA/SRE(2011)3*
[10] Dimopoulos S, Graham P W, Hogan J M, Kasevich M A and Rajendran S 2008 *Phys. Rev. D* **78** 122002
[11] Delva P and Rasel E M 2009 *J. Mod. Opt.* **56** 1999
[12] Hohensee M, Lan S Y, Houtz R, Chan C, Estey B, Kim G, Kuan P C and Müller H 2010 *Gen. Relativ. Gravit.* **43** 1905
[13] Hogan J M *et al* 2011 *Gen. Relativ. Gravit.* **43** 1953
[14] Chiow S W, Williams J and Yu N 2015 *Phys. Rev. A* **92** 063613
[15] Chaibi W, Geiger R, Canuel B, Bertoldi A, Landragin A and Bouyer P 2016 *Phys. Rev. D* **93** 021101
[16] Graham P W, Hogan J M, Kasevich M A, Rajendran S and Romani R W 2017 arXiv:1711.02225

[17] Hogan J M and Kasevich M A 2016 *Phys. Rev.* A **94** 033632
[18] Yu N and Tinto M 2010 *Gen. Relativ. Gravit.* **43** 1943
[19] Graham P W, Hogan J M, Kasevich M A and Rajendran S 2013 *Phys. Rev. Lett.* **110** 171102
[20] Hu L, Poli N, Salvi L and Tino G M 2017 *Phys. Rev. Lett.* **119** 263601
[21] Norcia M A, Cline J R K and Thompson J K 2017 *Phys. Rev.* A **96** 042118
[22] Bender P L 2014 *Phys. Rev.* D **89** 062004
[23] Müntinga H *et al* 2013 *Phys. Rev. Lett.* **110** 093602
[24] Kovachy T, Hogan J M, Sugarbaker A, Dickerson S M, Donnelly C A, Overstreet C and Kasevich M A 2015 *Phys. Rev. Lett.* **114** 143004
[25] Rudolph J 2016 Matter-wave optics with Bose–Einstein condensates in microgravity *PhD Thesis* Leibniz Universität Hannover
[26] Porsev S G and Derevianko A 2004 *Phys. Rev.* A **69** 042506
[27] Moore I D, Bailey K, Greene J, Lu Z T, Müller P, O'Connor T P, Geppert C, Wendt K D A and Young L 2004 *Phys. Rev. Lett.* **92** 153002
[28] Falke S *et al* 2014 *New J. Phys.* **16** 073023
[29] Gibble K 2015 private communication
[30] Sherman J A, Lemke N D, Hinkley N, Pizzocaro M, Fox R W, Ludlow A D and Oates C W 2012 *Phys. Rev. Lett.* **108** 153002
[31] Yi L, Mejri S, McFerran J J, Le Coq Y and Bize S 2011 *Phys. Rev. Lett.* **106** 073005
[32] Kulosa A P *et al* 2015 *Phys. Rev. Lett.* **115** 240801
[33] Kraft S, Vogt F, Appel O, Riehle F and Sterr U 2009 *Phys. Rev. Lett.* **103** 130401
[34] Santra R, Christ K V and Greene C H 2004 *Phys. Rev.* A **69** 042510
[35] Brickman K A, Chang M S, Acton M, Chew A, Matsukevich D, Haljan P C, Bagnato V S and Monroe C 2007 *Phys. Rev.* A **76** 043411
[36] Barber Z W, Hoyt C W, Oates C W, Hollberg L, Taichenachev A V and Yudin V I 2006 *Phys. Rev. Lett.* **96** 083002
[37] Petersen M, Chicireanu R, Dawkins S T, Magalhães D V, Mandache C, Le Coq Y, Clairon A and Bize S 2008 *Phys. Rev. Lett.* **101** 183004
[38] Taichenachev A V, Yudin V I, Oates C W, Hoyt C W, Barber Z W and Hollberg L 2006 *Phys. Rev. Lett.* **96** 083001
[39] Boyd M M, Zelevinsky T, Ludlow A D, Blatt S, Zanon-Willette T, Foreman S M and Ye J 2007 *Phys. Rev.* A **76** 022510
[40] Gaunt A L, Schmidutz T F, Gotlibovych I, Smith R P and Hadzibabic Z 2013 *Phys. Rev. Lett.* **110** 200406
[41] Mielec N, Altorio M, Sapam R, Horville D, Holleville D, Sidorenkov L A, Landragin A and Geiger R 2018 *Appl. Phys. Lett.* **113** 161108
[42] Cheinet P 2006 Conception et réalisation d'un gravimètre atomes froids *PhD Thesis* SYRTE
[43] Taie S, Takasu Y, Sugawa S, Yamazaki R, Tsujimoto T, Murakami R and Takahashi Y 2010 *Phys. Rev. Lett.* **105** 190401
[44] Nicholson T *et al* 2015 *Nat. Commun.* **6** 6896
[45] Mehlstäubler T 2005 Neuartige Kühlmethoden für einen optischen Magnesium Frequenzstandard *PhD Thesis* Leibniz Universität Hannover
[46] Takasu Y, Honda K, Komori K, Kuwamoto T, Kumakura M, Takahashi Y and Yabuzaki T 2003 *Phys. Rev. Lett.* **90** 023003
[47] Roy R, Green A, Bowler R and Gupta S 2016 *Phys. Rev.* A **93** 043403
[48] Stellmer S, Grimm R and Schreck F 2013 *Phys. Rev.* A **87** 013611
[49] Bongs K *et al* 2015 *C.R. Phys.* **16** 553
[50] Schiller S *et al* 2012 *European Frequency and Time Forum (EFTF), 2012* (Piscataway, NJ: IEEE) pp 412–8
[51] AOSense. web http://aosense.com/
[52] Mukaiyama T, Katori H, Ido T, Li Y and Kuwata-Gonokami M 2003 *Phys. Rev. Lett.* **90** 113002
[53] MenloSystems. web http://menlosystems.com/
[54] Adams C S, Lee H J, Davidson N, Kasevich M and Chu S 1995 *Phys. Rev. Lett.* **74** 3577
[55] Hartwig J, Abend S, Schubert C, Schlippert D, Ahlers H, Posso-Trujillo K, Gaaloul N, Ertmer W and Rasel E M 2015 *New J. Phys.* **17** 035011
[56] Leibrandt D R, Thorpe M J, Bergquist J C and Rosenband T 2011 *Opt. Express* **19** 10278
[57] Parker B, Marra G, Johnson L A M, Margolis H S, Webster S A, Wright L, Lea S N, Gill P and Bayvel P 2014 *Appl. Opt.* **53** 8157
[58] Ben Dahan M, Peik E, Reichel J, Castin Y and Salomon C 1996 *Phys. Rev. Lett.* **76** 4508
[59] Peik E, Ben Dahan M, Bouchoule I, Castin Y and Salomon C 1997 *Phys. Rev.* A **55** 2989
[60] Cladé P, de Mirandes E, Cadoret M, Guellati-Khelifa S, Schwob C, Nez F, Julien L and Biraben F 2006 *Phys. Rev.* A **74** 052109
[61] Sugarbaker A, Dickerson S M, Hogan J M, Johnson D M S and Kasevich M A 2013 *Phys. Rev. Lett.* **111** 113002
[62] Abend S *et al* 2016 *Phys. Rev. Lett.* **117** 203003
[63] Debs J E, Altin P A, Barter T H, Döring D, Dennis G R, McDonald G, Anderson R P, Close J D and Robins N P 2011 *Phys. Rev.* A **84** 033610
[64] Dickerson S M, Hogan J M, Sugarbaker A, Johnson D M S and Kasevich M A 2013 *Phys. Rev. Lett.* **111** 083001
[65] Hogan J M, Johnson D M S and Kasevich M A 2008 Light-pulse atom interferometry *Atom Optics and Space Physics: Proceedings of the International School of Physics* ed E Arimondo, W Ertmer, E M Rasel and W P Schleich (Amsterdam: IOS Press)
[66] Bongs K, Launay R and Kasevich M 2006 *Appl. Phys.* B **84** 599
[67] Louchet-Chauvet A, Farah T, Bodart Q, Clairon A, Landragin A, Merlet S and Pereira Dos Santos F 2011 *New J. Phys.* **13** 065025
[68] Tackmann G, Berg P, Schubert C, Abend S, Gilowski M, Ertmer W and Rasel E M 2012 *New J. Phys.* **14** 015002
[69] Guéry-Odelin D 2002 *Phys. Rev.* A **66** 033613
[70] Pedri P, Guéry-Odelin D and Stringari S 2003 *Phys. Rev.* A **68** 043608
[71] Pethick C J and Smith H 2001 *Bose–Einstein Condensation in Dilute Gases* (Cambridge: Cambridge University Press)
[72] Castin Y and Dum R 1996 *Phys. Rev. Lett.* **77** 5315
[73] Kagan Y, Surkov E and Shlyapnikov G 1996 *Phys. Rev.* A **54** R1753
[74] Huang K 1987 *Statistical Mechanics* (New York: Wiley)
[75] Shvarchuck I, Buggle C, Petrov D S, Kemmann M, von Klitzing W, Shlyapnikov G V and Walraven J T M 2003 *Phys. Rev.* A **68** 063603
[76] Giorgini S, Pitaevskii L P and Stringari S 2008 *Rev. Mod. Phys.* **80** 1215
[77] Ketterle W and Zwierlein M W 2008 Ultracold Fermi gases *Proc. Int. School of Physics 'Enrico Fermi' Course CLXIV* p 95
[78] Lassablière L and Quéméner G 2018 *Phys. Rev. Lett.* **121** 163402
[79] Condon G, Fortun A, Billy J and Guéry-Odelin D 2014 *Phys. Rev.* A **90** 063616
[80] Corgier R, Amri S, Herr W, Ahlers H, Rudolph J, Guéry-Odelin D, Rasel E M, Charron E and Gaaloul N 2018 *New J. Phys.* **20** 055002
[81] Rudolph J *et al* 2015 *New J. Phys.* **17** 065001
[82] Becker D *et al* 2018 *Nature* **562** 391
[83] van Zoest T *et al* 2010 *Science* **328** 1540
[84] Varoquaux G, Nyman R A, Geiger R, Cheinet P, Landragin A and Bouyer P 2009 *New J. Phys.* **11** 113010
[85] Elliott E R, Krutzik M C, Williams J R, Thompson R J and Aveline D C 2018 *NPJ Microgravity* **4** 16
[86] Gibney E 2018 *Nature* **557** 151

ACKNOWLEDGMENTS

CURRICULUM VITAE

PERSONAL INFORMATION

Name, Surname	Loriani Fard, Sina Leon
Date/place of birth	06.10.1993, Hamburg
Email	loriani@iqo.uni-hannover.de

EDUCATION

2017 –	PhD student · Institute of Quantum Optics, Leibniz University Hannover
2018-2019	Promotion Plus qualifiziert · Graduate Academy, Leibniz University Hannover
2014-2016	Master of Science (Physics) · Leibniz University Hannover
2011-2014	Bachelor of Science (Physics) · Leibniz University Hannover
2004-2011	Gymnasium Johanneum Lüneburg, Abitur 2011